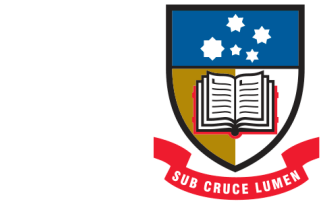

THE UNIVERSITY of ADELAIDE

Exploring the Composition, Dissolution Kinetics and Passivation of Jarosite from an Acid Sulfate Soil

Austin Trueman

School of Agriculture, Food and Wine

The University of Adelaide

This thesis is submitted in fulfilment of the requirements for the degree of Master of Philosophy

September 2020

Contents

Abstract

Jarosite minerals ($XFe(SO_4)_2(OH)_6$, where X is typically K or Na) are common secondary reaction products of iron sulfide oxidation. Consequently, jarosite is a diagnostic feature of sulfuric material (pH < 4) in acid sulfate soils (ASS), where it constitutes the principal source of retained acidity: an operationally defined pool of potential acidity associated with the hydrolysis of Al^{3+} and Fe^{3+} from minerals such as jarosite and schwertmannite. Soils containing considerable quantities of jarosite tend to exhibit hazardous properties (e.g. acidic and metalliferous drainage) for years to decades after the sulfuric material formed. This appears to be related to the slow mineral dissolution rate coupled with the ability of jarosite to buffer the soil solution between pH 3-4.

Effectively managing such soils requires an accurate understanding of jarosite-rich sulfuric material, its long-term behaviour and effects on soil and water quality, and potential remediation strategies. However, the results described in the literature concerning jarosite solubility and jarosite kinetics are highly variable. Furthermore, there are currently no effective means of directly nullifying the environmental risks associated with jarosite in soils. Conventional ASS management strategies such as liming or dewatering and filling/capping ASS may be costly, have limited ability to effectively nullify jarosite while preventing acidity export, and may limit land-use options. Mineral surface passivation techniques – where retained acidity remains *in situ*, but dissolution is slowed or prevented – may be an effective alternative remediation strategy. However, the efficacy of these techniques has not been trialled for jarosite in ASS.

Therefore, the work described in this thesis relates to three principal objectives: (1) to characterise jarosite-rich sulfuric material, (2) to provide a better understanding of how this material affects and is affected by the chemistry of the solution in which it dissolves; (3) to test potential jarosite passivation strategies.

In order to carry out these objectives, jarosite-rich segregations were extracted from an ASS in the Gillman area within the southern Barker Inlet estuary, South Australia. A range of chemical and physical assays were conducted, and showed that the jarosite-rich segregations were primarily composed of jarosite ($KFe_3(SO_4)_2(OH)_6$), and were admixed with minor amounts of quartz, halite, gypsum, muscovite and organic matter.

A gradient perfusion technique was utilised to describe the dissolution chemistry of this jarosite sample under constant flow conditions and at a range of pH values. The rate of dissolution (R) ranged from 3.16E-13 to 3.16E-11 mol/m^{2}s, and was strongly correlated to pH by the function: $\log_{10}R = 0.099pH^2 - 0.966pH - 9.914$. Monitoring differences between eluant (input) and eluate (output) pH clearly demonstrated that jarosite dissolution has a strongly acidifying effect, and should buffer soil pH around 4. Regardless of pH, the initial 12-24 hours of dissolution was characterised by the rapid release of Ca, Mg, Na and S (due to the dissolution of soluble minerals such as gypsum and halite). Consequently, flushing acidity from even highly weathered soils containing jarosite-rich sulfuric material is not advisable, as the resulting acidic, saline drainage may cause severe offsite environmental impacts. However, the dissolution experiments also suggest that the dissolution of jarosite under alkaline conditions is characterised by the formation of poorly-crystalline, ferric (oxyhydr)oxides that may possibly coat jarosite surfaces and hindered further dissolution. Therefore, promoting alkaline soil conditions may reduce the export of acidity by altering jarosite, or its surface, to more

chemically benign and environmentally stable ferric (oxyhydr)oxides. This study was published in *Chemical Geology* (Trueman et al., 2020).

In light of these conclusions, I examined the composition and dissolution kinetics of jarosite that was treated with a view to produce passivating coatings of ferric (oxyhydr)oxide (e.g. goethite, α-FeOOH) and ferric phosphate (e.g. strengite, $FePO_4.2H_2O$). I confirmed that under alkaline conditions jarosite readily decomposes to yield poorly-crystalline ferric (oxyhydr)oxides (i.e. two-line ferrihydrite). Moreover, these ferric (oxyhydr)oxides reacted with phosphoric acid to produce ferric phosphate; and reacted with monoammonium phosphate (MAP) to produce spheniscidite: an extremely rare ferric hydroxyphosphate. The direct alteration of jarosite to a ferric phosphate was constrained under ambient conditions. However, at elevated temperatures, jarosite reacted with phosphoric acid to produce phosphosiderite (a metastable dimorph of strengite) and gengenbachite ($KFe_3(HPO_4)_4(HPO_4)_2.6H_2O$); and reacted with MAP to produce an unnamed ammonium ferric phosphate ($H_2(NH_4)Fe(PO_4)_2$). The dissolution kinetics of the NaOH- and MAP-treated jarosite was examined using column perfusion experiments, which suggest these treatments do not offer any distinct advantages in terms of curtailing the release of potentially hazardous elements. However, the study provides key insights into jarosite alteration pathways, and sets a solid foundation upon which to further explore alternative methods of remediating jarosite-rich soils. This study was published in *Chemical Geology* (Trueman e al. 2021).

The findings presented in this thesis can be utilised to better predict the behaviour of jarosite in the environment and its effects on soil and water quality, and to design more effective remediation strategies for ASS with jarosite-rich sulfuric material.

References

Trueman, A.M., Fitzpatrick, R.W., Mosley, L.M., Mclaughlin, M.J., 2021. Exploring passivation-based treatments for jarosite from an acid sulfate soil. Chemical Geology, 561: 120034. https://doi.org/10.1016/j.chemgeo.2020.120034.

Trueman, A.M., Mclaughlin, M.J., Mosley, L.M., Fitzpatrick, R.W., 2020. Composition and dissolution kinetics of jarosite-rich segregations extracted from an acid sulfate soil with sulfuric material. Chemical Geology, 543: 119606. https://doi.org/10.1016/j.chemgeo.2020.119606.

Acknowledgements

Firstly, I am extremely grateful for the scholarship granted to me by the University of Adelaide.

I would like to thank my supervisors: Mike McLaughlin, Luke Mosley and Rob Fitzpatrick. Observing Mike interpret and extrapolate my results (often with very little context) was a highly valuable experience. Luke's constructive and reliable feedback and encouragement was greatly appreciated. Rob's enthusiasm for soil, science, and life in general, was energising.

I also would like to thank:

Bogumila Tomczak – for her company in the lab and for analysing quite literally several thousand eluate fractions.

Ashleigh Panagaris, Chandnee Ramkissoon, Colin Rivers, Emily Leyden, Emma Knight, Fein Degryse, Ivan Andelkovic, Pichu Rengasamy, Rodrigo Coqui da Silva, Roslyn Baird, and Shervin Kabiri – for their company and advice.

Thadeu Rodrigues de Melo – for his company and long discussions regarding the shared and respective quirks of English and Portuguese.

Ron Smernik – who plays a critical, yet undervalued, role in bolstering postgraduate mental health.

Cameron Grant – for his enthusiastic help and advice.

The South Australian Branch of Soil Science Australia – for supporting my participation in the 2018 National Soil Judging Competition.

Maggie – for her unwavering kindness and support.

Declaration

I, Austin Trueman, certify that this work contains no material which has been accepted for the award of any other degree or diploma in my name, in any university or other tertiary institution and, to the best of my knowledge and belief, contains no material previously published or written by another person, except where due reference has been made in the text. In addition, I certify that no part of this work will, in the future, be used in a submission in my name, for any other degree or diploma in any university or other tertiary institution without the prior approval of the

University of Adelaide and where applicable, any partner institution responsible for the joint-award of this degree.

I acknowledge that copyright of published works contained within this thesis resides with the copyright holder(s) of those works.

I also give permission for the digital version of my thesis to be made available on the web, via the University's digital research repository, the Library Search and also through web search engines, unless permission has been granted by the University to restrict access for a period of time.

I acknowledge the support I have received for my research through the provision of an Australian Government Research Training Program Scholarship.

_____

Date: 26.08.20

Figures

Chapter 1 – Introduction

Chapter 2 – Composition and dissolution kinetics of jarosite-rich segregations extracted from an acid sulfate soil with sulfuric material

Chapter 3 – Exploring passivation-based treatments for jarosite from an acid sulfate soil

Chapter 4 – Conclusion

Tables

Chapter 1 – Introduction

Chapter 2 – Composition and dissolution kinetics of jarosite-rich segregations extracted from an acid sulfate soil with sulfuric material

Chapter 3 – Testing passivation treatments for jarosite from an acid sulfate soil

Thesis structure

This thesis is composed of two published research chapters (Chapters 2 and 3), and unpublished introductory and concluding chapters. Chapters 2 and 3 and are equivalent to the results chapters in a traditional thesis format. These chapters are self-contained and include independent introduction, methods, results, discussion, and conclusion sections. Additionally, as these chapters are multi authored, the contributions of each author are ascribed in a standard form provided by the University of Adelaide at the start of each chapter.

Chapter 1 provides a brief overview of ASS, and the occurrence and nature of jarosite and its role as a source of potential acidity and trace elements. It reviews literature most relevant to the research objectives, identifying knowledge gaps, and defines the research objectives of the thesis.

Chapter 2 comprises a manuscript published in *Chemical Geology*. It details the composition and dissolution kinetics of pedogenic jarosite; and draws conclusions related to the key effects of jarosite dissolution on soil and water quality.

Chapter 3 comprises a manuscript published in *Chemical Geology*. It details the effects of select passivation-based treatments on the composition and dissolution kinetics of pedogenic jarosite; and draws conclusions related to the efficacy and practicality of these treatments in the field.

Chapter 4 provides an overall synthesis of the key findings contained in Chapters 2 and 3 and their significance, and includes recommendations for future work.

Chapter 1 – Introduction

1. Introduction

Jarosite ($KFe_3(SO_4)_2(OH)_6$) is commonly associated with acid sulfate soils (ASS), where it is thought to play a critical role in the regulation of acidity and mobility of trace elements. However, a comprehensive understanding of jarosite reactivity is required to better predict and mitigate the negative effects of jarosite dissolution on soil and water quality.

Acid sulfate soils are generally defined as soils that contain, or have the potential to produce, sulfuric acid in quantities that cause significant and long-lasting changes in key soil properties (Pons, 1973). Within the Australian Soil Classification, the term applies to soils that contain hypersulfidic, hyposulfidic and/or sulfuric materials (Isbell and The National Committee on Soils and Terrain, 2016). Hypersulfidic and hyposulfidic materials, which both have a field pH of 4 or more, contain defined thresholds of reduced inorganic sulfides (RIS) such as pyrite (FeS_2). While hypersulfidic material experiences a drop in pH to < 4 after at least 8 weeks of incubation, hyposulfidic material does not. This is due to a high pH buffering and acid neutralising capacity. Hypersulfidic and hyposulfidic materials tend to develop in oxygen-poor, nutrient-rich environments – and are relatively common in permanently or frequently waterlogged soil. Consequently, sulfidic materials often form part of, or are in close proximity to, aquatic systems (e.g. rivers, lakes, wetlands, and inlets), which are of great environmental and economic value.

Under oxygen-poor conditions, hypersulfidic material is unreactive. However, if aerobic conditions prevail – e.g. if the land is excavated or drained, or if the water table drops during a drought – hypersulfidic material will develop chemically hazardous characteristics (e.g. pH < 4) as the RIS oxidise to produce sulfuric acid (Pons, 1973). Soil material that is strongly acidic (pH < 4) due to the oxidation of hypersulfidic material is termed sulfuric material (Isbell and The National Committee on Soils and Terrain, 2016). The generation of acidity creates intense weathering conditions that liberate a range of elements as native soil minerals decompose. The fate of contaminants (e.g. acidity, metals and trace elements) is greatly affected by the nature (e.g. reactivity and solubility) of the secondary reaction products of RIS oxidation. For example, relatively soluble minerals – such as binary Al, Ca, Fe, and Mg sulfates – may drive dramatic seasonal changes in soil and water chemistry as they precipitate during dry periods and dissolve during wet periods (Fitzpatrick and Shand, 2008; Mosley et al., 2014c; van Breemen, 1973). Conversely, relatively insoluble minerals – such as jarosite – may exert considerable control over long-term trends in soil and water chemistry.

Members of the jarosite subgroup ($XFe_3(SO_4)_2(OH)_6$) are characterised by repeating layers of FeO_6 octahedra and sulfate tetrahedra, as well as monovalent interfoliar sites (X site) (Das et al., 1996; Dutrizac and Jambor, 2000; Stoffregen et al., 2000). The ideal endmember stoichiometry is $KFe_3(SO_4)_2(OH)_6$, however substitution for K, Fe and S is common. Natrojarosite (Na-dominant) and argentojarosite (Ag-dominant) species are likely the most common naturally occurring jarosite species after potassium jarosite. However, other K-site substitutions include: H_3O^+, NH_4^+, Rb^+, Ti^+, Ba^{2+}, Ca^{2+}, Cu^{2+}, Hg^{2+}, La^{3+}, Pb^{2+} and Sr^{2+}. Fe^{3+} is typically substituted by Al^{3+}, but a range of other Fe^{3+}-site substitutions have been recorded, including: Cu^{2+}, Ga^{3+}, Cr^{3+}, V^{3+}. Examples of sulfate substitution include AsO_4^{2-}, CrO_4^{2-}, and PO_4^{2-}. Although the array of substitutions described here may be relatively common, they rarely exceed 5 wt% (with the exceptions of Ag, Cu, H_3O, Na and Pb) (Dutrizac and Jambor, 2000). Therefore, although jarosite may exert some degree of influence over the mobility of trace

elements in the environment, its potential to generate acidity generally receives more attention in the literature.

Jarosite typically constitutes the principal source of Retained Acidity (RA) in soil with sulfuric material. RA refers to potential acidity associated with sparingly soluble Fe^{3+} and Al^{3+} minerals, which slowly undergo hydrolysis to produce H^+ (e.g. $Fe^{3+} + 3H_2O \rightarrow Fe(OH)_3 + 3H^+$) (Ahern et al., 2004; Sullivan et al., 2018; Vithana et al., 2013). As such, sulfuric soil and other geologic media with high levels of RA, tend to exhibit chemically hazardous properties long after the bulk of hypersulfidic material has weathered away. The significance of the widespread occurrences of jarosite-rich sulfuric material as a risk to soil and water quality was highlighted in South Australia during the Millennium Drought (esp. 2007-2010) when water table levels drastically fell. Additionally, post-drought reflooding resulted in subaqueous sulfuric soils, which presented a myriad of unique land management hurdles (Fitzpatrick et al., 2010; Fitzpatrick et al., 2018).

Due to record low rainfall and declines in groundwater levels, large swathes of soil with sulfidic material were exposed in the floodplains of the Lower Murray River – resulting in widespread acidification events (Mosley et al., 2017). Moreover, under post-drought conditions, the rapid rise of water levels remobilised contaminants in ASS profiles, resulting in acidic drainage channel water (pH 2-5) with soluble metal concentrations far above guidelines for ecosystem protection (Mosley et al., 2014a; Mosley et al., 2014b). Similarly, rewetting of exposed sediments in the Lower Lakes of the Murray-Darling Basin (Ramsar-listed ecosystem of international importance) led to substantial acidification (pH 2-3) and metal contamination of lake water (Mosley et al., 2014c). The total drought management costs in the Murraylands alone were estimated at AUD 2 billion – with greater than AUD 50 million required for direct acidification management (e.g. limestone dosing and engineering solutions) (Kingsford et al., 2011). Moreover, despite remediation efforts and return of regular rainfall patterns, large areas of soil remained strongly acidic. Mosley et al. (2017) suggested that this stunted or prolonged recovery of drought-affected ASS with sulfuric material was due to: (1) low microbial activity due to low pH and low availability of labile organic matter; (2) slow flushing of acidity due to low soil hydraulic conductivity; (3) persistent soil acidification due to jarosite dissolution.

This is one of many environmental catastrophes that demonstrate the need for national drought preparedness strategies that include the effective management of soils with sulfidic and sulfuric material. Hydrogeochemical models will likely play a vital role in the development of such strategies, but rely on accurate mineral data (e.g. mineral solubility). Although jarosite is relatively well described in the literature, reported solubility parameters vary dramatically. Moreover, the majority of these studies focus on synthetic jarosite, and were not conducted within the framework of ASS. Consequently, the long-term behaviour of jarosite-rich sulfuric material and its effect on soil and water quality requires further elucidation.

2. Jarosite formation and weathering in soil

Although the formation and behaviour of ASS is often highly site specific, a number of general trends can be collated to form a conceptual model (Fig. 1). Below the average water table, the soil profile is dominated by apedal (massive) sulfidic material (van Breemen, 1973). This horizon is often capped by a redoximorphic zone, which represents the average vertical fluctuations of water in the soil profile. Based on data from Thomas (2010), these transitional zones often display both sulfidic and sulfuric characteristics (e.g. the soil may contain substantial amounts of both RIS and RA). Consequently, accurate classifying this material may depend on the dry season pH (Isbell and The National Committee on Soils and Terrain, 2016).

During dry periods or following artificial drainage, the upper boundary of the hypersulfidic material is exposed to aerobic conditions and generates sulfuric acid and (through subsequent reactions) a range of secondary reaction products (e.g. sulfide gas and sulfate minerals) in a process referred to as sulfuricisation (Fanning et al., 2017). The mechanism and controlling factors of RIS oxidation are beyond the scope of this brief review. However, the literature supports the general conclusion that the oxidation of RIS in soil is microbially mediated (e.g. by *Acidithiobacillus spp.*) (Baker and Banfield, 2003; Hart, 1959; Ivarson et al., 1982). Therefore, factors controlling RIS reactivity as well as microbial activity are likely to greatly influence the rate of RIS oxidation in soils. Key factors include: pH, temperature, salinity, soil moisture, oxygen and organic matter availability, and RIS particle size and crystallinity (Rickard, 1973; van Breemen, 1973).

The oxidation of RIS produces a strongly acidic solution that is often immediately supersaturated with respect to a myriad of iron sulfates (Nordstrom, 1982). van Breemen (1988) suggests that short-lived hydrated ferrous sulfates, such as melanterite ($Fe^{2+}(H_2O)_6SO_4.H_2O$) initially form and then sequentially dehydrate to yield minerals such as rozenite ($Fe^{2+}SO_4.4H_2O$) and szomolnokite ($Fe^{2+}SO_4.H_2O$). As oxidising conditions prevail, so does the concentration of dissolved Fe^{3+}, resulting in mixtures of less soluble Al^{3+} and Fe^{2+}/Fe^{3+} sulfates (Bigham and Nordstrom, 2000; Fitzpatrick and Shand, 2008). Examples include alunogen ($Al_2(SO_4)_3.17H_2O$), copiapite ($Fe^{2+}Fe^{3+}{}_4(SO_4)_6(OH)_2.20H_2O$), jarosite and schwertmannite ($Fe^{3+}{}_{16}(OH,SO_4)_{12\text{-}13}O_{16}.10\text{-}12H_2O$). The groundwater, soil porewater and soil minerals (e.g. phyllosilicates, metal (oxyhydr)oxides, carbonates) provide a range of elements that influence the speciation of sulfate minerals following RIS oxidation. However, jarosite is by far the most common in sulfuric material, and is ubiquitously observed as pale yellow ped coatings and pore fillings (Fanning et al., 2017; Pons, 1973).

Jarosite has been observed in sulfuric material in: coastal ASS in South Australia (Fig. 2) (Fitzpatrick et al., 2008; Poch et al., 2009; Thomas, 2010); Victoria (Whitworth et al., 2020a, b); in the drained hypersulfidic material in the estuarine floodplain of the Anglesea River (Victoria) described by Fitzpatrick et al. (2007) and Yau et al. (2016); New South Wales (Johnston et al., 2009a; Vithana et al., 2013); Queensland (Johnston et al., 2009b; 2010; 2011; Hicks et al., 1999, 2009); and Western Australia (Appleyard et al., 2006). Similarly, jarosite has been identified in sulfuric material in the following inland areas of: (i) South Australian major lake and river systems during the Millennium drought (especially in the Lower Lakes), Currency Creek and Finniss River regions (Fitzpatrick and Shand, 2008; Fitzpatrick et al. 2010, 2018) and irrigation areas along the River Murray (Fitzpatrick et al., 2017); (ii) Victorian river systems during the Millennium drought along the Lower Loddon River and Burnt Creek regions (Thomas et al., 2009); (iii) Western Australian wheat belt region (Fitzpatrick et al., 2008); and (iv) Norfolk Island (Fitzpatrick et al., 2020).

If the water table level continues to fall, then over time both the sulfuric and hypersulfidic material may translocate down the soil profile as: the upper boundary of the hypersulfidic material oxidises to produce sulfuric material (thereby adding to the lower boundary of the sulfuric stratum); and as the upper boundary of the sulfuric material weathers to produce post-active acid sulfate soil material that is rich in ferric (oxyhydr)oxides such as ferrihydrite ($Fe_{10}O_{14}(OH)_2$), goethite (α-FeOOH), and hematite (Fe_2O_3) (Harmsen and van Breemen, 1975; van Breemen, 1973). Brown (1971) investigated the stability of jarosite and goethite, and concluded that the hydrolysis of jarosite to goethite is thermodynamically inevitable, but extremely sluggish under standard conditions. Therefore, under aerobic soil conditions jarosite should tend to slowly alter to goethite. Eventually the surface soil may ripen – a process

described by Dent (1986) as the physical, chemical and biological processes by which ASS develops into freely drained or dryland soils, which are referred to as a post-active ASS by Fanning et al. (2017).

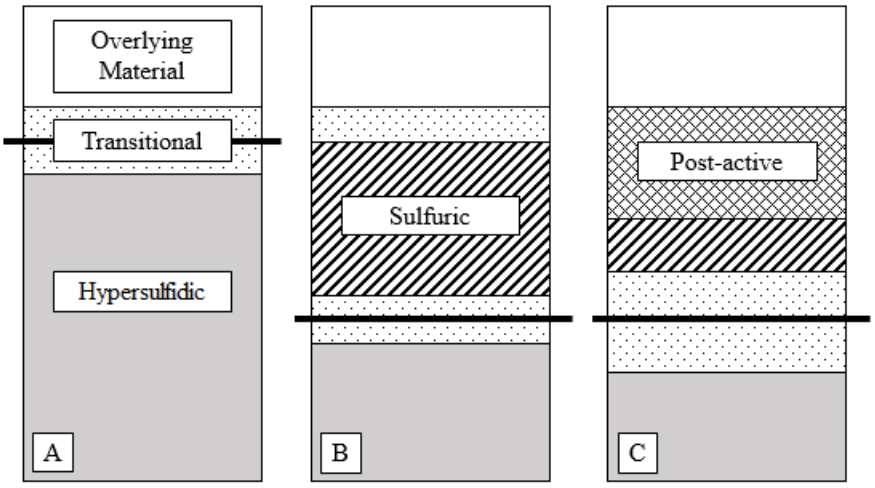

Figure 1. Simplified conceptual model showing the evolution of soil following the exposure of hypersulfidic material to aerobic conditions (adapted from van Breemen (1988)). (A) Initially, sulfidic material lies below the average water table level (bold, solid line). The vertical fluctuation of the water table level produces a transitional, redoximorphic zone. (B) As the average water table level falls (e.g. during a drought), the hypersulfidic material oxidises to produce sulfuric material. (C) Over time and many cycles of wetting and drying, the transitional zone between the hypersulfidic and sulfuric material widens. Moreover, the upper boundary of the sulfuric material weathers and ripens to produce post-active ASS material.

The general conceptual model shown in Figure 1 is congruent with field observations of ASS in Mediterranean environments in both coastal areas (e.g. Fitzpatrick et al., 2008; Poch et al., 2009; Thomas, 2010; Fig. 2) and inland areas (Fitzpatrick et al., 2012; Fitzpatrick and Shand, 2008; Fitzpatrick et al. 2017) of South Australia. However, this model is not universal. In wet tropical regions (e.g. Thailand), soils are often periodically submerged and drained during wet and dry seasons, respectively. Such drastic changes can have different effects on the formation and weathering of sulfidic and sulfuric material. For example, 7 months of complete saturation did not appear to affect the abundance of jarosite in a deeply-developed, matured ASS in Thailand (van Breemen, 1976, 1988). Conversely, in a nearby region, the bulk of jarosite in a younger, shallower ASS appeared to have converted back to sulfidic material within a few months of waterlogging. Moreover, sulfuric material with a high organic matter content was observed without jarosite, despite acidity and sulfate concentrations favourable to jarosite formation (van Breemen, 1976, 1988).

The formation of jarosite may be circumvented under certain conditions. For example, hematite pseudomorphs of pyrite in carbonate-rich soils suggest that the immediate neutralisation of acidity generated by RIS oxidation inhibited jarosite formation (Miedema et al., 1987). Additionally, Fitzpatrick (2004) reported that intense bushfires on recently exposed sulfidic soils converted pyrite to maghemite (Fe_2O_3).

Therefore, the formation and weathering of jarosite in soils is site specific and strongly influenced by a range of factors such as: pH, abundance of acidic and alkaline materials, soil structure (e.g. occurrence of aerobic cracks and pores), wetting and drying regime (and therefore rainfall and topography) and organic matter content.

Figure 2. Soil profile from Gillman, South Australia, showing conceptual strata as described in Fig. 1. Underlying hypersulfidic material is not shown, but occurs below the water table (at ca. 2 m depth). Image courtesy of R.W. Fitzpatrick.

3. Jarosite as an environmental risk

Products of RIS oxidation – particularly jarosite – play a key role in the regulation of actual and potential contaminants in soil and water. Ferrous sulfates such as melanterite (Eq. 1) and coquimbite do not generate or consume acidity, but may indirectly affect acidity by influencing the bisulfate-sulfate equilibrium (i.e. $HSO_4^- \rightleftharpoons SO_4^{2-} + H$) (Nordstrom et al., 2000).

$$Fe^{2+} + SO_4^{2-} + 7H_2O \rightarrow FeSO_4.7H_2O \ldots (1)$$

However, ferrous sulfates are generally short-lived due to their high solubility. Consequently, Fe^{2+} tends to quickly oxidise – a process that consumes acidity (Eq. 2) (Nordstrom et al., 2000; van Breemen, 1973).

$$Fe^{2+} + 0.25O_2 + H^+ \rightarrow Fe^{3+} + 0.5H_2O \ldots (2)$$

Hydronium-bearing ferric sulfate minerals such as rhomboclase ($(H_3O)Fe(SO_4)_2.3H_2O$) and hydronium jarosite may also directly influence acidity through the release or uptake of H_3O^+ (Eq. 3, 4) (Nordstrom et al., 2000).

$$Fe^{3+} + 2SO_4^{2-} + H^+ + 4H_2O \rightarrow (H_3O)Fe(SO_4)_2.3H_2O \ldots (3)$$
$$KFe_3(SO_4)_2(OH)_6 + H_3O^+ \rightarrow (H_3O)Fe_3(SO_4)_2(OH)_6 \ldots (4)$$

However, jarosite has a strong preference for K^+ (and Na^+) over H_3O^+ (Brophy and Sheridan, 1965; Brown, 1970; Desborough et al., 2010; Dutrizac and Jambor, 2000). Due to the prevalence of K^+ in most soils, it is unlikely that the uptake of hydronium by jarosite plays a meaningful role in the regulation of acidity in ASS.

The precipitation of minerals such as jarosite (Eq. 5) and copiapite generate acidity.

$$3Fe^{3+} + 2SO_4^{2-} + K^+ + 6H_2O \rightarrow KFe_3(SO_4)_2(OH)_6 + 6H^+ \ldots (5)$$

However, it can be argued that jarosite precipitation is relatively beneficial. Firstly, Fe^{3+} catalyses pyrite oxidation (Singer and Stumm, 1970). Therefore, the immediate precipitation of jarosite may help regulate pyrite oxidation and acid generation. Moreover, the immediate precipitation of jarosite (Eq. 6) theoretically generates less acidity than the complete oxidation of pyrite and hydrolysis of Fe^{3+} (Eq. 7) (van Breemen, 1973).

$FeS_2 + 15/4\ O_2 + 5/2\ H_2O + 1/3\ K^+ \rightarrow 1/3$ jarosite $+ 4/3\ SO_4^{2-} + 3H^+$ … (6)
$FeS_2 + 15/4\ O_2 + 7/2\ H_2O \rightarrow Fe(OH)_3 + 2SO_4^{2-} + 4H^+$ … (7)

However, the precipitation of jarosite has, in a sense, only delayed Fe^{3+} hydrolysis. Although jarosite is relatively insoluble, under normal supergene weathering conditions it will slowly hydrolyse and generate acidity (Eq. 8). As such, jarosite represents a source of potential acidity.

$KFe_3(SO_4)_2(OH)_6 + 3H_2O \rightarrow 3Fe(OH)_3 + 2SO_4^{2-} + K^+ + 3H^+$… (8)

Acid Base Accounting (ABA), namely, the practice of quantifying sources of acidity and alkalinity, is a critical aspect of managing ASS. The ABA system employed in Australian ASS guidance (e.g. Sullivan et al. (2018)) describe three operationally defined pools of acidity (mol H^+ per tonne dry soil). Potential Sulfidic Acidity (PSA) is a measure of the RIS that may oxidise to produce sulfuric acid. Titratable Actual Acidity (TAA) is a measure of soluble and exchangeable acidity. Retained Acidity is a measure of sparingly soluble, Al^{3+}- and Fe^{3+}-rich sulfates such as jarosite and schwertmannite. These pools of acidity are tallied against the Acid Neutralising Capacity (ANC) of the soil sample to calculate the net acidity.

In practice, the net acidity is used to prescribe liming rates for soils that have, or may be affected by RIS oxidation. As such, ABA often feeds into environmental risk/impact assessments and management plans, which play a key role in planning and development. However, no ABA system is perfect. Moreover, consistently determining the accurate jarosite content in soil has proven difficult. For example, Vithana et al. (2013) spiked soil samples with known amounts of jarosite, and found that the measured RA only accounted for 50-60% of the initial jarosite spike. Although it is recommended that RA values be doubled to compensate for this underestimation, it is possible that the risk of jarosite to soil and water quality may be frequently underestimated. Moreover, jarosite may also act as an important source and sink for trace elements. Welch et al. (2008) reported that over the course of around 12 days, 200 mg of pedogenic jarosite (in 100 mL of solution) released 10-30 mg/L of Mn, Sr and Zn, and 2-5 mg/L of Co, Cu, Ni and Rb. These are all above the ANZECC default trigger values for freshwater and marine ecosystems (ANZECC, 2000).

4. Measuring and predicting jarosite solubility

Multiple investigations of jarosite dissolution are described in the literature, however, they vary in methodology and results (Table 1). Precipitating jarosite is often employed to remove excess iron and sulfate during the extraction and purification of divalent metals from iron-rich ores (e.g. sphalerite, $(Zn,Fe)S_2$). Consequently, much of the information concerning jarosite chemistry stems from hydrometallurgical studies that aim to improve the jarosite precipitation process (Das et al., 1996; Dutrizac and Jambor, 2000). However, such investigations are conducted at high temperatures (e.g. 80-100℃) and have limited utility in most environmental contexts. The studies listed in Table 1 are not exhaustive, but are those which focus on jarosite dissolution under conditions more congruent with supergene environments. The results reported by these authors are not in agreement. Therefore, here we review the literature to understand trends and anomalies related to the measurement of jarosite solubility.

Table 1. Summary of the synthetic and natural jarosite solubility data from key instigations in the literature, expressed in terms of the solubility constant K_{sp} and rate of dissolution (R = mol/m^{2}s). *Dissolution rates calculated by Welch et al. (2008) using data from Smith et al. (2006). **Mean dissolution rate from tests using flowthrough reactors and unbuffered eluant (final pH 4.5-5).

Solubility ($log_{10}K_{sp}$)	**Jarosite Sample**	**Source**
-7.5	synthetic	Brown (1970)
-98.56	natural	Vlek et al. (1974)
-10.39 to -6.92	natural	Alpers et al. (1989)
-11.0	synthetic	Baron and Palmer (1996)
-11.3	synthetic	Smith et al. (2006)
Dissolution Rate ($log_{10}R$)		
-6.83 to -6.36	synthetic	Gasharova et al. (2005)
*-10.1 (pH 2) *-11.8 (pH 8)	synthetic	Smith et al. (2006)
-11.8 to -11.1 (short-term) -12.2 to -11.8 (long-term)	natural	Welch et al. (2008)
-9.8 to -6.5 (pH 1-11)	synthetic	Madden et al. (2012)
-9.5 to -6.5 (pH 1-10)	synthetic	Zahrai et al. (2013)
**-11.24 (unbuffered)	synthetic	Dixon et al. (2015)

4.1. Solubility product, ion activity product and saturation index

The solubility product (K_{sp}) is commonly measured and reported in the literature, as – in conjunction with the ion activity product (IAP) – it can be used to predict if a mineral will precipitate or dissolve under a given set of conditions (Ball and Nordstrom, 1991). The solubility product is the equilibrium constant (K) of a dissolution reaction, and may be described as either the stoichiometric (K_{sp}) or thermodynamic ($K°_{sp}$) solubility product. For example, for $A_aB_b \leftrightarrow aA + bB$: $K_{sp} = [A]^a[B]^b$, and $K°_{sp} = \{A\}^a\{B\}^b$ (where square and curly brackets denote the ionic concentrations and activities of A and B, respectively). In solutions with high ionic strength (e.g. saline ASS), the difference between the ionic concentrations and activities may be significant; and the latter becomes a more accurate representation of the solution chemistry (Christian et al., 2014). The IAP does not assume equilibrium (i.e. IAP = $\{A\}^a\{B\}^b$, where IAP $\neq K°_{sp}$). The saturation index (SI) is equal to $log_{10}(IAP/K_{sp})$, and indicates if a solution is saturated (SI = 0), undersaturated (SI < 0) or supersaturated (SI > 0) with respect to a given phase. Therefore, SI is frequently used to predict the behaviour of a mineral phase under certain conditions. However, K_{sp} values reported in the literature vary by several orders of magnitude – suggesting that accurately estimating the solubility of sparingly-soluble minerals is difficult even under relatively controlled conditions.

Brown (1970) investigated the properties of synthetic K-H_3O jarosite that was precipitated at 1 atm and 25 ℃. For the dissolution experiments, synthesised jarosite were added to a H_2SO_4 solution and stirred continually for 6 months at 1 atm and 25℃. The initial and final pH and E_h were measured, along with the concentration of Fe and sulfate. Ionic activities were determined using pH, E_h, ionic molalities, and from activity coefficients (γ) derived from multiple sources. Brown (1970) reported a $log_{10}K_{sp}$ value of -7.5.

Vlek et al. (1974) employed a novel, complexometric method, described by Norvell and Lindsay (1969), to investigate the solubility of several natural ferric hydroxides samples, including a natural jarosite sample. According to this method, the mineral sample is added to

a buffered solution containing EDTA and a 'competing ion' (Ca^{2+} or Zn^{2+}). The aim of the method is to use known chelated Fe^{3+}/Ca^{2+} (or Fe^{3+}/Zn^{2+}) molar ratios to calculate the concentration of complexed Fe^{3+}, in order to determine the formation constant (K_f, i.e. the equilibrium constant of the complexation reaction). K_{sp} was then calculated as the inverse of K_f. As outlined by Vlek et al. (1974), this method was susceptible to multiple sources of error, including: the heavy reliance upon data from other sources – primarily Sillen and Martell (1964); the assumptions made to calculate the Fe^{3+} concentration from the Fe and Ca (or Zn) complexes; and the calculation of the Fe^{3+} activity coefficient using estimations of the solution's ionic strength. Consequently, the chemical constants reported in this study are not recommended by more contemporary reviews such as Dutrizac and Jambor (2000). However, Vlek et al. (1974) was included in this review as: it is often cited in older literature (e.g. van Breemen, 1976), provides a novel approach, and is one of the few solubility studies conducted using jarosite collected from an ASS.

Alpers et al. (1989) conducted a study on a set of mine water samples in which jarosite had precipitated at some point after their collection 15 years earlier. WATEQ4F (a chemical equilibrium model) was used to calculate ionic activates based on measured concentrations of K^+, Fe^{3+} and SO_4^{2-}. Reported $\log_{10}K_{sp}$ values ranged from -10.39 to -6.92, with an average of -9.34.

Baron and Palmer (1996) investigated the solubility of synthetic jarosite between temperatures and pH values of 4-30℃ and 1.5-3, respectively. The dissolution reaction was assumed to have reached equilibrium after 80-125 days, that is, when the change in K concentration was less than $\pm$5%. The pH and total Fe, K and sulfate were measured at equilibrium, and used to calculate ionic activities using MINTEQ (a chemical equilibrium model). For comparison, the activities were calculated using the Davies and the extended Deybe-Huckel equation, and the difference was found to be negligible. The $\log_{10}K_{sp}$ of -11.0 was calculated from the measured pH and estimated ionic activities. The methods described by Baron and Palmer (1996) made fewer assumptions than those described by Brown (1970). Smith et al. (2006) conducted a similar investigation following the methods described by Baron and Palmer (1996), and reported a $\log_{10}K°_{sp}$ value of -11.3.

4.2. Dissolution rate

For the dissolution reaction $AB \leftrightarrow A + B$, the dissolution rate (R) is a measure of the loss of AB or gain of A or B over time; and is conventionally expressed as moles of solute dissolved per second, per gram or m^2 of the solute (mol/gs, mol/m^2s). The dissolution rate can be used estimate the longevity of a mineral phase under a given set of conditions. Therefore, accurately describing both the solubility and dissolution rate of a jarosite under a range of physicochemical conditions is vital for accurately predicting the behaviour of jarosite in the environment. However, Table 1 demonstrates the disparity between the few studies that have focused on the dissolution rate of jarosite.

Gasharova et al. (2005) employed atomic force microscopy (AFM) to conduct detailed micromorphological characterisations of synthetic K and H_3O-jarosite samples. AFM was employed to measure the change of jarosite volume over time, which was used to calculate the dissolution rate. Observed K- and H_3O-jarosite retreat rates of 1.37 and 4.25 nm/min corresponded to $\log_{10}R$ values of -6.84 and -6.36, respectively. Gasharova et al. (2005) concluded that the presence of structural hydronium accelerates jarosite dissolution.

Madden et al. (2012) investigated the dissolution of synthetic jarosite at initial pH values of 1-10, and temperatures of 3-50℃, and reported $\log_{10}R$ values ranging from ca. -9.8 to -6.5. Moreover, the rate of jarosite dissolution was found to be pH dependent, whereby the rate increased with increasing H^+ or OH^+ activity. Madden et al. (2012) proposed that at pH < 3.5, jarosite consumes H^+ and produces aqueous Fe^{3+} species. Consequently, aqueous ferric sulfate complexes should dominate at low pH values. At pH > 3.5, jarosite consumes OH^- and solid reaction products are formed – primarily ferrihydrite and maghemite. Zahrai et al. (2013) conducted similar experiments to Madden et al. (2012) in order to determine the solubility of Na jarosite at temperatures of 4, 20 and 50℃, and at pH values of 1, 2 8 and 10. Zahrai et al. (2013) reported $\log_{10}R$ values between ca. -9.5 and -6.5.

Welch et al. (2008) investigated the dissolution of jarosite extracted from an ASS. Natural jarosite samples from sulfuric material were added to six different solutions: (1) deionised water; (2) 0.1 mM HCl (~pH 4); (3) 1 mM HCl (~pH 3); (4) 0.05 mM H_2SO_4 (~pH 4); (5) 0.5 mM H_2SO_4 (~pH 3); (6) 1 mM oxalic acid (~pH 3). Oxalic acid was employed to simulate the chelating effect of organic acids. Aliquots were taken periodically for 12 days with the final sample taken after 1 year. Dissolution was relatively rapid over the first few hours of the experiments and decreased over time. Conversely, in the oxalate treatment, dissolution proceeded at a relatively regular rate over the duration of the experiment. Short-term (<12 days) experiments yielded $\log_{10}R$ values between -11.76 and -11.12. Overall dissolution rates during long-term (12-350 days) experiments were slower (i.e. $\log_{10}R$ values between -12.2 and -11.8). Moreover, there was a gradual shift from congruent to incongruent dissolution over time.

It has been suggested that variation in jarosite solubility be due to the nature of the sample, namely, whether the sample is synthetic or natural (Desborough et al., 2006; Dutrizac and Jambor, 2000). Generally speaking, the more crystalline and stoichiometrically ideal a mineral sample is, the less vulnerable it is to chemical attack and dissolution (Steefel, 2008). Both natural and synthetic jarosite tend to be inherently variable in terms of stoichiometry and crystallinity. Swayze et al. (2008) notes that jarosite formed in low temperature (< 100℃) environments tends to be non-stoichiometric, but may approach ideal stoichiometry through desiccation and recrystallization. Therefore, the common practice of drying synthetic jarosite at ≥ 100℃ or heating it at 200℃ to remove excess structural water (Baron and Palmer, 1996; Dixon et al., 2015; Gasharova et al., 2005; Madden et al., 2012; Smith et al., 2006) may amend site deficiencies and structural deformities. This logic implies that synthetic jarosite should be more ideal and therefore less soluble. However, the solubility data in Table 1 indicates that synthetic jarosite tends to be more soluble than natural jarosite. Therefore, although intrinsic differences between synthetic and natural jarosite may contribute to differences in solubility, without a comprehensive comparison, it is difficult to make any sound conclusions.

It is more likely that variation in the reported solubility of jarosite (Table 1) stems from variation in experimental design. For example, Smith et al. (2006) based their methods on those described by Baron and Palmer (1996) and both reported similar jarosite K_{sp} values. This is in spite of the considerable difference in jarosite morphology – i.e. the jarosite synthesised by Smith et al. (2006) was highly irregular and globular, while the jarosite synthesised by Baron and Palmer (1996) appears to be more crystalline. Similarly, Madden et al. (2012) and Zahrai et al. (2013) conducted similar experiments and reported relatively similar dissolution rates – e.g. compared to Welch et al. (2008). Therefore, the solubility data reported in Table 1 is somewhat operationally defined. Consequently, this data could be utilised to help predict the behaviour of jarosite-rich sulfuric material in the environment. However, due to the high

variance of this solubility data, such predictions would also be subject to a considerable degree of variance.

Jarosite dissolution has typically been tested using batch reactors (Madden et al., 2012; Welch et al., 2008). Batch reactors are useful tools for conducting simple tests in closed systems, but have limited utility in predicting complex geochemical reactions in open systems (Brantley and Conrad, 2008; Steefel et al., 2005). Flowthrough reactors (e.g. continuously stirred tank reactors (CSTR) and plug-flow reactors (PFR)) allow for more precise control over experimental parameters (e.g. solution residence time and chemistry). This enables more complex tests, and in turn facilitates more accurate upscaling of results (Brantley and Conrad, 2008; Steefel, 2008). PFR (e.g. packed-bed and column reactors), in which solution moves through a porous medium, more realistically mimics the solid-fluid phase interactions that occur in soil systems, and are therefore preferable over CTSR when investigating the behaviour of pedological jarosite. As a general trend, jarosite dissolution tends to be faster where dissolution experiments were conducted using batch reactors when compared to than those conducted with flowthrough reactors. Dixon et al. (2015) employed a flowthrough reactor to investigate the effect of flowrate on the dissolution chemistry of synthetic jarosite. The results indicate that the dissolution rate is largely unaffected by the flowrate. However, the study was conducted with a view to better understand jarosite longevity on Mars. Consequently, dissolution was measured using NaCl and $CaCl_2$ brines. Therefore, the results may have limited utility for predicting the behaviour of natural jarosite under constant flow conditions in soil.

Therefore, investigating the dissolution kinetics of pedogenic jarosite using a flowthrough reactor may help us to better predict and thus mitigate the risks to soil and water quality associated with jarosite dissolution.

5. Jarosite treatment strategies

Jarosite not only forms in soil, but is also associated with sulfidic ore, acid mine drainage (AMD), and is a common waste product of many metal refineries. Therefore, identifying and mitigating the environmental risk associated with jarosite has received attention in a number of fields.

As a mining waste, jarosite is produced to remove contaminants (e.g. As, Cr, Fe, SO_4) from acidic ore leachates (Dutrizac and Jambor, 2000). The recovery of iron from jarosite is uneconomical when compared to standard iron ores (Hage and Schuiling, 2000; Ismael and Carvalho, 2003). Moreover, although the use of jarosite waste (treated and untreated) as a building material has been explored, it does not appear to have been popularised (Gupta and Sachdeva, 2019; Sinha et al., 2012; Sinha et al., 2018). Consequently, jarosite waste is typically stored in conventional tailing impoundments, which invariably represent an extreme environmental risk (Hage and Schuiling, 2000). Therefore, considerable research efforts have gone towards devising methods of stabilising jarosite waste.

Alkaline material such as Portland cement (primarily $(CaO)_3.SiO_2$) or alkaline fly ash (primarily SiO_2, Al_2O_3 and CaO) has been shown to react with jarosite to form gypsum and a range of poorly-crystalline Ca-Al-Fe (oxyhydr)oxides and Ca-Al-Fe silicate sulfate-hydrates (Chen and Dutrizac, 2000; Chen and Dutrizac, 2001; Ding et al., 2002). These minerals help to cement the loose waste material into a more coherent solid with a lower overall hydraulic conductivity and higher resistance to chemical and physical weathering. As such, it is hoped that comingling jarosite waste with alkaline wastes will encourage the formation of self-sealing layers that passivate unreacted jarosite, immobilise hazardous elements and lower the overall

environmental risk of the tailings. However, the literature does not appear to describe the popularity and efficacy of such treatments outside of the laboratory. Moreover, while alkaline treatments are expected to have a similar passivating effect on jarosite in soil – this has not been directly investigated.

There are a range of ASS management and remediation strategies, which, for simplicity, are here broadly grouped as symptom- and source-oriented treatments. Symptom-oriented treatments aim to amend actual hazards such as acidic effluents produced during sulfuricisation. This is typically achieved through liming. However, liming soils with sulfuric material is expensive and often ineffective due to armouring: where lime reacts with acidic, metalliferous solutions to form a passivating coating of gypsum and ferric (oxyhydr)oxide (Hammarstrom et al., 2003). Conversely, source-oriented treatments aim to remove or prevent the actualisation of potential hazards such as pyrite oxidation. This generally involves ensuring that water levels remain or are returned above hypersulfidic materials; and may involve large scale earthworks projects (e.g. constructing levies and floodgates etc.). Maintaining adequately high water levels can be extremely challenging, especially in drought prone regions such as South Australia. Moreover, reflooding soils with sulfuric material can greatly increase the mobility of acidity and trace metals (Mosley et al., 2014d). Therefore, a once-off treatment designed to remove or passivate jarosite and immobilise other contaminants without adversely affecting soil and water quality, and overall land use opportunities, would be ideal.

Phosphate-based treatments have been used to remediate AMD-affected systems, and could potentially be used to treat ASS with jarosite-rich sulfuric material. Free Fe^{3+} greatly accelerates pyrite oxidation (Singer and Stumm, 1970). Adding phosphate (e.g. as apatite ($Ca_5(PO_4)_3(Cl/F/OH)$) should limit Fe^{3+} availability by complexing Fe^{2+} and by precipitating ferric phosphate minerals such as strengite ($FePO_4.2H_2O$) (Spotts and Dollhopf, 1992; Stiller et al., 1989). Additionally, the formation of ferric phosphate coatings over pyrite may also mitigate pyrite oxidation through surface passivation (Nyavor and Egiebor, 1995). Recently, Gao et al. (2020) investigated the effect of phosphate addition (as $NaH_2PO_4.H_2O$) on the biologically mediated reduction dissolution of (synthetic) jarosite. Relatively low phosphate concentrations (e.g. 0.02 g/L) supported the growth sulfate reducing bacteria (SRB), and therefore encouraged the reductive dissolution of jarosite. However, jarosite dissolution was lower at higher phosphate concentrations (e.g. 0.5 g/L). This effect was attributed to the sorption of phosphate by jarosite (up to 0.28 mg P per g jarosite), which may have shielded Fe^{3+} against SRB. Additionally, phosphate was shown to immobilise dissolved Fe^{2+} through the precipitation of vivianite ($Fe_3(PO_4)_2.8H_2O$). Therefore, phosphate treatments could possibly be utilized to stabilise jarosite and mitigate the formation of sulfidic material in subaqueous sulfuric material. However, as excess phosphate can greatly damage aquatic ecosystems (e.g. via eutrophication), more work is required to determine the efficacy, practicality, and potential risks of phosphate-based treatments with respect to ASS.

6. Conclusion

The dissolution of jarosite may have considerable influence over long-term changes in soil and water quality, and in many cases is likely responsible for impeding the remediation of ASS. Therefore, understanding the rate, controlling factors and effects of jarosite dissolution under a range of physicochemical conditions is a critical aspect of managing ASS.

The reported solubility of jarosite, both in terms of its solubility product and dissolution rate, ranges over several orders of magnitude. This variation likely stems from differences in

experimental design, rather than the nature of the jarosite sample. Due to differences in the experimental framework and design, it is difficult to recommend a value to represent the dissolution rate of jarosite-rich sulfuric material. Welch et al. (2008) provides the only dissolution rate of a natural jarosite sample, and reported long-term $\log_{10}R$ values between -12.2 and -11.8. However, these experiments employed a batch approach. Consequently, one of the principal objectives of this research is to build on the conclusions of Welch et al. (2008) to more accurately predict the long-term dissolution rate of jarosite-rich sulfuric material under a wider range of environmental conditions.

By exploring the dissolution kinetics of pedogenic jarosite and its potential effects on soil and water chemistry, I hope to develop more effective remediation strategies for ASS with jarosite-rich ASS. Jarosite mining waste is reported to be treated with alkaline material in order to passivate jarosite, immobilise trace elements and increase weather resistance through the formation of protective coatings. The passivation of jarosite in soil by applying conventional liming agents or alternative phosphate-based treatments, however, has not been systematically explored. Therefore, I aim to examine the validity of passivation-based treatments that encourage the alteration of jarosite to more stable ferric (oxyhydr)oxides or phosphates.

References

Ahern, C.R., Mcelnea, A.E., Sullivan, L.A., 2004. Acid sulfate soils laboratory methods guidelines, Queensland Department of Natural Resources, Mines and Energy, Indooroopily, Queensland, Australia.

Alpers, C.N., Nordstrom, D., Ball, J.W., 1989. Solubility of jarosite solid solutions precipitated from acid mine waters, Iron Mountain, California, U.S.A. Iron Mountain, California, U.S.A. Sciences Géologiques, bulletins et mémoires: 281-298.

Anzecc, 2000. Australian and New Zealand guidelines for fresh and marine water quality, aquatic ecosystems - rationale and background information Australian Water Association.

Appleyard, S., Angeloni, J., Watkins, R., 2006. Arsenic-rich groundwater in an urban area experiencing drought and increasing population density, Perth, Australia. Applied geochemistry, 21(1): 83-97.

Baker, B.J., Banfield, J.F., 2003. Microbial communities in acid mine drainage. FEMS Microbiology Ecology, 44(2): 139-152.

Ball, J.W., Nordstrom, D.K., 1991. WATEQ4F - User's manual with revised thermodynamic data base and test cases for calculating speciation of major, trace and redox elements in natural waters, Menlo Park, Calif.

Baron, D., Palmer, C.D., 1996. Solubility of jarosite at 4–35 °C. Geochimica et Cosmochimica Acta, 60(2): 185-195. https://doi.org/10.1016/0016-7037(95)00392-4.

Bigham, J.M., Nordstrom, D.K., 2000. Iron and aluminum hydroxysulfates from acid sulfate waters. Reviews in Mineralogy and Geochemistry, 40(1): 351-403.

Brantley, S.L., Conrad, C.F., 2008. Analysis of rates of geochemical reactions. In: Brantley, S.L., Kubicki, J.D., White, A.F. (Eds.), Kinetics of water-rock interaction. Springer New York, New York, NY, pp. 1-37.

Brophy, G.P., Sheridan, M.F., 1965. Sulfate studies IV: the jarosite-natrojarosite-hydronium jarosite solid solution series. American Mineralogist, 50(10): 1595-1607. ¯_(ツ)_/¯

Brown, J.B., 1970. A chemical study of some synthetic potassium-hydronium jarosites. The Canadian Mineralogist, 10(4): 696-703.

Brown, J.B., 1971. Jarosite-geoethite stabilities at 25°C, 1 ATM. Mineralium Deposita, 6(3): 245-252. https://doi.org/10.1007/bf00208032.

Chen, T., Dutrizac, J., 2000. A mineralogical study of Jarofix products for the stabilization of jarosite residues for disposal. Lead-Zinc 2000: 917-934.

Chen, T., Dutrizac, J., 2001. Jarofix: Addressing iron disposal in the zinc industry. JOM, 53(12): 32-35. https://doi.org/10.1007/s11837-001-0010-2.

Christian, G.D., Dasgupta, P.K., Schug, K.A., 2014. Analytical chemistry. John Wiley and Sons, Inc., Hoboken, N.J.

Das, G.K., Acharya, S., Anand, S., Das, R.P., 1996. Jarosites: a review. Mineral Processing and Extractive Metallurgy Review, 16(3): 185-210.

Dent, D., 1986. Acid sulphate soils: a baseline for research and development. International Institute for Land Reclamation and Improvement Wageningen, The Netherlands, 204 pp.

Desborough, G.A., Smith, K.S., Lowers, H.A., Swayze, G.A., Hammarstrom, J.M., Diehl, S.F., Driscoll, R.L., Leinz, R.W., 2006. The use of synthetic jarosite as an analog for natural jarosite, Proceedings of the Seventh International Conference on Acid Rock Drainage. St. Louis Missouri, pp. 458-475.

Desborough, G.A., Smith, K.S., Lowers, H.A., Swayze, G.A., Hammarstrom, J.M., Diehl, S.F., Leinz, R.W., Driscoll, R.L., 2010. Mineralogical and chemical characteristics of some natural jarosites. Geochimica et Cosmochimica Acta, 74(3): 1041-1056. https://doi.org/10.1016/j.gca.2009.11.006.

Ding, M., Schuiling, R., Van Der Sloot, H., 2002. Self-sealing isolation and immobilization: a geochemical approach to solve the environmental problem of waste acidic jarosite. Applied Geochemistry, 17(2): 93-103. https://doi.org/10.1016/S0883-2927(01)00099-3.

Dixon, E.M., Elwood Madden, A.S., Hausrath, E.M., Elwood Madden, M.E., 2015. Assessing hydrodynamic effects on jarosite dissolution rates, reaction products, and preservation on Mars. Journal of Geophysical Research: Planets, 120(4): 625-642.

Dutrizac, J.E., Jambor, J.L., 2000. Jarosites and their application in hydrometallurgy. Reviews in Mineralogy and Geochemistry, 40(1): 405-452. https://doi.org/10.2138/rmg.2000.40.8.

Fanning, D.S., Rabenhorst, M.C., Fitzpatrick, R.W., 2017. Historical developments in the understanding of acid sulfate soils. Geoderma, 308: 191-206. https://doi.org/10.1016/j.geoderma.2017.07.006.

Fitzpatrick, R., Degens, B., Baker, A., Raven, M., Shand, P., Smith, M., Rogers, S., George, R., 2008. Avon Basin, WA Wheatbelt: Acid sulfate soils and salt efflorescences in open drains and receiving environments, Inland acid sulfate soil systems across Australia. CRC LEME Open File Report No. 249, Perth, Australia, pp. 189-204.

Fitzpatrick, R., Grealish, G., Shand, P., Creeper, N., 2011. Monitoring and assessment of reflooded acid sulfate soil materials in Currency Creek and Finniss River Region, South Australia. Client Report R-325-8-6. Prepared for the South Australia Department of Environment and Natural Resources (DENR). CSIRO, Adelaide.

Fitzpatrick, R., Hicks, W., Marvanek, S., Dahlhaus, P., Cox, J., 2007. Scoping study of coastal and inland acid sulfate soil in the Corangamite CMA. Land and Water Science Report, 28(07). CSIRO, Adelaide.

Fitzpatrick, R., Thomas, B.P., Merry, R., Marvanek, S., 2012. A field guide to estuarine soil-landscapes in Barker Inlet, South Australia. Acid Sulfate Soils Centre (ASSC), The University of Adelaide.

Fitzpatrick, R.W., 2004. Changes in soil and water characteristics of natural, drained and re-flooded soils in the Mesopotamian marshlands: Implications for land management planning. CSIRO, Australia

Fitzpatrick, R.W., Grealish, G., Chappell, A., Marvanek, S., Shand, P., 2010. Spatial variability of subaqueous and terrestrial acid sulfate soils and their properties, for the Lower Lakes, South Australia, CSIRO Sustainable Agriculture National Research Flagship Client Report R-689-1-15 Australia. https://doi.org/10.4225/08/5852da2932c66.

Fitzpatrick, R.W., Philip, S., Wilson, P., Raven, M.D., Self, P., 2020. Peaty acid sulfate soils on Norfolk Island: Soil-landscape evolution models of wetlands during severe drought. Geoderma (In Press).

Fitzpatrick, R.W., Shand, P., 2008. Inland acid sulfate soil systems across Australia. CRC LEME Open File Report 249. CRC LEME, Perth, Australia, pp. 303.

Fitzpatrick, R.W., Shand, P., Mosley, L.M., 2017. Acid sulfate soil evolution models and pedogenic pathways during drought and reflooding cycles in irrigated areas and adjacent natural wetlands. Geoderma, 308: 270-290. https://doi.org/10.1016/j.geoderma.2017.08.016.

Fitzpatrick, R.W., Shand, P., Mosley, L.M., 2018. Soils in the Coorong, Lower Lakes and Murray Mouth Region. In: Mosley, L.M., Qifeng, Y., Shepard, S., Hemming, S., Fitzpatrick, R.W. (Eds.), Natural History of the Coorong, Lower Lakes and Murray Mouth Region. Royal Society of South Australia (Inc.), Adelaide, South Australia, pp. 227-251. https://doi.org/10.20851/natural-history-cllmm-2.9.

Gao, K., Hu, Y., Guo, C., Ke, C., He, C., Hao, X., Lu, G., Dang, Z., 2020. Effects of adsorbed phosphate on jarosite reduction by a sulfate reducing bacterium and associated mineralogical transformation. Ecotoxicology and Environmental Safety, 202: 110921.

Gasharova, B., Göttlicher, J., Becker, U., 2005. Dissolution at the surface of jarosite: an in situ AFM study. Chemical Geology, 215(1): 499-516. https://doi.org/10.1016/j.chemgeo.2004.06.054.

Gupta, T., Sachdeva, S., 2019. Investigations on Jarosite mixed cement concrete pavements. Arabian Journal for Science and Engineering, 44(10): 8787-8797.

Hage, J., Schuiling, R., 2000. Comparative column elution of jarosite waste and its autoclaved product-evidence for the immobilization of deleterious elements in jarosite. Minerals Engineering, 13(3): 287-296. https://doi.org/10.1016/S0892-6875(00)00008-X.

Hammarstrom, J.M., Sibrell, P.L., Belkin, H.E., 2003. Characterization of limestone reacted with acid-mine drainage in a pulsed limestone bed treatment system at the Friendship Hill National Historical Site, Pennsylvania, USA. Applied Geochemistry, 18(11): 1705-1721. https://doi.org/10.1016/S0883-2927(03)00105-7.

Harmsen, K., Van Breemen, N., 1975. Translocation of iron in acid sulfate soils: II. production and diffusion of dissolved ferrous Iron. Soil Science Society of America Journal, 39(6): 1148-1153. 10.2136/sssaj1975.03615995003900060034x.
Hart, M.G.R., 1959. Sulphur oxidation in tidal mangrove soils of Sierra Leone. Plant and Soil, 11(3): 215-236.
Hicks, W., Bowman, G., Fitzpatrick, R., 2009. Effect of season and landscape position on the aluminium geochemistry of tropical acid sulfate soil leachate. Soil Research, 47(2): 137-153.
Hicks, W.S., Bowman, G., Fitzpatrick, R.W., 1999. East Trinity acid sulfate soils part 1: Environmental hazards, CSIRO Land & Water Technical Report 14/99, Canberra.
Isbell, R.F., The National Committee on Soils and Terrain, 2016. The Australian soil classification. CSIRO publishing.
Ismael, M., Carvalho, J., 2003. Iron recovery from sulphate leach liquors in zinc hydrometallurgy. Minerals Engineering, 16(1): 31-39.
Ivarson, K.C., Ross, G.J., Miles, N.M., 1982. Microbiological transformations of iron and sulfur and their applications to acid sulfate soils and tidal marshes. In: Kittrick, J.A., Fanning, D.S., Hossner, L.R. (Eds.), Acid sulfate weathering. SSSA Special Publication. Soil Science Society of America, Madison, WI, pp. 57-75.
Johnston, S.G., Hirst, P., Slavich, P.G., Bush, R.T., Aaso, T., 2009a. Saturated hydraulic conductivity of sulfuric horizons in coastal floodplain acid sulfate soils: Variability and implications. Geoderma, 151(3): 387-394. https://doi.org/10.1016/j.geoderma.2009.05.010.
Johnston, S.G., Keene, A.F., Burton, E.D., Bush, R.T., Sullivan, L.A., Mcelnea, A.E., Ahern, C.R., Smith, C.D., Powell, B., Hocking, R.K., 2010. Arsenic mobilization in a seawater inundated acid sulfate soil. Environmental Science & Technology, 44(6): 1968-1973.
Johnston, S.G., Keene, A.F., Bush, R.T., Burton, E.D., Sullivan, L.A., Isaacson, L., Mcelnea, A.E., Ahern, C.R., Smith, C.D., Powell, B., 2011. Iron geochemical zonation in a tidally inundated acid sulfate soil wetland. Chemical Geology, 280(3-4): 257-270.
Johnston, S.G., Keene, A.F., Bush, R.T., Burton, E.D., Sullivan, L.A., Smith, D., Mcelnea, A.E., Martens, M.A., Wilbraham, S., 2009b. Contemporary pedogenesis of severely degraded tropical acid sulfate soils after introduction of regular tidal inundation. Geoderma, 149(3-4): 335-346.
Kingsford, R.T., Walker, K.F., Lester, R.E., Young, W.J., Fairweather, P.G., Sammut, J., Geddes, M.C., 2011. A Ramsar wetland in crisis – the Coorong, Lower Lakes and Murray Mouth, Australia. Marine and Freshwater Research, 62(3): 255-265.
Madden, M.E., Madden, A.S., Rimstidt, J.D., Zahrai, S., Kendall, M.R., Miller, M.A., 2012. Jarosite dissolution rates and nanoscale mineralogy. Geochimica et Cosmochimica Acta, 91: 306-321. https://doi.org/10.1016/j.gca.2012.05.001.
Miedema, R., Jongmans, A., Slager, S., 1987. Micromorphological observation on pyrite and its oxidation products in four Holocene alluvial soils in The Netherlands. Soil Micromorphology, pp. 313-337.
Mosley, L.M., Biswas, T.K., Cook, F.J., Marschner, P., Palmer, D., Shand, P., Yuan, C., Fitzpatrick, R.W., 2017. Prolonged recovery of acid sulfate soils with sulfuric materials following severe drought: causes and implications. Geoderma, 308: 312-320. https://doi.org/10.1016/j.geoderma.2017.03.019.
Mosley, L.M., Fitzpatrick, R.W., Palmer, D., Leyden, E., Shand, P., 2014a. Changes in acidity and metal geochemistry in soils, groundwater, drain and river water in the Lower Murray River after a severe drought. Science of The Total Environment, 485-486: 281-291. https://doi.org/10.1016/j.scitotenv.2014.03.063.
Mosley, L.M., Palmer, D., Leyden, E., Cook, F., Zammit, B., Shand, P., Baker, A., W. Fitzpatrick, R., 2014b. Acidification of floodplains due to river level decline during drought. Journal of Contaminant Hydrology, 161: 10-23. https://doi.org/10.1016/j.jconhyd.2014.03.003.
Mosley, L.M., Shand, P., Self, P., Fitzpatrick, R., 2014c. The geochemistry during management of lake acidification caused by the rewetting of sulfuric (pH<4) acid sulfate soils. Applied Geochemistry, 41: 49-61. https://doi.org/10.1016/j.apgeochem.2013.11.010.
Mosley, L.M., Zammit, B., Jolley, A.-M., Barnett, L., Fitzpatrick, R., 2014d. Monitoring and assessment of surface water acidification following rewetting of oxidised acid sulfate soils. Environmental Monitoring and Assessment, 186(1): 1-18. https://doi.org/10.1007/s10661-013-3350-9.
Nordstrom, D.K., 1982. Aqueous pyrite oxidation and the consequent formation of secondary iron minerals. Soil Science Society of America.
Nordstrom, D.K., Alpers, C.N., Ptacek, C.J., Blowes, D.W., 2000. Negative pH and extremely acidic mine waters from Iron Mountain, California. Environmental Science & Technology, 34(2): 254-258. https://doi.org/10.1021/es990646v.
Norvell, W.A., Lindsay, W.L., 1969. Reactions of EDTA complexes of Fe, Zn, Mn, and Cu with coils. Soil Science Society of America Journal, 33(1): 86-91. https://doi.org/10.2136/sssaj1969.03615995003300010024x.

Nyavor, K., Egiebor, N.O., 1995. Control of pyrite oxidation by phosphate coating. Science of the Total Environment, 162(2-3): 225-237.
Pons, L.J., 1973. Outline of the genesis, characteristics, classification and improvement of acid sulfate soils. In: Dost, H. (Editor), International Symposium on Acid Sulfate Soils. International Institute for Land Reclamation and Improvement, Wageningen, The Netherlands.
Rickard, D., 1973. Sedimentary iron sulfide formation In: Dost, H. (Editor), Acid Sulfate Soils. Internal Institute for Land Reclamation and Improvement, Wageningen, The Netherlands.
Sillen, L.G., Martell, A.E., 1964. Stability constants of metal-ion complexes. Special Publication no. 17, 3rd Ed. The Chemical Society, London.
Singer, P.C., Stumm, W., 1970. Acidic Mine Drainage: The rate-determining step. Science, 167(3921): 1121. https://doi.org/10.1126/science.167.3921.1121.
Sinha, A., Havanagi, V., Arora, V., Ranjan, A., Mathur, S., 2012. Recycling Jarofix waste as a construction material for embankment and sub grade. The Journal of Solid Waste Technology and Management, 38(3): 169-181.
Sinha, A.K., Havanagi, V.G., Shahu, J.T., 2018. Characterisation of jarofix for use in geotechnical projects. Proceedings of the Institution of Civil Engineers-Geotechnical Engineering, 171(5): 439-450.
Smith, A.M.L., Hudson-Edwards, K.A., Dubbin, W.E., Wright, K., 2006. Dissolution of jarosite [KFe3(SO4)2(OH)6] at pH 2 and 8: Insights from batch experiments and computational modelling. Geochimica et Cosmochimica Acta, 70(3): 608-621. https://doi.org/10.1016/j.gca.2005.09.024.
Spotts, E., Dollhopf, D.J., 1992. Evaluation of phosphate materials for control of acid production in pyritic mine overburden. Journal of environmental quality, 21(4): 627-634. https://doi.org/10.2134/jeq1992.00472425002100040017x.
Steefel, C.I., 2008. Geochemical kinetics and transport. In: Brantley, S.L., Kubicki, J.D., White, A.F. (Eds.), Kinetics of water-rock interaction. Springer New York, New York, NY, pp. 545-589. 10.1007/978-0-387-73563-4_11.
Steefel, C.I., Depaolo, D.J., Lichtner, P.C., 2005. Reactive transport modeling: An essential tool and a new research approach for the Earth sciences. Earth and Planetary Science Letters, 240(3-4): 539-558.
Stiller, A.H., Renton, J.J., Rymer, T.E., 1989. An experimental evaluation of the use of rock phosphate (apatite) for the amelioration of acid-producing coal mine waste. Mining Science and Technology, 9(3): 283-287. https://doi.org/10.1016/S0167-9031(89)90985-7.
Stoffregen, R.E., Alpers, C.N., Jambor, J.L., 2000. Alunite-jarosite crystallography, thermodynamics, and geochronology. Reviews in Mineralogy and Geochemistry, 40(1): 453-479.
Sullivan, L.A., Ward, N.J., Toppler, N., Lancaster, G., 2018. National acid sulfate soils guidance: National acid sulfate soils identification and laboratory methods manual. Department of Agriculture and Water Resources, Canberra, ACT.
Swayze, G.A., Desborough, G.A., Smith, K.S., Lowers, H.A., Hammarstrom, J.M., Diehl, S.F., Leinz, R.W., Driscoll, R.L., 2008. Understanding jarosite - from mine waste to Mars. In: Verplanck, P.L. (Ed.), Understanding contaminants associated with mineral deposits. U.S. Geological Survey Circular 1328.
Thomas, B.P., 2010. Coastal acid sulfate soil processes in Barker Inlet, South Australia, The University of Adelaide, Australia.
Thomas, B.P., Merry, R.H., Creeper, N.L., Fitzpatrick, R.W., Shand, P., Raven, M.D., Jayalath, N., 2009. Acid sulfate soil assessment of the Lower Loddon River and Burnt Creek, Central Victoria, CSIRO Land & Water Science Report CLW 18/09.
Trueman, A.M., Mclaughlin, M.J., Mosley, L.M., Fitzpatrick, R.W., 2020. Composition and dissolution kinetics of jarosite-rich segregations extracted from an acid sulfate soil with sulfuric material. Chemical Geology, 543: 119606. https://doi.org/10.1016/j.chemgeo.2020.119606.
van Breemen, N., 1973. Soil forming processes in acid sulfate soils. In: Dost, H. (Ed.), Proceedings of the international symposium on acid sulfate soils. Internal Institute for Land Reclamation and Improvement, Wageningen, The Netherlands, pp. 66-130.
van Breemen, N., 1976. Genesis and solution chemistry of acid sulfate soils in Thailand, Wageningen University, Wageningen.
van Breemen, N., 1988. Redox Processes of iron and sulfur involved in the formation of acid sulfate soils. In: Stucki, J. (Ed.), Iron in Soils and Clay Minerals. Reidel Publishing Company, Dordrecht, Holland.
Vithana, C.L., Sullivan, L.A., Bush, R.T., Burton, E.D., 2013. Acidity fractions in acid sulfate soils and sediments: contributions of schwertmannite and jarosite. Soil Research, 51(3): 203-214. https://doi.org/10.1071/SR12291.
Vlek, P.L.G., Blom, T.J.M., Beek, J., Lindsay, W.L., 1974. Determination of the solubility product of various iron hydroxides and jarosite by the chelation method. Soil Science Society of America Journal, 38(3): 429-432.

Welch, S.A., Kirste, D., Christy, A.G., Beavis, F.R., Beavis, S.G., 2008. Jarosite dissolution II - Reaction kinetics, stoichiometry and acid flux. Chemical Geology, 254(1): 73-86. https://doi.org/10.1016/j.chemgeo.2008.06.010.

Whitworth, A.J., Brand, H.E., Frierdich, A.J., 2020a. Iron isotope exchange and fractionation between jarosite and aqueous Fe (II). Chemical Geology. https://doi.org/10.1016/j.chemgeo.2020.119802.

Whitworth, A.J., Brand, H.E., Wilson, S.A., Frierdich, A.J., 2020b. Iron isotope geochemistry and mineralogy of jarosite in sulfur-rich sediments. Geochimica et Cosmochimica Acta, 270: 282-295.

Yau, C., Wong, V., Kennedy, D., 2016. Soil chemistry and acidification risk of acid sulfate soils on a temperate estuarine floodplain in southern Australia. Soil Research, 54(7): 787-796.

Zahrai, S.K., Elwood Madden, M.E., Madden, A.S., Rimstidt, J.D., 2013. Na-jarosite dissolution rates: the effect of mineral composition on jarosite lifetimes. Icarus, 223(1): 438-443. https://doi.org/10.1016/j.icarus.2012.12.020.

Chapter 2

Composition and dissolution kinetics of jarosite-rich segregations extracted from an acid sulfate soil with sulfuric material

Statement of Authorship

Title of Paper	Composition and dissolution kinetics of jarosite-rich soil segregation extracted from an acid sulfate soil with sulfuric material
Publication Status	☒ Published ☐ Accepted for publication ☐ Submitted for publication ☐ Unpublished and unsubmitted work written in manuscript style
Publication Details	Submitted to *Chemical Geology* on 29.01.20. Published on 03.04.20.

Principal Author

Name of Principal Author (Candidate)	Austin Trueman
Contribution to the Paper	Experimental design, laboratory and data analyses, and manuscript preparation.
Overall Percentage (%)	85%
Certification:	This paper reports on original research I conducted during the period of my Higher Degree by Research candidature and is not subject to any obligations or contractual agreements with a third party that would constrain its inclusion in this thesis. I am the primary author of this paper.
Signature:	Date: 26.08.20

Co-Author Contributions

By signing the Statement of Authorship, each author certifies that:

i. the candidate's stated contribution to the publication is accurate (as detailed above);
ii. permission is granted for the candidate to include the publication in the thesis; and
iii. the sum of all co-author contributions is equal to 100% less the candidate's stated contribution.

Name of Co-Author	Michael McLaughlin
Contribution to the Paper	Experimental design and critical review of manuscript.
Overall Percentage (%)	5
Signature:	Date: 26.08.20

Name of Co-Author	Luke Mosley
Contribution to the Paper	Experimental design and critical review of manuscript.
Overall Percentage (%)	5
Signature:	Date: 26.08.20

Name of Co-Author	Rob Fitzpatrick
Contribution to the Paper	Experimental design and critical review of manuscript.
Overall Percentage (%)	5
Signature:	Date: 26.08.20

Chemical Geology 543 (2020) 119606

Contents lists available at Science Direct

Chemical Geology

journal homepage: www.elsevier.com/locate/chemgeo

Composition and dissolution kinetics of jarosite-rich segregations extracted from an acid sulfate soil with sulfuric material

A.M. Trueman *[a,b], M.J. McLaughlin [a], L.M. Mosley [b], R.W. Fitzpatrick [b, c]

[a] School of Agriculture, Food and Wine, The University of Adelaide, Adelaide SA 5064, Australia
[b] Acid Sulfate Soils Centre (ASSC), School of Biological Sciences, The University of Adelaide, Adelaide SA 5064, Australia
[c] CSIRO Land and Water, Adelaide SA 5064, Australia

ARTICLE INFO

Editor: Karen Johannesson

Keywords:
Jarosite
Acid sulfate soil
Sulfuric material
Kinetics
Column perfusion

ABSTRACT

Jarosite ($KFe_3(SO_4)(OH)_6$) is known to play a key role in perpetuating chemically aggressive properties in acid sulfate soils with sulfuric material (pH < 4) – primarily through the release of retained acidity. The purpose of this study was to describe: (i) the composition of jarosite-rich segregations handpicked from sulfuric material and (ii) the dissolution chemistry of the jarosite-rich segregations under constant flow conditions and at a range of pH values. The jarosite segregations were primarily composed of K-jarosite and were admixed with minor amounts of quartz, halite, gypsum, muscovite and organic matter. The first 12-24 hours of dissolution is characterised by the rapid release of Ca, Mg, Na and S, which is attributable to the dissolution of soluble minerals such as gypsum and halite. Monitoring the differences between eluant and eluate pH showed that the release of acidity due to jarosite dissolution will resist pH increases above pH 4. The Fe/S, Fe/K and S/K molar ratios suggests that dissolution was only congruent under extremely acidic conditions (pH < 2) or in the presence of a chelating agent. Incongruent dissolution was characterised by precipitation of Fe-rich solids, which immobilised trace metal(loid)s and may have slowed jarosite dissolution through surface passivation. The rate of dissolution (in terms of $\log_{10}R$, R = mol/m^{2}s) ranged from -10.5 to 12.5. Moreover, $\log_{10}R$ and pH were nonlinearly related, so that dissolution was slowest between pH 4 and 5, and increased with both increasing and decreasing pH. These results suggest that jarosite dissolution may be able to maintain acidic soil conditions (e.g. pH < 5) even if the soil is constantly flushed. This is consistent with field observations of acid sulfate soils with sulfuric materials. Therefore, flushing acidity from soils containing jarosite-rich sulfuric material may not be a viable remediation strategy. Alternatively, promoting alkaline soil conditions may convert jarosite to more chemically benign and stable Fe (hydr)oxides.

1. Introduction

Jarosite ($KFe_3(SO_4)_2(OH)_6$) – a common secondary reaction product of ion sulfide oxidation – plays a key role in perpetuating chemically aggressive conditions in acid sulfate soils (ASS) with sulfuric material. Sulfuric material refers to soil material that exhibits a pH_{water} < 4, due to the oxidation of iron sulfide (typically pyrite, FeS_2) (Isbell and The National Committee on Soils and Terrain, 2016). In addition to being a diagnostic feature of sulfuric material, jarosite is also considered to be the principal source of retained acidity (RA) in soils with sulfuric material (Fanning et al., 2017). Retained Acidity refers to a form of potential or latent acidity that is released through the hydrolysis of poorly-crystalline, sparingly-soluble, Al^{3+} and/or Fe^{3+} minerals (Sullivan et al., 2018; Vithana et al., 2013; Vithana et al., 2014). The release of RA is suspected of preventing the pH of soil layers containing jarosite-rich sulfuric material from increasing above 4 despite years or, in some cases, decades for the acidity to be removed through natural processes (Mosley et al., 2017). This is especially evident in Gillman (South Australia), which constitutes ca. 770 ha of intertidal and supratidal land within the Southern Barker Inlet. Large swathes of soil in Gillman contains layers abundant in RA (e.g. 1000-4000 mol H^+/ton soil), and have displayed chemically aggressive properties (e.g. highly acidic, metalliferous soil drainage) since the area was drained around 1935 (Fitzpatrick et al., 2020; Poch et al., 2009). Therefore, understanding jarosite dissolution and its effect on soil and water chemistry is vital in effectively managing soils containing sulfuric material.

A number of previous studies have investigated jarosite dissolution kinetics. Baron and Palmer (1996) investigated the thermochemistry and kinetics of synthetic jarosite dissolution using a stirred batch reactor. The experimental design of this study likely formed a basis for similar investigations such as: Smith et al. (2006), Welch et al. (2008), Madden et al. (2012), Pritchett et al. (2012), Kendall et al. (2013), Zahrai et al. (2013) and Reyes et al. (2017). These studies provide insights into the behaviour of jarosite dissolution under a range of physicochemical conditions such as pH, temperature and salinity. The results reported in these studies are variable (e.g. reported reaction rates vary by several orders of magnitude). This is likely due to differences in experimental design and the nature of the mineral sample employed for testing. However, the overall trends presented in the literature provide useful insights into the role of jarosite in the environment. The relationship between the rate of jarosite dissolution and pH is of particular importance in better understanding how jarosite can promote chemically aggressive conditions in soil. Madden et al. (2012) showed that the rate of jarosite dissolution was lowest between pH 3-4, and increased with increasing acidity and alkalinity. Madden et al. (2012) suggested this was due to a bimodal dissolution mechanism, whereby the overall jarosite dissolution reaction consumed and

*Corresponding author at: School of Agriculture, Food and Wine, The University of Adelaide, Adelaide, SA 5064, Australia.
E-mail address: austin.trueman@adelaide.edu.au (A.M. Trueman)

https://doi.org/10.1016/j.chemgeo.2020.119606
Received 29 January 2020; Received in revised form 24 March 2020; Accepted 31 March 2020
Available online 03 April 2020

released H^+ at pH values below and above 3.5, respectively. In a practical sense, these results suggest that jarosite would act to buffer soil pH around 3.5, as noted by Mosley et al. (2017).

The majority of jarosite dissolution studies utilised closed batch systems, which – although powerful tools for describing mineral chemistry and predicting water-rock interactions – do not take into account mass transport: a critical aspect of environmental geochemistry (Steefel et al., 2005). Qian et al. (2019) studied the dissolution of natural jarosite under quiescent (i.e. static or semi-static) conditions using unstirred batch reactors and column leaching experiments; and reported reaction rates several order of magnitude slower than those observed using batch dissolution techniques. While gravity-driven column leaching experiments more realistically simulate water-mineral interactions in the environment, they do not provide precise control over mass transport conditions within the column. Conversely, flowthrough reactors also mimic natural water-mineral interactions, but facilitates testing under constant flow conditions. Dixon et al. (2015) employed a flowthrough reactor to investigate the effect of flowrate on the dissolution chemistry of synthetic jarosite. The results indicate that the dissolution rate is largely unaffected by the flowrate, and provide a better understanding of jarosite longevity. However, the relationship between jarosite dissolution and pH is not explored. Therefore, the aim of this study is to describe the composition of jarosite-rich segregations extracted from an ASS with sulfuric material in Gillman, South Australia; and to describe the dissolution chemistry of this jarosite-rich sample in a flowthrough reactor under constant flow and variable pH conditions. Monitoring eluate pH and the efflux of major ions during jarosite dissolution will be utilised to better describe jarosite's role in perpetuating chemically aggressive conditions in an ASS with sulfuric material.

2. Methods

2.1. Sample characterisation

2.1.1. Sample preparation and physical characterisation

Soil collected from the jarosite-bearing horizon (Figure 1) from a site at Gillman (34°49'47.21"S 138°32'39.77"E) was oven dried at 80℃ for 48 hours, gently broken-apart and sieved into the multiple size fractions (to make manual extraction more manageable). Jarosite-rich soil segregations (pale yellow soil mottles in Figure 1) were removed by hand, pulverised with a mortar and pestle, and sieved to < 250 μm. The resulting mineral powder was thoroughly mixed to form a single composite sample: herein referred to as the jarosite-rich sample. Although pulverising the sample may have affected its reactivity, the priority was to produce a homogenous sample in order to lower experimental variation.

The particle size distribution of the jarosite-rich sample was determined using a Malvern Mastersizer 2000 and refraction (n) and absorbance (k) refraction coefficients of 1.80 and 0.3, respectively.

Figure 1. (Left) A typical soil profile in the study site at Gillman, South Australia. (Right) Jarosite-rich soil segregations (pale-yellow soil mottles) that were handpicked from the soil for characterisation and the dissolution experiments.

For the dissolution experiments, the handpicked jarosite-rich sample was mixed with acid-washed quartz sand (210-297 μm, Sigma Aldrich) in a 1:1 weight ratio to promote uniform flow conditions in the reactor. Pore volume is required to express dissolution results in terms of porewater equivalents or porewater velocity. As such, the pore volume of the jarosite-rich sample and the jarosite-sand mixture was determined from bulk density and particle density (g/cm^3) after the methods described by Blake and Hartge (1986a,b). Bulk density was determined by weighing the sample in a container with a known volume. Particle density was determined with a pycnometer by weighing the sample submerged in a nonpolar organic liquid (kerosene) degassed under a partial vacuum. The sample volume is calculated from the mass and the density of the liquid displaced by the sample.

Reaction rates are conventionally normalised to the specific surface area (SSA, m^2/g) of the reactive solid phase. SSA was determined via methylene blue (MB) adsorption following the methods described by Hang and Brindley (1970) and Yang et al. (2014). 100 mg of the jarosite-rich sample was added to 45 mL of a 20 mg/L solution of MB, shaken (end-over-end) for 24 hours and centrifuged (2620 g for 10 min). The remaining concentration of MB in the supernatant was determined via UV-vis spectroscopy at 665 nm.

2.1.2. Elemental composition

Six 1 g ($\pm$ 0.005 g) subsamples of the jarosite-rich sample were digested in *aqua regia* in two steps: 1 hour at 80℃, and 3 hours at 125℃. The digests were diluted with MilliQ water (18.20 MΩ.cm) and the concentration of the following elements was measured using an Avio 200 Inductively Coupled Plasma Optical Emission Spectrometer (ICP-OES): Al, As, Cr, Fe, K, Mg, Mn, Na, Pb, S and Zn. Analyte concentrations derived from *aqua regia* digestion are referred to herein as *pseudototal concentration*s to acknowledge that the *aqua regia* digestion does not extract structural elements from silicate minerals that may be present in the sample.

2.1.3. Acid Base Accounting

Acid Base Accounting (ABA) involves a suite of analyses that quantify three operationally defined pools of acidity: potential sulfidic acidity (PSA), actual acidity (AA) and retained acidity (RA). Samples of soil were oven dried at 80 °C for 48 h prior to crushing (< 0.5 mm) and analysis for full ABA parameters using the methods from Ahern et al. (2004).

2.1.4. XRD analysis

The mineralogy of the jarosite-rich sample was analysed using a PANalytical X'Pert Pro Multipurpose Diffractometer. Diffraction patterns (Figure S.1, S.2.) were obtained using Fe filtered Co Kα radiation, an auto divergence slit, a 2° anti-scatter slit and a fast X'Celerator Si strip detector. The diffraction patterns were recorded in steps of 0.016° 2 theta and a 0.4 s counting time per step. Qualitative analysis was performed on the data using in-house XPLOT and commercial software HighScore Plus from PANalytical with the PDF4+ 2014 database from the International Centre for Diffraction Data (ICDD).

2.1.5. SEM and EDXS

For SEM and EDXS analysis, samples of the jarosite-rich segregations were mounted using an Araldite two-part epoxy resin, while the milled samples were mounted using carbon adhesive discs. Analysis was conducted on uncoated samples using a Quanta 450 SEM fitted with a Silicon Drift Detector (SDD) (Oxford Instruments) for EDXS. Images in Figure 4 were captured in high vacuum mode with a beam voltage of 20 kV and a scan time of 30 μS. X-ray spectra were acquired with the SDD and AZtecOne software, using the Point and ID method with a sampling time of 10-15 seconds.

2.2. Column perfusion experiments

The overall experimental setup, described by Baird et al. (2019), is shown in Figure 2. A peristaltic pump was used to drive the eluant through Tygon

tubing (Ø = 1.02 mm) and the polypropylene column perfusion reactor (Ø = 16 mm, h = 14.7 mm, V ~ 32 mL), while the eluate was collected in 12 mL polypropylene tubes by a Gilson FC 204 fraction collector. The flow rate was iteratively calibrated to 5 mL/h by adjusting the pump speed and tube tension until the variance in eluate weight was < 5% over an 18 hour period.

One gram of the jarosite-rich sample was mixed with one gram of acid-washed quartz sand and loaded into the reactor between glass wool. The desired eluant pH was obtained via the stepwise addition of HCl or NaOH. The effect of eluant pH on jarosite dissolution was tested in a stepped fashion by swapping the eluant solution every 48-72 hours to another eluant of a different pH. Dissolution was tested against a range of eluant pH values between 1 and 12. Collected eluate fractions were acidified to a concentration of 0.6% v/v with 70%, AR Grade nitric acid, then weighed and analysed for As, Al, Ca, Fe, K, Mg, Na, S and Zn via ICP-OES. Eluate pH was measured using a calibrated Orion 9110DJWP micro pH probe. To avoid K contamination from the glass electrode reference electrolyte, even and odd numbered fractions were used for elemental analysis and pH analysis, respectively.

A solution of 'acid oxalate' (0.1 M ammonium oxalate and 0.1 M oxalic acid, adjusted to pH 3 with either compound) is commonly used to extract poorly-crystalline Al and Fe phases from soil (Rayment and Lyons, 2011; Skjemstad et al., 1992). In light of this, dissolution tests were also conducted using acid oxalate as the eluant to obtain results that were representative of congruent dissolution. Therefore, the acid oxalate experiment, in effect, constituted a positive control.

The results of five such dissolution experiments are described here. Experiments A, B and C refer to the two-step, pH variable experiments, where the eluant pH was changed from: pH 4 to 8 (experiment A), pH 3 to 1 (experiment B), and pH 10 to 12 (experiment C). Experiment D refers to the multi-step, pH variable dissolution experiment where the eluant pH was sequentially changed from pH 2 to 12 in intervals of 2. The dissolution where the acid oxalate solution was used as an eluant will be be referred to as the acid oxalate experiment.

The Saturation Index (SI) of jarosite and other common Fe minerals (e.g. hematite and goethite) was calculated with Visual MINTEQ (version 3.1), using analyte concentrations and pH of the eluate fractions. Saturation Index values were primarily utilised to gauge which minerals may have formed during the different dissolution tests.

In order to gauge the pH of the jarosite dissolution reaction at equilibrium, a mixture of 1 part jarosite-rich sample to 5 parts RO water (w/w) was shaken end-over-end for 48 hours and centrifuged (10 min at 2620 g). The pH was then measured using a Mettler Toledo InLab Expert Pro pH probe.

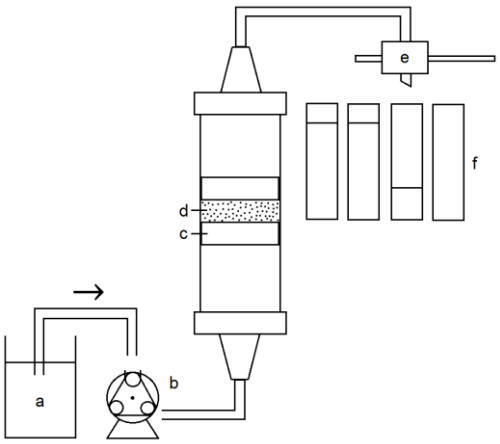

Figure 2. Column perfusion setup. A peristaltic pump (b) moves the eluant (a), through the sample (d), while a fraction collector (e) collects the eluate in plastic tubes (f). Mass transport of particulate matter is reduced by glass wool barriers (c) within the perfusion column.

3. Results and discussion

3.1. Sample characterisation

3.1.1. Particle size distribution, particle density, and specific surface area

The results of the particle size distribution analysis (Figure 3) show that the median particle diameter (d0.5) was 37 μm, while the dominant mode (i.e. the tallest peak in Figure 3) was around 138 μm. However, analysis of the sample using SEM showed that individual jarosite crystals were < 5 μm in diameter, and were typically grouped in clusters < 50 μm across (Figure 4). Consequently, it was suspected that the jarosite-rich sample had flocculated during particle size analysis. To gauge the effect of flocculation on particle size distribution, the sample was also analysed after 5 minutes of sonication. After sonication, the mean and dominant particle sizes were found to be 9.8 μm and 105 μm, respectively. This indicates the jarosite-rich sample tends to flocculate. The flocculation of the sample and subsequent formation of preferential flow paths during the column perfusion experiments may interfere with uniform flow conditions within the reactor. Consequently, the jarosite-rich sample was mixed with sand to promote uniform conditions.

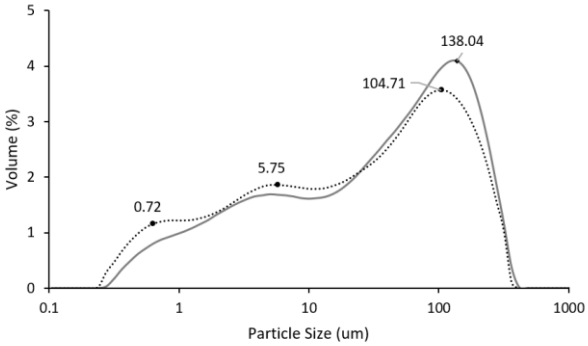

Figure 3. Particle size distribution of the jarosite-rich sample. The dotted line relates to the sample that was sonicated before analysis. Several points are labelled to show the particle size (μm) around the maxima.

The measured particle density of the jarosite-rich sample (2.72 g/cm^3) was lower than that of ideal jarosite (3.1 g/cm^3); however, the sample was admixed with other minerals and organic materials that may have contributed to the lower-than-expected results. Note that the bulk density of the jarosite-rich sample (required, along with the particle density, to calculate pore volume) was 0.68 g/cm^3.

The SSA of the jarosite-rich material at Gillman was found to be 13.6 (± 0.18) m^2/g. This was higher than the SSA values (BET-determined) reported by Sasaki and Konno (2000), Gasharova et al. (2005), Smith et al. (2006) and Wang et al. (2006) of 4, 1.3, 1.4, and 3.8-5.5 m^2/g, respectively, for synthetic jarosite. Welch et al. (2008) estimated a geometric surface area of 1.68 m^2/g for natural jarosite. Therefore, the SSA value of 13.6 m^2 reported here is more than double the highest value reported in the literature. However, the sample was shown to contain trace amounts of organic matter and muscovite, and likely contains traces of poorly-crystalline Fe oxides – all of which may have contributed to the higher-than-expected SSA.

The SSA determined using the MB adsorption method may have been partly dependent on factors such as the adsorption time and pH. For example, poorly-crystalline weathering products often exhibit high intraparticle porosity, and may display a two-step adsorption process: rapid and reversible adsorption to the external surfaces within 24 hours, followed by slow surface diffusion along micropore walls (Chorover and Brusseau, 2008; Trivedi and Axe, 1999). Similarly, changes in surface geometry (e.g. the formation of etch pits) as the jarosite dissolves would also increase measured SSA. Additionally, the pH of the MB solution containing the jarosite-rich sample was 3.9 (± 0.4). It is reasonable to assume that adjusting the pH would affect the surface charge and

therefore MB adsorption capacity of the jarosite-rich sample. However, the effect of factors such as adsorption time and pH on the measured SSA and other physical properties of the jarosite-rich sample was outside the scope of this study. Moreover, as discussed in section 3.2, the SSA used to normalise the reaction rate does not have a major impact on the overall conclusions of this study.

3.1.2. Acid base accounting

Table 1 shows that the potential and actual acidity fractions of the parent soil are insignificant with respect to RA. Consequently, the RA is expected to exert the greatest control over long-term chemistry of this soil. Additionally, the RA value of the jarosite-rich sample (4927 mol H^+/t) is of immediate practical utility, as it represents an extreme upper limit of RA for soils containing sulfuric material. The proportion of total carbon and nitrogen in the jarosite-rich sample and the soil from which it was extracted are included in Table 1. Not only is the C content of the parent soil high, but the C/N ratios of both the jarosite-rich sample and its parent soil are below 25, indicating that the organic matter is generally suitable for microbial respiration (Bruce and Rayment, 1982). This suggests that biological processes in the soil could return if this organic material was available to microbes, sulfuric materials were removed and other the chemically aggressive properties were ameliorated. Indeed, recent laboratory incubation findings of Kölbl et al. (2018) found microbial reduction reactions raised the Gillman soil pH following additional of ≥ 50% native soil organic carbon and pre-adjustment of pH to values ≥ 5.0. Therefore, the remediation of soils containing high RA values may be difficult, but ultimately achievable.

Table 1. Acid-base accounting (ABA) for the jarosite-rich sample (A) and the soil from which it was extracted (B). TC and TN refer to total carbon and total nitrogen, respectively. PSA, AA and RA respectively denote Potential Sulfidic Acidity, Actual Acidity, and Retained Acidity. AA, PSA and RA are expressed here in moles of H^+ per tonne (dry weight) of sample.

	%TC	%TN	TC/TN	pH_{KCl}	AA	PSA	RA
A	1.69	0.14	12.1	3.65	35	12	4927
B	4.76	0.23	20.7	3.82	46	17	1543

3.1.3. Elemental and mineralogical composition

The acid digestion results in Table 2 show that the jarosite stock is primarily composed of Fe, S and K, and contains minor amounts of Na, Al, Mg and Ca, and traces of As, Cr and Zn. Low RSD values (< 10%) show that the elemental variation of the sample is low, and should not be a primary source of error in the dissolution experiments. The formula according to the results in Table 2 is $K_{0.71}Fe_{2.86}(SO_4)_2(OH)_6$. Although the wt% of Na is relatively high, XRD analysis (Figure S.1, S.2) did not detect natrojarosite ($NaFe_3(SO_4)_2(OH)_6$). Therefore, Na is attributable to halite, which was present in trace amounts. The Fe/S, Fe/K and S/K ratios of the jarosite-rich sample were 1.44, 4.05 and 2.82, respectively. While the Fe/S ratio of the sample was slightly less than ideal, the Fe/K and S/K ratios were both greater than ideal, indicating that the sample is enriched in Fe and S relative to K. Alternative sources of Fe and S in the sample include iron oxides and sulfate minerals such as the gypsum, which were likely admixed with the jarosite-rich sample.

XRD analysis showed that the sample was primarily jarosite, with minor quartz (SiO_2) and traces of halite, gypsum and muscovite ($KAl_2Si_3AlO_{10}(OH)_2$) (Figure S.1). Consequently, Fe, K and S are primarily attributable to jarosite, while Na, Ca and Al are associated with the other trace minerals. The jarosite-rich sample contained traces of As, Cr and Zn, which may have been admixed with, adsorbed by or incorporated in jarosite as it formed (Dutrizac and Jambor, 2000).

Table 2. Results of the acid digestion of the jarosite-rich sample. Pseudototal elemental abundance is expressed in moles analyte per gram sample, and as a weight percent (wt%). Fe, S and K molar ratios are also included. The relative standard deviation (RSD) is included (n = 6).

	mol/g	wt%	RSD (%)
Fe	5.05E-03	28.2	4.2
S	3.53E-03	11.3	9.3
K	1.25E-03	4.90	8.3
Na	8.45E-04	1.94	8.9
Al	1.36E-04	0.37	11.2
Mg	7.47E-05	0.18	8.3
Ca	2.32E-05	0.09	7.4
As	3.25E-06	0.02	7.8
Cr	6.83E-07	0.004	28
Zn	2.54E-07	0.002	13.8
Fe/S	1.44		7.6
Fe/K	4.05		7.4
S/K	2.82		2.1

The SEM and EDXS analyses (Figure 4) compliment the conclusions drawn from the results of the acid digestion and XRD analyses, and provide insight into the formation of jarosite and its relationship with other minerals. Jarosite is commonly observed as spherical clusters (Figure 4a), similar to pyrite framboids – *c.f.* Fitzpatrick and Shand (2008). The jarosite crystals themselves are primarily octahedral (Figure 4b, EDXS: 78% O, 9.3% Fe, 7.9% S, 2.9% K), but may also display more isometric structures (Figure 4c, EDXS: 74.2% O, 9.5% Fe, 7.3% S, 2.2% K). These features suggest that the jarosite formed as a pseudomorph of pyrite (i.e. jarosite after pyrite) (Furbish, 1963). Jarosite is often associated with organic residue (Figure 4a and f), which was presumably derived from the mangrove trees (*Avicennia marina*) that originally stood in Gillman (Fitzpatrick et al., 2012). Mg sulfate - possibly epsomite ($MgSO_4 . 7H_2O$) and/or hexahydrite ($MgSO_4 . 6H_2O$) – was commonly observed as clusters of tabular crystals (Figure 4d, EDXS: 73.4% O, 11.7 Mg, 11.2% S), and were often adjacent to jarosite. Large, acicular crystals of gypsum are shown in Figure 4e. Halite (NaCl) was present as large, anhedral crystals (Figure 4f, EDXS: 80.9% O, 10.2% S, 9.0% Ca) or as surface coatings.

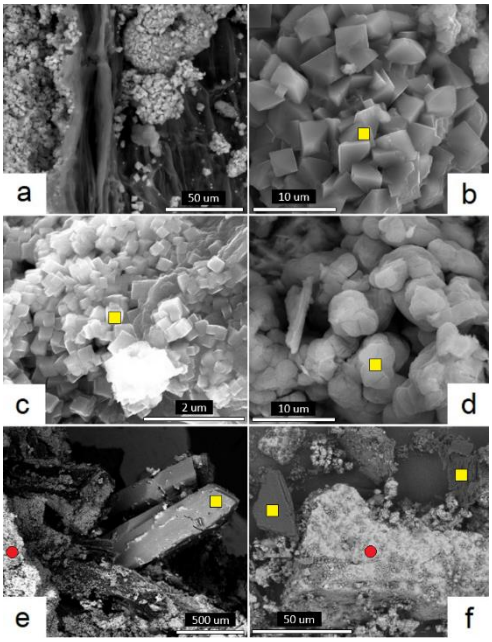

Figure 4. SEM images of a jarosite-rich soil segregation. Coloured shapes represent the EDXS sample sites. Figures 4a to 4e show different areas of the same unaltered jarosite-rich segregation. Conversely, Figure 4f shows an area of the pulverised and sieved jarosite-rich sample. (a) Jarosite clusters against the organic residue of the mangrove root in which the jarosite formed. (b) A cluster of jarosite crystals (78% O, 9.3% Fe, 7.9% S, 2.9% K) displaying a typical octahedral morphology. (c) Jarosite crystals (74.2% O, 9.5% Fe, 7.3% S, 2.2% K) displaying a pseudocubic morphology. (d) Magnesium sulfate crystals (73.4% O, 11.7 Mg, 11.2% S) displaying a tabular morphology. (e) Acicular gypsum crystals (yellow square; 80.9% O, 10.2% S, 9.0% Ca) jutting out from organic residue, which is encrusted with jarosite (red circle; 78.8% O, 9.2% Fe, 8.0% S, 2.4% K). (f) Organic residue (yellow squares), and a large, weathered halite crystal (red circle; 51.1% Cl, 48.9% Na) encrusted with smaller sulfates.

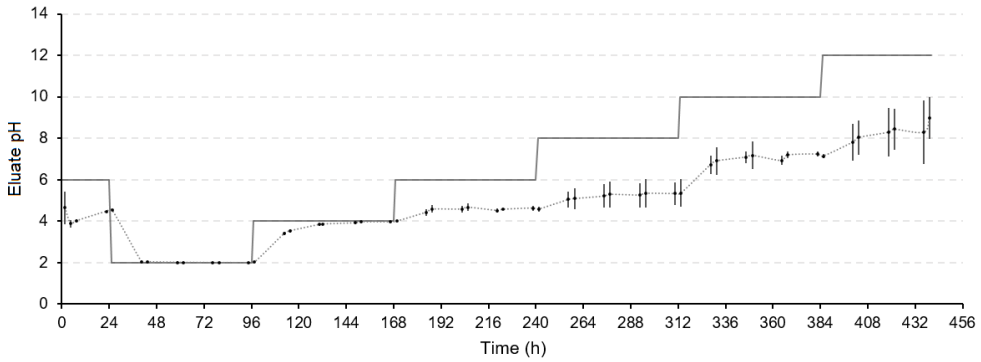

Figure 5. Change in eluate pH (dotted line) over time relative to changes in eluant pH (solid line) for experiment D. Error bars represent standard deviation.

3.2. Column perfusion tests

The pH_{water} of the 1:5 extract was measured to gauge the pH of the jarosite dissolution reaction near equilibrium and was found to be 3.65. Therefore, it was expected that the eluate would tend towards pH 3.65, regardless of eluant pH. Figure 5 shows the change of eluate pH, relative to eluant pH, over the course of an experiment where the eluant pH was increased from 2 to 12 (in 6 steps) over three weeks. In cases where the eluant pH > 4, the eluate pH was less than the eluant pH by approximately 1.5-3 pH units. There was no appreciable difference between eluant and eluate pH where eluant pH was < 4. In a practical sense, these results clearly demonstrate that the dissolution of jarosite is capable of buffering subsurface soil layers around pH 4 – as suggested by Mosley et al. (2017).

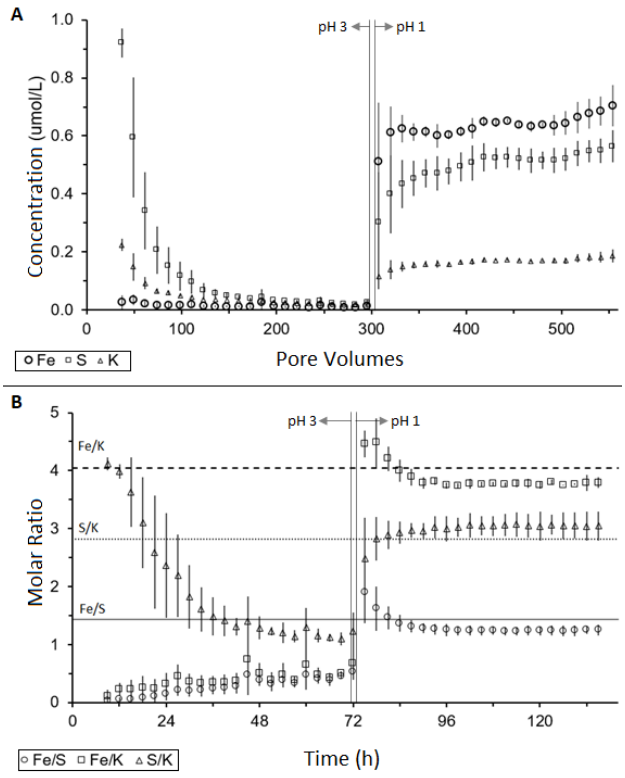

Figure 6. Results from a dissolution experiment B, in which the eluant pH was decreased from 3 to 1 after 72 hours (ca. 300 pore volumes). (a) Fe, S and K concentrations (μmo/L) expressed as a function of porewater volumes. (b) Change of Fe, S and K molar ratios over time, where the solid, dashed and dotted horizontal lines respectively denote the Fe/S, Fe/K and S/K molar ratios of the jarosite-rich sample. Error bars represent standard deviation.

Figure 6 shows a typical data set from a single-step experiment – in this case the eluant pH was decreased from 3 to 1 after 72 hours. Initial S concentrations are several times greater than those of Fe and K, and was attributed to the dissolution of more soluble sulfates (primarily gypsum) admixed with the jarosite-rich sample. The presence of soluble sulfates prohibits an accurate calculation of the jarosite dissolution rate from dS/dt. Therefore, subsequent experiments began with a 24 hour rinse phase, where RO water was used as the eluant to remove soluble minerals. Fe, S and K concentrations reach a relatively steady state by 48 hours. The Fe, S and K molar ratios show that dissolution is incongruent at pH 3. The decrease in eluant pH from 3 to 1 at 72 hours (ca. 300 pore volumes) is marked by a large increase in Fe, S and K concentrations (Figure 6a). Moreover, after the decrease in pH, the Fe, S and K molar ratios (Figure 6b) tend towards values that would be expected if the dissolution reaction was congruent (i.e. the Fe, S and K molar ratios of the jarosite-rich sample in Table 2). Note that the Fe/S and Fe/K ratios during the pH 1 treatment are initially marked by a positive inflection, but then decrease over the next 20 hours. This suggests that Fe accumulated in the reactor during the pH 3 treatment, due to incongruent dissolution and accompanying formation of Fe-rich solids.

Figure 7 shows the Fe, S and K ratios at the conclusion of each treatment, and demonstrates that the dissolution is only congruent under strongly acidic conditions or in the presence of a chelating agent (i.e. oxalate). This is in agreement with studies such as Smith et al. (2006) and Madden et al. (2012), with the former proposing that the selective dissolution of K and S is due to the high stability of the FeO_6 octahedra, and the lower stability of the $KFe(OH)_4$ surface relative to the $Fe_2(SO_4)_2(OH)_2$ surface.

Table 3 summarises the amount of each analyte that dissolved during the different treatments; and are expressed as percentage of the pseudototal amount of that analyte in the jarosite-rich sample (i.e. the results in Table 2). Dissolution of all elements was greatest using the oxalate treatment. Most Ca, Mg and Na was released in the rinse phase due to the dissolution of Ca and Mg sulfate and halite. Around 6.5% of Zn was also dissolved during the rinse phase, suggesting it was incorporated in soluble minerals or weakly adsorbed to charged surfaces. In a practical sense, the initial, rapid release of major cations and trace elements such as Zn indicates that an initial increase in salinity may be a key management concern associated with the rewetting of soils containing jarosite-rich segregations.

The release of Al, As, Fe and Zn generally increased with decreasing pH as jarosite dissolution became more congruent and these elements became more soluble. Moreover, the release of Al, As and Fe increased dramatically when eluant pH was increased from pH 10 to 12. It may be reasonable to assume that the high pH environment not only accelerated the alkaline decomposition of jarosite, but also promoted the dissolution the Fe-rich reaction products (and associated Al and As). The formation of these Fe-rich solids in the environment may present a risk to soil and water quality through the release of RA and trace metal(loid)s. Moreover, these Fe-rich solids may also pose a risk to infrastructure (e.g. may clog pipes) and water amenity (e.g. may cause rust-coloured water).

Table 3 may also be utilised alongside Tables 1 and 2 to make quick estimations of mineral longevity and release of acidity and key elements. For example, the rate at which Fe was released can be used to estimate jarosite longevity under the same experimental conditions, assuming a zero order reaction, and that dissolved Fe was primarily derived from jarosite. At pH 1, roughly 4% of the pseudototal Fe dissolved over 72 hours, hence 100% of the Fe would dissolve in 1800 hours or 75 days. Moreover, the acidity generated by the subsequent hydrolysis of dissolved Fe^{3+} may present a management concern and may also be estimated from Table 3. For example, at pH 4, 0.02 % of the pseudototal Fe dissolved over 48 hours, equating to 1.01E-06 mol Fe per 48 hours or

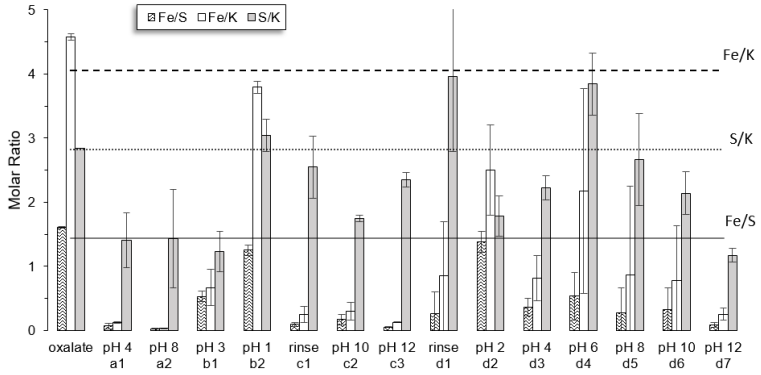

Figure 7. Molar ratios of Fe, S and K in the final eluate fraction of each of the treatments. For pH-variable experiments, the letter and number below the treatment denotes the experiment and order of testing. For example, in experiment b, dissolution was tested at pH 3 (pH 3-b1) and then pH 1 (pH 1-b2). The solid, dashed and dotted line respectively denote the Fe/S, Fe/K and S/K ratios of the jarosite-rich sample (c.f. Fe, S and K molar ratios in Table 2). Error bars represent standard deviation.

Table 3. The amount of each analyte dissolved during the treatment, expressed as a percentage of the pseudototal amount of that analyte in the jarosite-rich sample (i.e. results in Table 2). Matching superscript letters indicates that the treatments were tested in the same experiment, while the superscript numbers give the order in which the treatments were tested. For example, for pH 3^{b1} and pH 1^{b2}, dissolution was tested at pH 3 then 1. Results for Ca and K are not available (na) for pH 4^{a1} and pH 8^{a2}.

Trt.	t (h)	Al	As	Ca	Fe	K	Mg	Na	S	Zn
oxalate	48	4.13	17.3	7.72	8.87	9.41	69.2	59.5	9.02	38.5
pH 4^{a1}	48	0.96	0.41	na	0.02	na	72.0	62.7	1.30	17.5
pH 8^{a2}	48	0.16	0.10	na	0.00	na	1.15	0.50	0.15	0.42
pH 3^{b1}	72	0.41	0.08	24.2	0.07	0.76	14.0	9.20	0.57	6.60
pH 1^{b2}	72	2.29	10.5	3.58	3.59	3.76	0.92	1.31	4.00	8.82
rinse^{c1}	24	0.20	0.05	71.9	0.01	1.00	64.9	61.3	1.15	9.09
pH 10^{c2}	72	0.06	0.14	6.58	0.04	0.38	4.73	4.97	0.34	0.52
pH 12^{c3}	72	0.81	1.69	1.71	0.22	9.27	0.59	6.55	7.96	0.78
rinse^{d1}	24	0.16	0.17	70.5	0.02	0.82	69.9	49.9	1.11	6.42
pH 2^{d2}	72	1.34	0.32	33.5	0.19	0.84	24.0	14.4	0.77	21.6
pH 4^{d3}	72	0.16	0.65	0.96	0.04	0.21	0.20	0.16	0.20	5.27
pH 6^{d4}	72	0.09	0.50	0.83	0.05	0.15	0.00	0.40	0.18	1.23
pH 8^{d5}	72	0.24	0.54	2.33	0.01	0.18	0.00	0.40	0.16	1.05
pH 10^{d6}	72	0.21	0.07	2.31	0.02	0.25	0.09	0.18	0.16	0.24
pH 12^{d7}	72	0.37	1.49	0.65	0.18	0.63	0.06	9.85	0.70	0.72

2.10E-08 mol Fe per hour. Therefore, the acid generation rate due to Fe hydrolysis would be 2.10E-08 mol H^+ per hour – assuming 1 mole of Fe^{3+} hydrolyses to yield 1 mole of H^+ (Ahern et al., 2004). Similarly, these results may be used to gauge elemental toxicity in selected ecosystems. For example, at pH 4, 0.96% of the pseudototal Al dissolved over 48 hours, equating to 2.72E-08 mol Al per hour. Assuming a flow rate of 5 mL per hour, the average Al concentration during the pH 4 test was 5.44E-06 mol per L – or around 147 μg/L. This is more than double the ANZECC (2000) freshwater (pH < 6.5) moderate reliability trigger value for dissolved Al (55 μg/L). Therefore, drainage associated with soil containing jarosite-rich segregations could pose substantial threats to receiving waterways and related freshwater and marine ecosystems.

Figure 8 shows the relationship between the dissolution rate of the jarosite-rich sample ($\log_{10}$R) and the eluate pH. This relationship was found to be quadratic, so that the reaction rate was slowest between 4 and 5, and increased with both increasing and decreasing pH. Madden et al. (2012) and Qian et al. (2019) show similar, nonlinear relationships between dissolution rate and pH, but with the slowest rates occurring around pH 4.4 and 3.4, respectively. As previously noted, the pH_{water} of the jarosite-rich sample was 3.65, suggesting that jarosite is most stable at this pH. Qian et al. (2019) studied dissolution under quiescent conditions, which allowed jarosite dissolution to tend closer towards equilibrium than the methods used in this study, where a constant supply of fresh solution encouraged far-from-equilibrium dissolution. In a practical sense, this relationship between dissolution rate and pH indicates that jarosite dissolution may be able to maintain acidic soil conditions (i.e. pH < 5) even if the soil is continually flushed.

In terms of magnitude, the reaction rates determined in this study ($\log_{10}$R values ca. between -10.5 and -12.5) are more aligned with those for natural jarosite samples described by Welch et al. (2008) ($\log_{10}$R values ca. between -11 and -12) and Qian et al. (2019) ($\log_{10}$R values ca. between -12 and -14). However, the reaction rates presented in Figure 8 were normalised with a SSA of 13.57 m^2/g, while the literature reports SSA values between 1.3 and 5.5 m^2/g. For comparison, normalising the rates in this study to 2 m^2/g, results in $\log_{10}$R values roughly ranging from -9.5 to -11.5. These rates are still slower than the majority of rates reported in the literature. Therefore, the SSA used to normalise the reaction rates does not wholly account for the difference in dissolution rates reported here and by other authors.

Jarosite dissolution at circumneutral and alkaline conditions was marked by the accumulation of Fe-rich solids in the reactor, which may have affected the rate of jarosite dissolution. The formation of poorly-crystalline Fe-rich solids has frequently been observed during jarosite dissolution, and are described at length by Madden et al. (2012). In this study, within 24 hours of increasing the eluant pH from 10 to 12, the sample developed dark red mottles. Moreover, extremely fine, red solids were observed in the Tygon tubing and in several eluate fractions. At the conclusion of the pH 12 treatment, the eluant was switched to the acid oxalate solution in order to gauge the composition of the red solids. This resulted in the Fe/S and Fe/K ratios increasing by 519 and 89 times, respectively – indicating that the red solids were primarily composed of Fe. Furthermore, eluate SI values obtained using Visual MINTEQ, were positive for common Fe (hydr)oxides (e.g. goethite and hematite) at eluate pH values > 1. Similarly, the onset of the oxalate treatment resulted in dramatic spikes in concentrations of Al, As and Zn, suggesting other metal(loid)s precipitated out of solution with Fe. As noted by Welch et al. (2008) and Madden et al. (2012), the formation of Fe-rich coatings on the jarosite surface may hinder further dissolution. If this were the case, then the dissolution rates should decrease with increasing pH, but this was not observed. Therefore, although these Fe-rich weathering products may provide some protection against jarosite dissolution under circumneutral conditions, they do not guard against chemical attack under extreme pH conditions.

The rate of jarosite dissolution and formation of Fe-rich solids may also be related to the solid/liquid ratio, as greater ratios may lower the time required for the solution to become saturated with respect to jarosite and Fe (hydr)oxide. The highest pR values reported in the literature also had the highest solid/liquid ratios. The solid/liquid ratio described in Welch et al. (2008), Qian et al. (2019) and in this study were 0.002, 0.008 and 0.06, respectively.

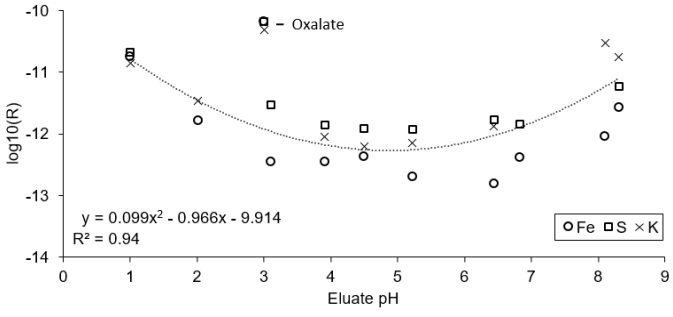

Figure 8. Jarosite dissolution rates (R, mol/m^2s) expressed in $\log_{10}$ form and as a function of eluate pH. Reaction rates derived from the release of Fe, S and K are plotted separately as circles, squares and crosses, respectively. Conversely, the quadratic regression line corresponds to the mean dissolution rate (i.e. the arithmetic mean of the Fe-, S- and K-derived rates). The minimum of this function (i.e. the slowest rate) occurs at pH 4.87. The set of points labelled 'Oxalate' correspond to the results of the acid oxalate experiment.

Conversely, other solid/liquid ratios in the literature range from 0.001 (Pritchett et al., 2012) to 0.0002 (Baron and Palmer, 1996; Smith et al., 2006). Agitating the sample during dissolution (e.g. with stirrers and shakers) may encourage dissolution by preventing Fe solids from settling or by removing them from jarosite surfaces.

4. Conclusion

This study describes the composition and dissolution chemistry of jarosite-rich soil segregations obtained from chemically aggressive ASS in Gillman, South Australia. Several analytical methods (acid digestion, acid base accounting, SEM and XRD) indicate that the sample was primarily K-jarosite, and contained minor amounts of quartz, gypsum, halite, muscovite and organic residue. The soluble minerals admixed with jarosite were responsible for high initial Ca, Mg, Na and S concentrations in eluates. Jarosite dissolution was congruent only in the presence of a chelating agent or under strongly acidic conditions (pH < 2). In a closed system, the solution pH should tend towards 3.65. Conversely, under constant flow conditions, the release of RA as jarosite dissolves will resist increases in pH above pH 4. Incongruent dissolution is marked by the formation of Fe-rich solids, which immobilise other metal(loid)s such as Al, As and Zn; and, under circumneutral conditions, may hinder further jarosite dissolution through surface passivation. The $\log_{10}R$ values ranged from approximately -10.5 to -12.5. Additionally, $\log_{10}R$ and pH were found to be non-linearly related (quadratic), where the dissolution rate was lowest between pH 4 and 5, increased with both increasing and decreasing pH.

In terms of managing soils containing jarosite-rich segregations, this study has shown that the initial release of acidity and salinity associated with soluble minerals and readily exchangeable ions represents an acute risk to soil and water quality. Conversely, jarosite dissolution represents a chronic risk of acidification and metal(loid) toxicity. Flushing the soil to remove acidity is not recommended, as jarosite may be able to maintain acidic soil conditions even with constant flushing. Alternatively, promoting alkaline soil conditions may convert jarosite to more chemically benign Fe (hydr)oxides, which may even act to passivate the remaining jarosite. However, partially hydrolysed ferric (hydr)oxides also represent a source of RA; and may also damage infrastructure (e.g. by clogging pipes) and affect water amenity (e.g. cause rust-coloured water). Moreover, if these precipitates are subsequently acidified, they may release noxious metal(loid)s previously scavenged from the soil. In light of this, passivating jarosite by encouraging the formation of a chemically stable and benign mineral coatings represents a potential remediation strategy, but requires further investigation. Therefore, management strategies concerning soils containing jarosite should prioritise liming, passivation and hydraulic isolation rather than attempting to dissolve jarosite and flush acidity from the soil profile. If limiting soil water input is impractical or undesirable, then great care should be taken to collect and amend soil drainage.

Acknowledgements

We would like to acknowledge: Bogumila Tomczak for ICP-OES analysis, Mark Raven and Peter Self for XRD analysis, Stuart McClure for SEM and EDXS analysis, and the Environmental Analysis Laboratory (Lismore, NSW) for ABA. Additionally, we would like to thank the anonymous reviewers for their constructive comments.

This work was supported by Australian Research Council Discovery Project (DP170104541) funding.

References

Ahern, C.R., McElnea, A.E., Sullivan, L.A., 2004. Acid sulfate soils laboratory methods guidelines, Queensland Department of Natural Resources, Mines and Energy, Indooroopily, Queensland, Australia.

ANZECC, 2000. Australian and New Zealand guidelines for fresh and marine water quality, aquatic ecosystems - rationale and background information. Australian Water Association, Artarmon, New South Wales, Australia.

Baird, R., da Silva, R.C., Degryse, F., McLaughlin, M.J., 2019. A column perfusion test to assess the kinetics of nutrient release by soluble, sparingly soluble and coated granular fertilizers. Journal of Plant Nutrition and Soil Science, 182(5): 763-771.

Baron, D., Palmer, C.D., 1996. Solubility of jarosite at 4-35°C. Geochimica et Cosmochimica Acta, 60(2): 185-195.

Blake, G.R., Hartge, K.H., 1986a. Bulk density, Methods of soil analysis: part 1 - physical and mineralogical methods. Soil Science Society of America book series. Soil Science Society of America, American Society of Agronomy, Madison, WI, pp. 363-375.

Blake, G.R., Hartge, K.H., 1986b. Particle density, Methods of soil analysis: part 1 - physical and mineralogical methods. Soil Science Society of America book series. Soil Science Society of America, American Society of Agronomy, Madison, WI, pp. 377-382.

Bruce, R.C., Rayment, G., 1982. Analytical methods and interpretations used by the agricultural chemistry branch for soil and land use surveys. Queensland Department of Primary Industries.

Chorover, J., Brusseau, M.L., 2008. Kinetics of sorption-desorption. In: Brantley, S.L., Kubicki, J.D., White, A.F. (Eds.), Kinetics of water-rock interaction. Springer New York, New York, NY, pp. 109-149.

Dixon, E.M., Madden, A.S., Hausrath, E.M., Madden, M.E., 2015. Assessing hydrodynamic effects on jarosite dissolution rates, reaction products, and preservation on Mars. Journal of Geophysical Research: Planets, 120(4): 625-642.

Dutrizac, J.E., Jambor, J.L., 2000. Jarosites and their application in hydrometallurgy. Reviews in Mineralogy and Geochemistry, 40(1): 405-452.

Fanning, D.S., Rabenhorst, M.C., Fitzpatrick, R.W., 2017. Historical developments in the understanding of acid sulfate soils. Geoderma, 308: 191-206.

Fitzpatrick, R., Thomas, B.P., Merry, R., Marvanek, S., 2012. A field guide to estuarine soil-landscapes in Barker Inlet, South Australia. Acid Sulfate Soils Centre (ASSC), the University of Adelaide.

Fitzpatrick, R.W., Shand, P., 2008. Inland acid sulfate soil systems across Australia. CRC LEME Open File Report 249. CRC LEME, Perth, Australia, pp. 303.

Fitzpatrick, R.W., Thomas, B.P., Kölbl, A., Raven, M.D., Trueman, A.M., Stiglingh, A.D., Smernik, R.J., McLaughlin, M.J., Mosley, L.M., 2020. Contemporary and relict pedogenic processes in a disturbed coastal acid sulfate soil sequence from a tidal estuary in South Australia. Geoderma, sumbitted.

Furbish, W.J., 1963. Geologic implications of jarosite, pseudomorphic after pyrite. American Mineralogist: Journal of Earth and Planetary Materials, 48(5-6): 703-706.

Gasharova, B., Göttlicher, J., Becker, U., 2005. Dissolution at the surface of jarosite: an in situ AFM study. Chemical Geology, 215(1): 499-516.

Hang, P.T., Brindley, G., 1970. Methylene blue absorption by clay minerals. Determination of surface areas and cation exchange capacities (clay-organic studies XVIII). Clays and Clay Minerals, 18(4): 203-212.

Isbell, R.F., The National Committee on Soils and Terrain, 2016. The Australian soil classification. CSIRO publishing.

Kendall, M.R., Madden, A.S., Madden, M.E., Hu, Q., 2013. Effects of arsenic incorporation on jarosite dissolution rates and reaction products. Geochimica et Cosmochimica Acta, 112: 192-207.

Kölbl, A., Marschner, P., Mosley, L., Fitzpatrick, R., Kögel-Knabner, I., 2018. Alteration of organic matter during remediation of acid sulfate soils. Geoderma, 332: 121-134.

Madden, M.E. et al., 2012. Jarosite dissolution rates and nanoscale mineralogy. Geochimica et Cosmochimica Acta, 91: 306-321.

Mosley, L.M. et al., 2017. Prolonged recovery of acid sulfate soils with sulfuric materials following severe drought: causes and implications. Geoderma, 308: 312-320.

Poch, R.M., Thomas, B.P., Fitzpatrick, R.W., Merry, R.H., 2009. Micromorphological evidence for mineral weathering pathways in a coastal acid sulfate soil sequence with mediterranean-type climate, South Australia. Soil Research, 47(4): 403-422.

Pritchett, B.N., Madden, M.E., Madden, A.S., 2012. Jarosite dissolution rates and maximum lifetimes in high salinity brines:

implications for earth and mars. Earth and Planetary Science Letters, 357-358: 327-336.
Qian, G. et al., 2019. Evaluation of the rate of dissolution of secondary sulfate minerals for effective acid and metalliferous drainage mitigation. Chemical Geology, 504: 14-27.
Rayment, G.E., Lyons, D.J., 2011. Soil chemical methods: Australasia. CSIRO publishing.
Reyes, I.A. et al., 2017. Dissolution rates of jarosite-type compounds in H_2SO_4 medium: a kinetic analysis and its importance on the recovery of metal values from hydrometallurgical wastes. Hydrometallurgy, 167: 16-29.
Sasaki, K., Konno, H., 2000. Morphology of jarosite-group compounds precipitated from biologically and chemically oxidized Fe ions. The Canadian Mineralogist, 38(1): 45-56.
Skjemstad, J., Fitzpatrick, R.W., Zarcinas, B., Thompson, C., 1992. Genesis of podzols on coastal dunes in southern Queensland. II. Geochemistry and forms of elements as deduced from various soil extraction procedures. Soil Research, 30(5): 615-644.
Smith, A.M.L., Hudson-Edwards, K.A., Dubbin, W.E., Wright, K., 2006. Dissolution of jarosite $[KFe_3(SO_4)(OH)_6]$ at pH 2 and 8: insights from batch experiments and computational modelling. Geochimica et Cosmochimica Acta, 70(3): 608-621.
Steefel, C.I., DePaolo, D.J., Lichtner, P.C., 2005. Reactive transport modeling: an essential tool and a new research approach for the earth sciences. Earth and Planetary Science Letters, 240(3-4): 539-558.
Sullivan, L.A., Ward, N.J., Toppler, N., Lancaster, G., 2018. National acid sulfate soils guidance: national acid sulfate soils identification and laboratory methods manual. Department of Agriculture and Water Resources, Canberra, ACT.
Trivedi, P., Axe, L., 1999. A comparison of strontium sorption to hydrous aluminum, iron, and manganese oxides. Journal of Colloid and Interface Science, 218(2): 554-563.
Vithana, C.L., Sullivan, L.A., Bush, R.T., Burton, E.D., 2013. Acidity fractions in acid sulfate soils and sediments: contributions of schwertmannite and jarosite. Soil Research, 51(3): 203-214.
Vithana, C.L., Sullivan, L.A., Bush, R.T., Burton, E.D., 2014. Jarosite quantification in soils: an enhanced sequential extraction procedure. Applied Geochemistry, 51: 130-138.
Wang, H., Bigham, J.M., Tuovinen, O.H., 2006. Formation of schwertmannite and its transformation to jarosite in the presence of acidophilic iron-oxidizing microorganisms. Materials Science and Engineering: C, 26(4): 588-592.
Welch, S.A., Kirste, D., Christy, A.G., Beavis, F.R., Beavis, S.G., 2008. Jarosite dissolution II - reaction kinetics, stoichiometry and acid flux. Chemical Geology, 254(1): 73-86.
Yang, C. et al., 2014. All-solid-state asymmetric supercapacitor based on reduced graphene oxide/carbon nanotube and carbon fiber paper/polypyrrole electrodes. Journal of Materials Chemistry A, 2(5): 1458-1464.
Zahrai, S.K., Madden, M.E., Madden, A.S., Rimstidt, J.D., 2013. Na-jarosite dissolution rates: the effect of mineral composition on jarosite lifetimes. Icarus, 223(1): 438-443

Supplementary Material

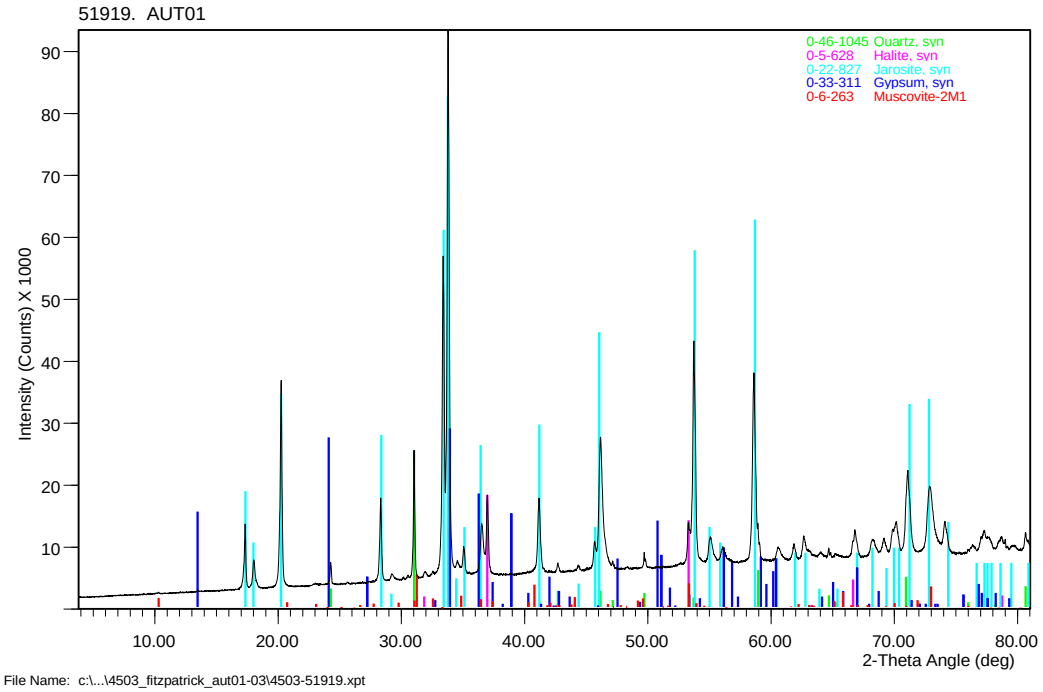

Figure. S.1. Diffraction pattern of the jarosite-rich sample (sample code: AUT01) obtained using a PANalytical X'Pert Pro Multipurpose Diffractometer. The pattern indicates that the sample was dominant in jarosite, and contained minor amounts of quartz and trace amounts of halite, gypsum and mica.

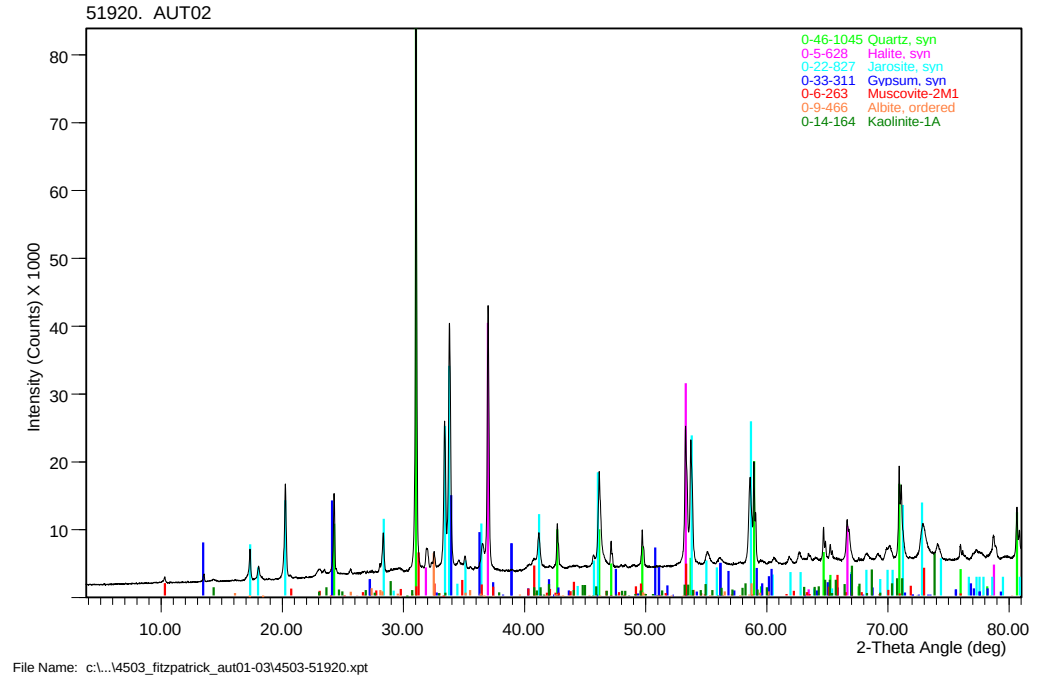

Figure. S.2. Diffraction pattern of the soil from which the jarosite-rich sample was extracted (sample code: AUT02) obtained using a PANalytical X'Pert Pro Multipurpose Diffractometer. The pattern indicates that the sample was codominant in jarosite and quartz, and contained minor amounts of halite and minor, and trace amounts of gypsum.

Chapter 3

Exploring passivation-based treatments for jarosite from an acid sulfate soil

Statement of Authorship

Title of Paper	Exploring passivation-based treatments for jarosite from an acid sulfate soil
Publication Status	☒ Published ☐ Accepted for publication ☐ Submitted for publication ☐ Unpublished and unsubmitted work written in manuscript style
Publication Details	Submitted to *Chemical Geology* on 18.08.20. Published 06.01.21

Principal Author

Name of Principal Author (Candidate)	Austin Trueman
Contribution to the Paper	Experimental design, laboratory and data analyses, and manuscript preparation.
Overall Percentage (%)	85%
Certification:	This paper reports on original research I conducted during the period of my Higher Degree by Research candidature and is not subject to any obligations or contractual agreements with a third party that would constrain its inclusion in this thesis. I am the primary author of this paper.
Signature:	Date: 26.08.20

Co-Author Contributions

By signing the Statement of Authorship, each author certifies that:

iv. the candidate's stated contribution to the publication is accurate (as detailed above);
v. permission is granted for the candidate to include the publication in the thesis; and
vi. the sum of all co-author contributions is equal to 100% less the candidate's stated contribution.

Name of Co-Author	Michael McLaughlin
Contribution to the Paper	Experimental design and critical review of manuscript.
Overall Percentage (%)	5
Signature:	Date: 26.08.20

Name of Co-Author	Luke Mosley
Contribution to the Paper	Experimental design and critical review of manuscript.
Overall Percentage (%)	5
Signature:	Date: 26.08.20

Name of Co-Author	Rob Fitzpatrick
Contribution to the Paper	Experimental design and critical review of manuscript.
Overall Percentage (%)	5
Signature:	Date: 26.08.20

Contents lists available at Science Direct

Chemical Geology

journal homepage: www.elsevier.com/locate/chemgeo

Exploring passivation-based treatments for jarosite from an acid sulfate soil

A.M. Trueman *[a,b], R.W. Fitzpatrick [b, c], L.M. Mosley [b], M.J. McLaughlin [a]

[a] School of Agriculture, Food and Wine, The University of Adelaide, Adelaide SA 5064, Australia
[b] Acid Sulfate Soils Centre (ASSC), School of Biological Sciences, The University of Adelaide, Adelaide SA 5064, Australia
[c] CSIRO Land and Water, Adelaide SA 5064, Australia

ARTICLE INFO

Editor: B. Sherwood-Lollar

Keywords:
Jarosite
Passivation
Strengite
Phosphosiderite
Gengenbachite
Spheniscidite

ABSTRACT

Jarosite ($KFe_3(SO_4)_2(OH)_6$) is a common secondary reaction product of iron sulfide oxidation and can pose a considerable risk to soil and water quality. The overarching objective of this study was to explore the possibility of employing passivation-based treatments to mitigate the risks associated with jarosite-rich materials by investigating the alteration of pedogenic jarosite to a relatively benign, sparingly-soluble mineral such as goethite or strengite. Samples of jarositic phytotubules (from an acid sulfate soil with sulfuric material) were treated with: (i) alkaline solutions with a view to produce ferric (oxyhydr)oxide; (ii) phosphate solutions with a view to produce ferric phosphate; and (iii) alkaline solutions, followed by phosphate solutions, with a view to produce ferric phosphate. These treatments were conducted at both ambient (25℃) and elevated temperatures (80℃) to explore the effects of temperature on the extent of jarosite alteration. Under alkaline conditions, jarosite readily decomposed to yield poorly-crystalline ferric (oxyhydr)oxides (e.g. two-line ferrihydrite), regardless of temperature. These ferric (oxyhydr)oxides readily reacted with phosphoric acid to yield ferric phosphate; and with monoammonium phosphate (MAP) to yield spheniscidite ($(NH_4,K)(Fe,Al)_2(PO_4)_2(OH).2H_2O$). Jarosite reacted with phosphoric acid to produce strengite or phosphosiderite (depending on the reaction temperature) and, to a lesser extent, gengenbachite ($KFe_3(HPO_4)_4(H_2PO_4)_2.6H_2O$). Similarly, jarosite reacted with MAP to produce hydrogen ammonium ferric phosphate ($H_2(NH_4)Fe(PO_4)_2$). The direct alteration of jarosite to ferric phosphate appears to be very limited under ambient conditions. However, this study predominantly focuses on changes to the bulk chemical composition of jarosite. Consequently, further investigation (e.g. SEM analysis) is recommended to explore subtle changes in surface chemistry and the related effects on jarosite reactivity. Column perfusion experiments were also conducted to study the release of key elements during the dissolution of NaOH- and MAP-treated jarosite. The results suggest that these treatments do not considerably lower the risks to soil and water quality posed by jarosite dissolution. The practicality of the treatments is discussed, including the potential negative side effects. Further investigation is required to determine if these, or alternative, passivation treatments could be employed in the field to effectively mitigate the environmental risk associated with jarosite.

1. Introduction

1.1. Jarosite as a risk to soil and water quality

Jarosite minerals ($XFe_3(SO_4)_2(OH)_6$, where X is typically K or Na) represent a considerable risk to soil and water quality. In the context of acid sulfate soils (ASS), jarosite forms through the oxidation of reduced iron sulfides such as pyrite (FeS_2), and is the principal source of retained acidity (Fanning et al., 2017; Vithana et al., 2013). Retained acidity is an operationally defined form of potential acidity associated with sparingly-soluble minerals, often including alunite ($KAl_3(SO_4)_2(OH)_6$) and schwertmannite ($Fe_{16}(OH,SO_4)_{12\text{-}13}O_{16}.10\text{-}12H_2O$) (Bigham et al., 2002; Vithana et al., 2013, 2014). These minerals slowly release Al^{3+} and Fe^{3+}, which hydrolyse to generate acidity (e.g. $Fe^{3+} + 3H_2O \rightarrow Fe(OH)_3 + 3H^+$). Consequently, soils containing jarosite-rich sulfuric material may display chemically aggressive properties (e.g. pH < 4) for years to decades after the jarosite has formed (Fanning et al., 2017; Mosley et al., 2017; Van Breemen, 1973). Additionally, jarosite has a strong affinity for a range of trace elements (e.g. As, Cr, Pb, Sr and Zn), and may greatly affect their mobility in terrestrial and aquatic ecosystems (Dutrizac and Jambor, 2000; Mosley et al., 2017; Trueman et al., 2020; Welch et al., 2007).

Treatment options for soils containing high amounts of jarosite-rich sulfuric material are limited. Where the disturbance of ASS materials is unavoidable, standard management guidelines emphasise applying alkaline materials (e.g. limestone, $CaCO_3$) to neutralise acidic or potentially acidic soil material (Ahern et al., 2004; Dear et al., 2002; Sullivan et al., 2018). Liming rates are based on the net acidity (mol H^+/tonne), which is a function of the actual and potential pools of soil acidity and alkalinity (i.e. net acidity = actual acidity + retained acidity – acid neutralising capacity). Trueman et al. (2020) describes sulfuric material with 1606 mol H^+/tonne of net acidity, and an accompanying lime requirement of 121 kg $CaCO_3$/tonne. To put this into perspective, liming one hectare of this soil to a depth of 1 m would require 1573 t of $CaCO_3$ (assuming a soil bulk density of 1.3 kg/m^3). In addition to the expense and logistical hurdles posed by such a task, liming efficacy is often greatly reduced by armouring, namely, the formation gypsum ($CaSO_4.2H_2O$) and mixed aluminium and iron (oxyhydr)oxides and hydroxysulfates, which coat and passivate the lime (Hammarstrom et al., 2003).

Due to its insolubility, flushing jarosite from the soil profile is also not a practical option (Trueman et al., 2020). Permanently saturating the soil and adding fresh organic matter should encourage the biologically mediated

*Corresponding author at: School of Agriculture, Food and Wine, The University of Adelaide, Adelaide, SA 5064, Australia.
E-mail address: austin.trueman@adelaide.edu.au (A.M. Trueman)

https://doi.org/10.1016/j.chemgeo.2020.120034
Received 18 August 2020; Received in revised form 15 December 2020; Accepted 16 December 2020

reductive dissolution of jarosite (Kölbl et al., 2018; Yuan et al., 2015). This may be feasible in coastal areas, but is highly impractical inland – especially in drought-prone regions. Moreover, flooding land greatly limits land use opportunities.

Rewetting exposed sulfuric material may present a myriad of risks to the environment and the communities that depend on them (Mosley et al., 2014; Sullivan et al., 2018). For example, post-drought flooding of sulfuric material in the lower River Murray catchment (South Australia) was associated with the acidification and metal(loid) contamination of surface waters in economically and environmentally significant lake-wetland systems (Fitzpatrick et al., 2019; Mosley et al., 2014). Therefore, in the absence of adequate environmental protection laws, land developers may seek to hydraulically isolate sulfuric material (e.g. through land filling and capping practices) to mitigate rewetting. However, this does not remove the environmental risk. Consequently, land treated in this manner is often rezoned for waste disposal, public infrastructure, or industry, which (from an environmental conservation perspective) constitutes an unfortunate loss of valuable soil resource. Therefore, nullifying the environmental risk associated with jarosite without limiting land use opportunities represents an appealing remediation strategy. Passivating jarosite by, for example, encouraging the formation of relatively inert mineral coatings, aligns with this strategy.

1.2. Jarosite passivation strategies

Jarosite is produced as an industrial waste product during the recovery of divalent metals from iron-rich ores (e.g. sphalerite, ZnS_2). Jarosite waste/residue is generally not considered commercially valuable (Dutrizac and Jambor, 2000). Moreover, the recovery of iron from the waste (e.g. through the alkaline or thermal decomposition of jarosite to iron (oxyhydr) oxide) is generally considered uneconomical (Hage and Schuiling, 2000). Consequently, jarosite waste is usually stored in impoundments, which pose considerable risks to soil and water quality (Hage and Schuiling, 2000). Responsibly disposing of jarosite waste has largely motivated the jarosite passivation strategies described below.

Under aerobic, supergene conditions, jarosite typically weathers to form iron (oxyhydr)oxides such as hematite (Fe2O3) and goethite (α-FeOOH) (Brown, 1971; Dutrizac and Jambor, 2000; Van Breemen, 1973). Iron minerals such as these are extremely long-lived (Bigham et al., 2002; Schwertmann and Taylor, 1989); and the apparent persistence of jarosite outside its stability field has been partly accredited to the formation of iron (oxyhydr)oxide rinds or coatings that impede further weathering (Van Breemen, 1973; Welch et al., 2007). The alteration of jarosite to ferric (oxyhydr)oxides can be rapidly achieved by treating jarosite with alkaline materials.

Chen and Dutrizac (2001) found that, after three months, Portland cement (principally $(CaO)_3.SiO_2$) had reacted with the water and jarosite waste to form Ca-Al-Fe oxides and a range of Ca-Al-Fe silicate sulfate-hydrate phases. The overall composition of the treated jarosite product ("Jarofix") was found to be partly reacted jarosite and gypsum ($CaSO_4.2H_2O$). Jarosite treated in this manner was more resistant to physical and chemical weathering (Chen and Dutrizac, 2001). Similarly, jarosite treated with alkaline fly ash (principally SiO_2, Al_2O_3 and CaO) developed a low porosity layer (a mixture of gypsum and poorly-crystalline, iron (oxyhydr)oxides) that lowered the material's overall hydraulic conductivity – and which should mitigate risks associated with leaching (Ding et al., 1998; Ding et al., 2002).

The conversion of jarosite to a sparingly-soluble, ferric phosphate mineral represents a possible alternative passivation strategy. Phosphating is a widely employed metal passivation technique. The process involves treating the metal surface with a phosphate solution to produce a protective coating of relatively inert minerals such as strengite ($FePO_4.2H_2O$), phosphophylite ($Zn_2Fe(PO4)_2.4H_2O$), and hopeite ($Zn_3(PO4)_2.4H_2O$) (Sankara Narayanan, 2005). Similarly, commercially available rust converters primarily contain phosphoric acid, which rapidly alters iron (oxyhydr)oxides to strengite (Ocampo et al., 2004).

Phosphate-based passivation strategies have also been employed to mitigate pyrite oxidation and the accompanying generation of Acid Mine Drainage (AMD). The presence of free Fe^{3+} accelerates pyrite oxidation (Singer and Stumm, 1970). Consequently, several studies describe treating AMD or AMD-affected systems with phosphate salts (e. g. apatite, $Ca_5(PO_4)_3(Cl/F/OH)$) or phosphate-rich solutions in order to complex Fe^{2+}, and to remove Fe^{3+} through the precipitation of ferric phosphate (Spotts and Dollhopf, 1992; Stiller et al., 1989). Similarly, the formation of ferric phosphate coatings over the pyrite also appears to limit pyrite oxidation through surface passivation (Nyavor and Egiebor, 1995). Many ASS with sulfuric material also contain underlying sulfidic material – i.e. soil material (pH > 4) containing substantial quantities of reduced inorganic sulfides (Isbell and The National Committee on Soils and Terrain, 2016). Therefore, phosphate-based treatments may have the potential to amend sulfuric material and curtail further iron sulfide oxidation. However, phosphate-based passivation treatments have yet to be tested on sulfuric material. The principal objectives of this investigation were to: (1) assess whether the surface chemistry of jarosite could be modified to produce sparingly-soluble, relatively benign minerals such as goethite and strengite (2) describe the dissolution chemistry of the treated jarosite.

2. Methods

2.1. Extraction and treatment

The method for extracting and preparing the jarosite was described in Trueman et al. (2020). Large subsoil samples were collected from an ASS with sulfuric material in Gillman, South Australia. The soil contains jarositic segregations that formed around relict mangrove roots, and are referred to as phytotubules (Brewer and Sleeman, 1988). These jarositic phytotubules were hand-picked from the dried soil, then ground down using a mortar and pestle, and sieved to < 250 μm. The resulting mineral powder was thoroughly mixed to create a homogeneous sample, herein referred to as the jarositic powder. The jarositic powder was previously characterised by Trueman et al. (2020), and found to be primarily composed of potassium jarosite with minor quartz and traces of gypsum.

A number of preliminary experiments were performed to gauge the validity of the phosphate-based treatments. These experiments greatly affected the focus and experimental design of the overall investigation, and are therefore outlined here. For the first set of preliminary experiments, 1 g of the jarositic powder was added to 1 L of 0.01 M NH4H2PO4 (monoammonium phosphate, MAP). Air was continually bubbled through the solution with polypropylene tubing to promote mixing and aeration (i.e. to mitigate Fe3+ reduction). This was repeated with 1 L of RO water as a control. After 8 days the solids were separated (using a centrifuge) and oven dried at 40°C for 48 h. The initial aim of this experiment was to employ SEM analysis to describe the nature of any coatings that may have formed during the 0.01 M MAP treatment. However, restrictions to the SEM prohibited this route of investigation. Therefore, the focus shifted from promoting the formation of passivating coatings to promoting changes in the bulk chemical composition that could be measured with available equipment. The bulk chemical composition and dissolution kinetics of the reaction products would then be used to gain insight into jarosite reactivity and the potential use of these treatments to passivate jarosite. Therefore, in order to promote measurable changes in the bulk chemical composition of jarosite, more reactive reagents such as H3PO4 and NaOH were employed for the treatments, and the treatment concentration was increased from 0.01 M to 1 M.

The jarositic powder was treated with the following solutions: 1 M NaOH (pH ~ 14), 10 g/L CaOH2 (pH ~ 13), 1 M MAP (pH 4), and 1 M H3PO4 (pH 1). The aim of the NaOH and CaOH2 treatments were to drive to alkaline decomposition of jarosite to ferric (oxyhydr)oxide. Conversely, the aim of the MAP and H3PO4 treatments were to promote the alteration of jarosite to ferric phosphate. The NaOH and H3PO4 treatments were chosen for their high solubility and reactivity, while

CaOH2 and MAP were selected for their lower cost and greater commercial availability. Control samples were treated with reverse osmosis (RO) water (≥ 18.20 MΩcm). For all these tests, 2 g of the jarositic powder was combined with 40 mL of the treatment solution in 50 mL polypropylene tubes, which were placed in a rotary mixer for 8 days. Treated solids were separated using a centrifuge, oven dried at 40 °C for 48 h, then gently ground using a mortar and pestle, and sieved to < 250 μm to obtain a relatively homogeneous powder for analysis. All treatments were performed in triplicate.

It was suspected during the 1 M MAP and 1 M H3PO4 treatments that the alteration of jarosite to ferric phosphate was sluggish/limited under ambient conditions or low phosphate concentrations. Consequently, a sample of untreated jarositic phytotubule was submerged in 85% H3PO4 to determine if a reaction would proceed under more acidic, phosphate-rich conditions. As discussed in Section 3.1.2, this treatment gradually produced noticeable changes (e.g. colour), which suggested that the transformation of jarosite to ferric phosphate was spontaneous but slow. Consequently, a set of phosphate treatments were also conducted at 80°C in an attempt to improve the reaction kinetics. For these treatments, 4 g of jarositic powder was combined with 80 mL of 1 M MAP or 1 M H3PO4 solution in a stoppered conical flask, which was stirred and heated for 48 h at 80°C using a hotplate stirrer. It was also suspected that any changes caused by the 1 M MAP or H3PO4 treatments alone may have been insignificant or undetectable. Consequently, a set of "two-step" treatments were also conducted to ensure a ferric phosphate sample was obtained for analysis. For these two-step experiments, the jarositic powder was treated with 1 M NaOH (step one) to form ferric (oxyhydr)oxide, then treated with 1 M MAP or 1 M H3PO4 (step two) to produce ferric phosphate. All treatments were performed in triplicate.

2.2. Characterisation

The treated samples were digested in *aqua regia* in two steps: 1 h at 80℃ followed by 3 h at 125℃. The digested samples were then diluted and analysed for the following elements with an Avio 200 Inductively Coupled Plasma Optical Emission Spectrometer (ICP-OES): Al, As, Ca, Fe, K, Mg, Na, P, S and Zn.

Mineralogy was determined using a PANalytical X'Pert Pro Multipurpose Diffractometer. Diffraction patterns were obtained using iron filtered cobalt Kα radiation, an auto divergence slit, a 2° anti-scatter slit, and and a fast X'Celerator silicon strip detector. Diffraction patterns were recorded in steps of 0.016° 2 theta and a 0.4 s counting time per step. Qualitative analysis was performed on the collected data using in-house XPLOT and commercial software HighScore Plus from PANalytical with the PDF4+ 2014 database from the International Centre for Diffraction Data (ICDD).

2.3. Column perfusion experiments

Column perfusion experiments – as described by Baird et al. (2019) and Trueman et al. (2020) – were utilised to assess how certain treatments described in Section 2.1 may have affected the dissolution kinetics of the jarositic powder. As a control, 1 g of untreated jarositic powder was mixed with 1 g of acid-washed quartz sand (210–297 μm, Sigma Aldrich) and loaded into a polypropylene column reactor (V ~ 32 mL) between two pieces of glass wool. The jarositic powder was eluted for 72 h with dilute HCl (pH 4, unbuffered), then for another 72 h with dilute NaOH (pH 10, unbuffered). The leachate, or eluate, was collected in 12 mL polypropylene tubes by a Gilson FC 204 fraction collector. The flowrate was maintained at 5 mL/h by iteratively adjusting the pump speed and tube tension. The pH of the eluate fractions was measured using an Orion 911DJWP micro pH probe. The eluate fractions were acidified with AR grade nitric acid to 0.6% (v/v) and analysed for the following elements using ICP-OES: As, Al, Ca, Fe, K, Mg, Na, P, S, and Zn. This experiment was repeated using 1 g samples of the jarositic powder that had been previously treated (at ambient temperatures) with either 1 M MAP or 1 M NaOH – as per the methods described in Section 2.1. While an eluant pH of 4 was chosen to reflect the pH of a typical ASS with sulfuric material, an eluant pH of 10 was chosen to induce a dramatic change in dissolution dynamics without triggering rapid alkaline decomposition of the jarosite – which tends to occur at eluant pH > 10 (Trueman et al., 2020). Drastic pH jump scenarios such as this can provide key insights into mineral solubility and pH buffering capacity. All column perfusion experiments were performed in triplicate.

3. Results and discussion

The results of the chemical treatment experiments and column dissolution experiments are separately presented and discussed in Sections 3.1 and 3.2, respectively. Section 3.1 is subdivided into three sections that separately discuss the effects that the (i) alkaline treatments (ii) phosphate treatments, and (iii) two-step treatments have on the bulk composition of the jarositic powder. Tables 1 and 2 respectively relate to the results of the acid digestion and XRD analysis described in Section 2.2 of the methods. The results discussed in Section 3.2 only relate to jarositic powder that was treated with 1 M NaOH or 1 M MAP under ambient conditions. Fig. 1 highlights the differences between the eluant (input) and eluate (output) pH over the dissolution test, which helps to contextualise the release rates of key elements (Figs. 2–3). Finally, Section 3.3 provides a brief discussion on the practical concerns and potential negative side effects associated with the application of these treatments in the field.

3.1. Characterisation of the treatment products

3.1.1. NaOH and $Ca(OH)_2$ products

Sodium and calcium hydroxide both readily reacted with the jarositic powder to form dark red solids (2.5YR 3/6) (Fig. S.1). The red solids were primarily composed of iron (Table 1); and displayed two broad XRD peaks (Fig. S.7), which is indicative of two-line ferrihydrite (Eggleton and Fitzpatrick, 1988; Jambor and Dutrizac, 1998). The formation of poorly-crystalline, ferric (oxyhydr)oxides from the alkaline decomposition of jarosite is well documented (e.g. Salinas et al. (2001) and Madden et al. (2012)). For example, Madden et al. (2012) suggests that ferrihydrite and maghemite are the dominant reaction products where pH > 7.5; and that these minerals may be replaced by hematite over time. In addition to the poorly-crystalline ferric (oxyhydr)oxides, the NaOH treatment produced minor amounts of thénardite (Na_2SO_4) (Table 2).

3.1.2. MAP and H_3PO_4 treatments

The MAP and H_3PO_4 treatments that were conducted at ambient temperatures did not produce any changes to the jarositic powder that were apparent with the naked eye. However, both treatments significantly increased the proportion of iron with respect to potassium and sulfur (Table 1). Moreover, both treatments lowered the Fe/P molar ratio from around 550 to 7–9. This was likely a combination of phosphorus adsorption and the formation of new iron-phosphorus phases. Increasing the treatment concentration or temperature appeared to increase the extent of jarosite alteration. For example, submerging an untreated jarositic phytotubule in 85% H_3PO_4 resulted in the slow conversion of jarosite to a white solid over the course of 1 to 2 weeks (Fig. S.2a). Moreover, treating jarosite with 1 M H_3PO_4 at 80℃, resulted in the apparently complete conversion of jarosite to finely textured, white solids (7.5YR 8.5/1) within 6 h (Fig. S.2b). These white solids had an Fe/P ratio of around 0.9, and were found to be principally composed of phosphosiderite (monoclinic $FePO_4.2H_2O$), with minor amounts of gengenbachite ($KFe_3(HPO_4)_4(H_2PO_4)2.6H_2O$) and strengite (orthorhombic $FePO_4.2H_2O$). This suggests that the alteration of jarosite to ferric phosphate is constrained at low temperatures by a high activation energy. Additionally, the initial formation of a ferric phosphate coating could hinder further jarosite alteration.

Table 1. The elemental composition (μmol/g) and selected molar ratios of the untreated and treated jarosite. Values in bold are not statistically different with respect to the untreated jarosite. The first six columns ("untreated" to "NaOH H3PO4") relate to the treatments conducted at ambient temperatures, while the final three columns relate to those conduced at 80◦C. Corresponding RSD and p values are provided in Table S.1.

	25℃						80℃		
	untreated	NaOH	$CaOH_2$	MAP	H_3PO_4	NaOH H_3PO_4	H_2O	MAP	H_3PO_4
micromoles per gram									
Al	137	**119**	**115**	**129**	**153**	539	82.2	71.9	35.7
As	3.25	0.24	3.89	**3.07**	2.21	0.18	5.85	0.10	0.30
Ca	23.2	30.7	2020	3.26	1.64	2.02	**20.8**	16.9	1.45
Fe	5050	6770	4290	**5100**	**5050**	729	2440	2360	2390
K	1250	76.4	154	983	1000	70.7	518	25.7	20.9
Mg	74.7	**78.2**	**70.9**	11.8	12.9	50.3	**71.2**	**68.1**	3.32
Na	845	3380	54.3	270	255	45.2	541	87.8	18.8
P	9.33	2.99	12.6	725	589	1340	7.64	2630	1970
S	3530	173	1890	**2940**	2810	35.5	1540	12.8	64.2
Zn	0.25	0.18	0.11	0.12	0.13	**0.27**	0.15	0.19	**0.26**
molar ratio									
Fe/Al	37.3	56.5	**37.4**	**39.4**	**33.1**	1.35	29.8	32.7	67.0
Fe/K	4.05	88.7	27.8	5.19	5.05	10.5	4.72	92.0	114
Fe/P	549	2370	340	7.03	8.57	0.54	320	0.90	1.24
Fe/S	1.44	39.2	2.27	1.74	1.80	20.7	**1.60**	184	37.4
S/K	2.82	2.26	12.2	2.99	**2.81**	0.50	**2.97**	0.50	3.07

Eqs. (1)–(3) describe possible overall reactions between jarosite and H_3PO_4 to yield strengite/phosphosiderite (Eq. (1)) or gengenbachite (Eq. (2)), along with aqueous potassium and sulfur. The initial pH of the batch solution during the treatment was 0.90 (± 0.02). The final pH was < 0.90, but was subject to considerable drift. Given that the pK_{a1} of H_3PO_4 is 1.95, it is reasonable to assume that H_3PO_4 was the dominant phosphate species during the reaction.

$KFe_3(SO_4)_2(OH)_{6(s)} + 3H_3PO_{4(aq)} \rightarrow 3FePO_4.2H_2O_{(s)} + K^+_{(aq)} + 2SO_4^{2-}{}_{(aq)} + 3H^+_{(aq)}$, (1)

$KFe_3(SO_4)_2(OH)_{6(s)} + 6H_3PO_{4(aq)} \rightarrow KFe_3(HPO_4)_4(H_2PO_4)_2.6H_2O_{(s)} + 2SO_4^{2-}{}_{(aq)} + 4H^+_{(aq)}$, (2)

$KFe_3(SO_4)_2(OH)_{6(s)} + 4.5H_3PO_{4(aq)} \rightarrow 0.5KFe_3(HPO_4)_4(H_2PO_4)_2.6H_2O_{(s)} + 1.5FePO_4.2H_2O_{(s)} + 0.5K^+_{(aq)} + 2SO_4^{2-}{}_{(aq)} + 3.5H^+_{(aq)}$, (3)

Phosphosiderite and gengenbachite may have formed contemporaneously via independent reaction pathways, or sequentially. Jarosite dissolves relatively congruently under extremely acidic conditions (i.e. pH < 2) (Trueman et al., 2020). The pH in the reactor remained well below 2 throughout the treatment. Therefore, jarosite may have dissolved congruently until the solution became supersaturated with respect to phosphosiderite and gengenbachite – the former precipitating out of solution in greater amounts. Alternatively, jarosite may have been sequentially altered to gengenbachite then phosphosiderite (e.g. through the successive substitution of structural sulfate for phosphate).

Accounts of naturally occurring gengenbachite are rare, but considering natural occurrences may provide insight into jarosite alteration pathways. Gengenbachite and haigerachite ($KFe_3(HPO_4)_2(H_2PO_4)_2.4H_2O$) found in the Silberbrunnle Mine (Germany) tailings occurred as crusts on quartz, and were associate with pyrite, gypsum, jarosite and diadochite ($Fe_2(PO_4)(SO_4)_2(OH).5H_2O$) (Walenta et al., 2007). This assemblage suggests that gengenbachite formed through sequential alteration of pyrite, for example: pyrite → jarosite and gypsum → gengenbachite, haigerachite and diadochite. Additionally, the lack of strengite in this assemblage suggests that alteration of jarosite to strengite is not favourable under supergene conditions, which is consistent with the results of the 25℃ H_3PO_4 treatment.

Reacting jarosite with MAP at 80℃ produced a hydrogen ammonium ferric phosphate ($H_2(NH_4)Fe(PO_4)_2$) (herein referred to as HAIP), and minor amounts of spheniscidite ($(NH_4,K)(Fe,Al)_2(PO_4)_2(OH).2H_2O$) (Table 2). The HAIP appeared as small (< 0.5 mm), spherical crystals or crystalline aggregates (colourless, vitreous lustre) (Fig. S.3b). Roughly half of the jarosite remained after the treatment. This suggests that the reaction between jarosite and MAP was constrained – even at elevated temperatures. Eq. (4) provides a possible overall reaction for the direct alteration of jarosite to HAIP. The alteration of jarosite to spheniscidite is not presented as it is more likely that spheniscidite formed from ferric (oxyhydr)oxide – as discussed in Section 3.1.3. Ammonium jarosite was not detected. Jarosites (including ammonium jarosite) are commonly prepared at 1.7 < pH < 2.3 and 60–100℃ (Das et al., 1996). The reactor pH during the 80℃ MAP treatment hovered around 3.87 (± 0.13). Consequently, the relatively high pH and concentration of phosphate (as H_2PO_4) was likely more favourable for the formation of HAIP than ammonium jarosite.

$KFe_3(SO_4)_2(OH)_{6(s)} + 6NH_4H_2PO_{4(aq)} \rightarrow 3H_2(NH_4)Fe(PO_4)_{2(s)} + K^+_{(aq)} + 2SO_4^{2-}{}_{(aq)} + 3NH_4^+{}_{(aq)} + 6H_2O$, (4)

3.1.3. Two-step treatment

As discussed in Section 3.1.1, jarosite has been shown to rapidly undergo alkaline decomposition to produce ferric (oxyhydr)oxides. Moreover, iron (oxyhydr)oxides have been shown to rapidly react with H_3PO_4 to produce strengite (Ocampo et al., 2004). Therefore, it was assumed that sequentially treating the jarositic powder with an alkaline solution then a H_3PO_4 solution would yield strengite. The product of this two-step treatment could thus be utilised as an additional tool to compare and contrast the products of the phosphate treatments described in Section 3.1.2. Additionally, the two-step treatments provided unexpected insights into the formation of other phosphate minerals.

As a preliminary experiment, an untreated jarositic phytotubule was immersed in 1 M NaOH for 48 h, rinsed with RO water, then immersed in 1 M H_3PO_4. Over a few hours in the H_3PO_4 solution, the jarosite changed colour from red to white. The beaker containing this sample was left out under ambient conditions for 3 weeks, during which the liquid evaporated and small, spherical aggregates (waxy to dull lustre) appeared (Fig. S.4a). It was suspected that these aggregates were strengite, which tends to be poorly-crystalline at low temperatures, but begins to

Table 2. Reaction products (confirmed via XRD analysis) of the high temperature treatments (with the exception of the NaOH treatment). Estimated abundances were normalised to 100% and are included only as a rough guide. The relevant XRD spectra are provided in the supplementary materials. Hydrogen ammonium iron phosphate is abbreviated as HAIP.

Treatment	T (℃)	Reaction Products	Formula
H_2O	80	Jarosite (95%)	$KFe_3(SO_4)_2(OH)_6$
		Quartz (5%)	SiO_2
1 M NaOH	25	Non-crystalline (major)	–
		Quartz (minor)	SiO_2
		Thénardite (minor)	Na_2SO_4
		Rutile (trace)	TiO_2
1 M H_3PO_4	80	Phosphosiderite (71%)	$FePO_4.2H_2O$ (monoclinic)
		Gengenbachite (19%)	$KFe^{3+}{}_3(HPO_4)_4(H_2PO_4)_2.6H_2O$
		Strengite (5%)	$FePO_4.2H_2O$ (orthorhombic)
		Quartz (4%)	SiO_2
1 M $NH_4H_2PO_4$	80	HAIP (45%)	$H_2(NH_4)Fe(PO_4)_2$
		Jarosite (44%)	$KFe_3(SO_4)_2(OH)_6$
		Biphosphammite (5%)	$NH_4(H_2PO_4)$
		Quartz (4%)	SiO_2
		Spheniscidite (3%)	$(NH_4,K)(Fe^{3+},Al)_2(PO_4)_2(OH).2H_2O$
1 M NaOH then 1 M $NH_4H_2PO_4$	80	Spheniscidite (93%)	$(NH_4,K)(Fe^{3+},Al)_2(PO_4)_2(OH).2H_2O$
		Quartz (4%)	SiO_2
		Biphosphammite (2%)	$NH_4(H_2PO_4)$

crystallise at around 75℃ (Cate et al., 1959). Consequently, the beaker was placed in an oven at 80℃. Over the course of three days, the white aggregates recrystallised as individual euhedral crystals, which displayed a vitreous lustre and appeared to have a monoclinic (or possibly trigonal) symmetry (Fig. S.4b-d). These characteristics are consistent with phosphosiderite: a monoclinic, metastable dimorph of strengite (orthorhombic). Under ambient conditions, these crystals decomposed back into the white, spherical aggregates.

Following this preliminary experiment, a two-step treatment was trialled, whereby jarosite was first reacted with NaOH to produce ferric (oxyhydr)oxides, which were then treated with H_3PO_4 or MAP with the intent of producing strengite. At ambient and elevated temperatures, H_3PO_4 reacted with the ferric (oxyhydr)oxides to produce finely textured, white solids (Fig. S.2b). The bulk elemental composition of these white solids was considerably different than that of the control (Table 1), being principally composed of aluminium, iron and phosphorous. The Fe/Al ratio of 1.3 is suggestive of aluminium strengite ($(Fe,Al)PO_4.2H_2O$). Alternatively, the sample may have contained both strengite and an aluminium phosphate species such as variscite ($AlPO_4.2H_2O$). A Fe/P ratio of 0.54 is lower than that of ideal strengite (Fe/ P = 1). This may have simply been due to an excess of phosphate in the sample. Alternatively, if both strengite and variscite are assumed to have been present in, for example, equal proportions, then Fe/P and Al/P values respectively increase to 1.09 and 0.81. Unfortunately, restricted access to appropriate equipment precluded further investigation of the sample's mineralogy.

Treating jarosite with NaOH then MAP at 80℃ produced finely textured, brown solids (7.5YR 5/4). Spherical crystals or crystalline aggregates (colourless to red, vitreous lustre, 30–80 μm) were apparent upon magnification (Fig. S.5). These crystals were likely spheniscidite, which the XRD results indicate was the principal reaction product of the 80℃ NaOH-MAP treatment. In contrast, only trace amounts of spheniscidite formed during the 80℃ MAP treatment. This suggests that spheniscidite does not form directly through jarosite alteration, but through the reaction of ferric (or aluminium) (oxyhydr)oxides with MAP (Eqs. (5)–(7)).

$$Fe(OH)_{3(s)} + NH_4H_2PO_{4(aq)} + 0.5H^+_{(aq)} \rightarrow 0.5NH_4Fe_2(PO_4)_2(OH).2H_2O_{(s)} + 0.5NH_4^+{}_{(aq)} + 1.5H_2O, \quad (5)$$

$$FeO(OH)_{(s)} + NH_4H_2PO_{4(aq)} + 0.5H^+_{(aq)} \rightarrow 0.5NH_4Fe_2(PO_4)_2(OH).2H_2O_{(s)} + 0.5NH_4^+{}_{(aq)} + 0.5H_2O, \quad (6)$$

$$Fe_2O_{3(s)} + 2NH_4H_2PO_{4(aq)} + 3H^+_{(aq)} \rightarrow NH_4Fe_2(PO_4)_2(OH).2H_2O_{(s)} + NH_4^+{}_{(aq)}, \quad (7)$$

3.2. Column perfusion experiments

Column perfusion experiments were utilised to describe the dissolution chemistry of the jarosite samples treated at ambient temperatures with either: (i) RO water (i.e. the control), (ii) 1 M NaOH, and (iii) 1 M MAP. The changes in eluant pH, relative to eluate pH, during the dissolution experiment is shown in Fig. 1. It is immediately evident that the NaOH-treated jarosite contained enough residual alkalinity to completely neutralise the acidic eluant. Similarly, the MAP remaining in the MAP-treated jarosite may have provided some pH buffering capacity. Conversely, there was very little difference between the eluant and eluate pH during the dissolution of the control sample at pH 4.

During the pH 10 test, the average absolute difference between eluant and eluate pH was 3.5 (± 0.89) for the control, 4.36 (± 0.79) for the MAP-treated jarosite, and 2.17 (± 0.30) for the NaOH-treated jarosite. The higher pH buffering capacity of the MAP-treated jarosite was likely due to the pH buffering effect of residual MAP. The NaOH-treated jarosite also appears to have released acidity or consumed hydroxide during the pH 10 test. It's possible that, despite the NaOH treatment, the sample still contained partially hydrolysed aluminium and iron, which consumed hydroxide during the pH 10 interval. Similarly, other trace elements may also have formed relatively stable hydroxide phases at pH 8–10 (e.g. Mg(OH)2, Zn(OH)).

The rates at which key elements were released during the dissolution experiments are summarised in Fig. 2. The rates were calculated over 72 h intervals, namely, from 0 to 72 h and 72–144 h. For discussion purposes the first and second intervals are referred to herein as the "pH 4 interval" and "pH 10 interval", respectively, in reference to the eluant pH. Note that Table S.2 provides the rate values presented in Fig. 2.

Ideally, the passivation treatments should have dramatically reduced the release of iron, which is a key risk associated with jarosite dissolution. The MAP-treated jarosite displayed a significantly lower rate of iron release during the pH 10 interval. However, this was the only significant difference observed. In Fig. 3 it appears that the control released several times more iron than both treatments. However, this difference was not

significant – primarily due to the high degree of error (ca. 50–73% RSD) in the control test. Consequently, it could be argued that the control contains and outlier.

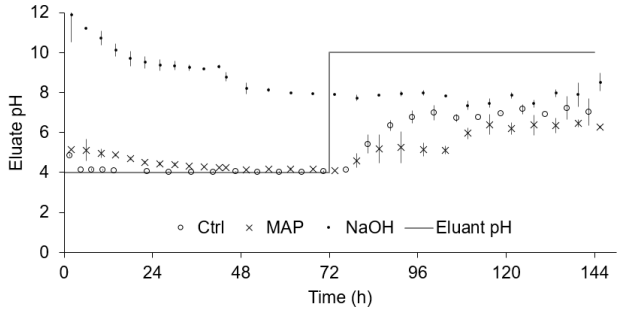

Fig 1. Eluate pH during the dissolution of the control ("Ctrl"), the 25◦*C* MAP-treated jarosite ("MAP") and the 25◦*C* NaOH-treated jarosite ("NaOH"). The eluant pH is shown as a solid line. Error bars represent standard deviation.

To test this, pseudoreplicates were obtained from a number of similar dissolution experiments described by Trueman et al. (2020). Analysing the control dataset along with the pseudoreplicates suggests that the upper extreme (fastest rate) in the control dataset is an outlier. Repeating the tests with and without this upper extreme results in no significant differences between the control and treatments. Note that this argument is given in more detail, and with the relevant statistical evidence, in Section 2 of the supplementary material. In light of these results, it is unlikely that the treatments meaningfully reduced the release of iron.

The source of variance during the control test isn't completely clear, but could be related to a leaky reactor. The release of iron from the first replicate is initially greater than the other replicates by a factor of 14. This factor decreases to 4 by 58 h, to 2 by 120 h and to 1.5 by 144 h. Therefore, it is likely jarosite powder was initially leaking from the column into the eluate fractions; and that this leak subsided over time.

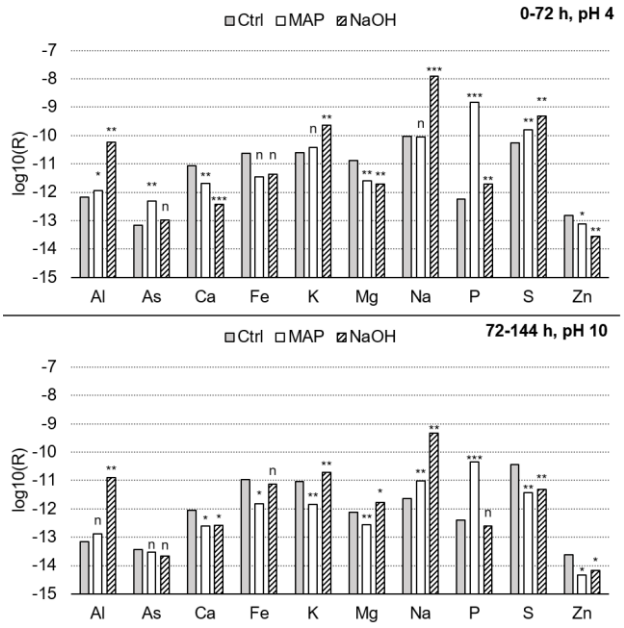

Fig. 2. Analyte release rates (R, mol/s), expressed in log form, during the dissolution of untreated jarosite ("Ctrl"), MAP-treated jarosite ("MAP"), and NaOH-treated jarosite ("NaOH"). The top graph (labelled "0-72 h, pH 4") shows analyte release rates during the first 72 h of the experiment, where the solid was eluted with dilute HCl (pH 4). Conversely, the bottom graph (labelled "72-144 h, pH 10") shows analyte release rates during the second half of the experiment (i.e. 72–144 h), where the solid was eluted with dilute NaOH (pH 10). Significance indicators correspond to a 95% confidence interval (n = 3).

The NaOH-treated jarosite released aluminium at a rate 1–2 orders of magnitude greater than the control and MAP-treated jarosite (regardless of eluant pH). Consequently, in this way the NaOH-treated jarosite could pose a greater environmental risk than untreated jarosite. Similarly, aluminium and arsenic were released at a significantly greater rate by the MAP-treated jarosite. Conversely, both treatments released zinc at a significantly lower rate than the control.

Relative to the control, the NaOH-treated jarosite released significantly more sulfur during the pH 4 interval, and less sulfur during the pH 10 interval. Similarly, the MAP-treated jarosite released more sulfur during the pH 4 interval and less potassium and sulfur during the pH 10 interval. Trueman et al. (2020) showed that the release of sulfur and potassium (as well as calcium, magnesium and sodium) is initially relatively rapid – regardless of pH – due to the dissolution of more soluble phases admixed with the sample (e.g. gypsum). This pattern is apparent in Fig. 3. Consequently, the treatments effectively increased the relative proportion of soluble potassium and sulfur phases. While the NaOH treatment produced thénardite, the MAP treatment did not produce any distinct sulfur-rich solids. Consequently, a portion of sulfate released during the MAP treatment (possibly encouraged by sulfate-phosphate substitution) may have simply become adsorbed to the bulk solid phase.

The NaOH- and MAP-treated jarosite, contained more sodium and phosphorus, respectively, than the untreated jarosite. Therefore it is not surprising that the NaOH- and MAP-treated jarosite released significantly more sodium and phosphorus, respectively (regardless of pH).

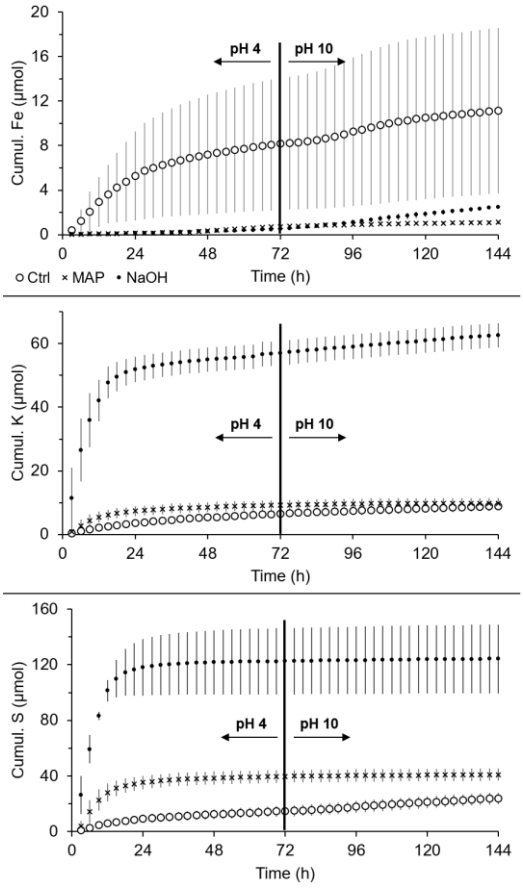

Fig. 3. Cumulative release of Fe, K and S during the dissolution of the untreated jarosite ("Ctrl"), MAP-treated jarosite ("MAP") and NaOH-treated jarosite ("NaOH"). Samples were eluted with dilute HCl (pH 4, unbuffered) for the first 72 h, then with dilute NaOH (pH 10, unbuffered) for another 72 h. Error bars represent standard deviation.

3.3. Practical considerations

The practicality of these treatments in the field, although outside the scope of this study, is worth briefly discussing here. Administering these treatments in the field presents a number of concerns and logistical

hurdles. The hydraulic conductivity of sulfuric material is highly variable (Johnston et al., 2009). Consequently, evenly incorporating treatments (as a solid or solution/slurry) with the soil at depth (e.g. through deep tilling techniques) may be required to bring the treatment in contact with jarosite. However, not only would this be costly, it may not be practically possible in some cases. For example, the soil may be too poorly-structured, saturated or cohesive to support effective tilling.

The uncertain behaviour of the different treatments in soils with sulfidic and sulfuric materials is also an issue. Compared to other soil materials (e.g. basic sulfate salts, metal (oxyhydr)oxides, organic matter and phyllosilicates), jarosite is relatively inert (at least under acidic conditions) and has a low surface area. Consequently, the treatment may be consumed, immobilised or passivated before interacting with jarosite. Therefore, an excess of the treatment would likely be required to achieve the desired results and may generate other on- and off-site risks. For example, an excess of alkalinity may mobilise a range of elements as various minerals begin to decompose. In the case of a phosphate-based treatment, an excess of phosphate (and, in the case of MAP, ammonium) may result in the eutrophication of adjacent aquatic ecosystems. Note too that the reaction between jarosite and H3PO4 appeared to generate acidity (Eqs. (1)–(3)), which is counterproductive to the goal of reducing the release of retained acidity. Therefore, additional land management efforts may be required to mitigate these risks (e.g. collecting and treating soil drainage). In some cases, managing acute risks such as these may be desirable when compared to chronic risk imposed by unmitigated jarosite weathering. However, in general, the logistical hurdles and environmental risks posed by the treatments described here greatly detract from their suitability as ameliorants for jarosite-rich soil and sediment. That being said, the results of this study are not conclusive enough to dismiss passivation-based remediation strategies altogether. Therefore, the shortcomings identified in this study should be utilised to design more effective, practical passivation-based treatments for jarosite-rich materials.

4. Conclusions

In the context of remediating ASS with jarosite-rich sulfuric material, a once-off treatment designed to remove or passivate jarosite without reducing soil and water quality, and land use options is extremely appealing. Jarosite, extracted from an ASS with sulfuric material, was treated with a view to produce sparingly-soluble, relatively benign minerals such as goethite and strengite. Jarosite readily reacted with NaOH and Ca(OH)2 under ambient and elevated temperatures to produce poorly-crystalline ferric (oxyhydr)oxides. However, due to the high pH of these treatments, a substantial portion of aluminium was mobilised, as demonstrated by the dissolution experiments. Consequently, treating jarosite-rich soil with strongly alkaline material may remove jarosite through alkaline decomposition, but may mobilise hazardous elements such as aluminium.

Treating jarosite with phosphate-rich solutions produced ferric phosphate minerals such as strengite/phosphosiderite, gengenbachite and H2(NH4)Fe(PO4)2. However, the alteration of jarosite to ferric phosphate appears to be very limited at ambient temperatures. Investigating the changes to jarosite surface chemistry (e.g. using SEM) may help clarify why the reaction is limited at ambient temperatures. For example, the initial formation of a ferric phosphate coating over the jarosite may have hindered further reaction. Additionally, it may be worth exploring the use of chemical additives to, for example, catalyse the alteration reaction, or change certain characteristics (e.g. thickness, uniformity or porosity) of any coatings that may formed. The two-step treatments provided an alternative route of converting jarosite to ferric phosphate at ambient temperatures; and also showed how spheniscidite may form through the alteration of ferric (oxyhydr)oxides.

The dissolution experiments suggest that neither the NaOH nor MAP treatment offers any distinct advantages in terms of curtailing the release of potentially hazardous elements. However, these experiments only provide a glimpse of how altered jarosite may be expected to behave in the environment. Consequently, in light of the results of both the alteration and dissolution experiments, the treatments described in this study do not appear to be suitable for mitigating the environmental risk associated with the dissolution of jarosite. However, passivation-based remediation strategies as a whole are still very appealing and worth pursuing. Therefore, further investigation is required to determine if these or alternative passivation treatments could be employed in the field; and how such treatments compare to other conventional and alternative remediation strategies.

Declaration of Competing Interest

The authors declare that they have no known competing financial interests or personal relationships that could have appeared to influence the work reported in this paper.

Acknowledgements

We would like to acknowledge Bogumila Tomczak for ICP-OES analysis, and Mark Raven and Peter Self for XRD analysis. This work was supported by Australian Research Council Discovery Project (DP170104541) funding.

References

Ahern, C.R., Mcelnea, A.E., Sullivan, L.A., 2004. Acid sulfate soils laboratory methods guidelines, Queensland Department of Natural Resources, Mines and Energy, Indooroopily, Queensland, Australia.

Baird, R., Da Silva, R.C., Degryse, F., Mclaughlin, M.J., 2019. A column perfusion test to assess the kinetics of nutrient release by soluble, sparingly soluble and coated granular fertilizers. Journal of Plant Nutrition and Soil Science, 182(5): 763-771. https://doi.org/10.1002/jpln.201800666.

Bigham, J., Fitzpatrick, R.W., Schulze, D., 2002. Iron oxides. In: Dixon, J.B., Schulze, D. (Eds.), Soil mineralogy with environmental applications. SSSA, pp. 323-366.

Brown, J.B., 1971. Jarosite-geoethite stabilities at 25°C, 1 atm. Mineralium Deposita, 6(3): 245-252. https://doi.org/10.1007/bf00208032.

Chen, T., Dutrizac, J., 2001. Jarofix: Addressing iron disposal in the zinc industry. JOM, 53(12): 32-35. https://doi.org/10.1007/s11837-001-0010-2.

Dear, S.E., Moore, N.G., Dobos, S.K., Watling, K.M., Ahern, C.R., 2002. Soil management guidelines, Department of Natural Resources and Mines, Indooroopilly, Queensland, Australia.

Ding, M., Geusebroek, M., Van Der Sloot, H., 1998. Interface precipitation affects the resistance to transport in layered jarosite/fly ash. Journal of Geochemical Exploration, 62(1-3): 319-323. https://doi.org/10.1016/S0375-6742(97)00062-9.

Ding, M., Schuiling, R., Van Der Sloot, H., 2002. Self-sealing isolation and immobilization: A geochemical approach to solve the environmental problem of waste acidic jarosite. Applied Geochemistry, 17(2): 93-103. https://doi.org/10.1016/S0883-2927(01)00099-3.

Dutrizac, J.E., Jambor, J.L., 2000. Jarosites and their application in hydrometallurgy. Reviews in Mineralogy and Geochemistry, 40(1): 405-452. https://doi.org/10.2138/rmg.2000.40.8.

Fanning, D.S., Rabenhorst, M.C., Fitzpatrick, R.W., 2017. Historical developments in the understanding of acid sulfate soils. Geoderma, 308: 191-206. https://doi.org/10.1016/j.geoderma.2017.07.006

Hage, J., Schuiling, R., 2000. Comparative column elution of jarosite waste and its autoclaved product – evidence for the immobilization of deleterious elements in jarosite. Minerals Engineering, 13(3): 287-296. https://doi.org/10.1016/S0892-6875(00)00008-X.

Hammarstrom, J.M., Sibrell, P.L., Belkin, H.E., 2003. Characterization of limestone reacted with acid-mine drainage in a pulsed limestone bed treatment system at the Friendship Hill National Historical Site, Pennsylvania, USA. Applied Geochemistry, 18(11): 1705-1721. https://doi.org/10.1016/S0883-2927(03)00105-7.

Isbell, R.F., The National Committee on Soils and Terrain, 2016. The Australian soil classification. CSIRO publishing.
Johnston, S.G., Hirst, P., Slavich, P.G., Bush, R.T., Aaso, T., 2009. Saturated hydraulic conductivity of sulfuric horizons in coastal floodplain acid sulfate soils: Variability and implications. Geoderma, 151(3): 387-394. https://doi.org/10.1016/j.geoderma.2009.05.010.
Kölbl, A., Marschner, P., Mosley, L., Fitzpatrick, R., Kögel-Knabner, I., 2018. Alteration of organic matter during remediation of acid sulfate soils. Geoderma, 332: 121-134. https://doi.org/10.1016/j.geoderma.2018.06.024.
Madden, M.E., Madden, A.S., Rimstidt, J.D., Zahrai, S., Kendall, M.R., Miller, M.A., 2012. Jarosite dissolution rates and nanoscale mineralogy. Geochimica et Cosmochimica Acta, 91: 306-321. https://doi.org/10.1016/j.gca.2012.05.001.
Mosley, L.M. et al., 2017. Prolonged recovery of acid sulfate soils with sulfuric materials following severe drought: Causes and implications. Geoderma, 308: 312-320. https://doi.org/10.1016/j.geoderma.2017.03.019.
Mosley, L.M., Shand, P., Self, P., Fitzpatrick, R., 2014. The geochemistry during management of lake acidification caused by the rewetting of sulfuric (pH<4) acid sulfate soils. Applied Geochemistry, 41: 49-61. https://doi.org/10.1016/j.apgeochem.2013.11.010.
Nriagu, J.O., 1972. Solubility equilibrium constant of strengite. American Journal of Science, 272(5): 476-484.
Nyavor, K., Egiebor, N.O., 1995. Control of pyrite oxidation by phosphate coating. Science of the Total Environment, 162(2-3): 225-237.
Ocampo, L.M., Margarit, I., Mattos, O.R., Córdoba-De-Torresi, S., Fragata, F.D.L., 2004. Performance of rust converter based in phosphoric and tannic acids. Corrosion Science, 46(6): 1515-1525. https://doi.org/10.1016/j.corsci.2003.09.021.
Salinas, E., Roca, A., Cruells, M., Patiño, F., Córdoba, D., 2001. Characterization and alkaline decomposition–cyanidation kinetics of industrial ammonium jarosite in NaOH media. Hydrometallurgy, 60(3): 237-246. https://doi.org/10.1016/S0304-386X(01)00149-9.
Sankara Narayanan, T., 2005. Surface pretretament by phosphate conversion coatings – a review. Reviews in Advanced Materials Science, 9: 130-177.
Schwertmann, U., Taylor, R.M., 1989. Iron oxides. In: Dixon, J.B., Weed, S.B. (Eds.), Minerals in soil environments. SSSA, Madison, WI, pp. 379-438. https://doi.org/10.2136/sssabookser1.2ed.c8.
Singer, P.C., Stumm, W., 1970. Acidic mine drainage: The rate-determining step. Science, 167(3921): 1121. https://doi.org/10.1126/science.167.3921.1121.
Spotts, E., Dollhopf, D.J., 1992. Evaluation of phosphate materials for control of acid production in pyritic mine overburden. Journal of Environmental Quality, 21(4): 627-634. https://doi.org/10.2134/jeq1992.00472425002100040017x.
Stiller, A.H., Renton, J.J., Rymer, T.E., 1989. An experimental evaluation of the use of rock phosphate (apatite) for the amelioration of acid-producing coal mine waste. Mining Science and Technology, 9(3): 283-287. https://doi.org/10.1016/S0167-9031(89)90985-7.
Sullivan, L., Ward, N., Toppler, N., Lancaster, G., 2018. National acid sulfate soils guidance: National acid sulfate soils identification and laboratory methods manual, Department of Agriculture and Water Resources, Canberra, ACT. CC BY 4.0.
Trueman, A.M., Mclaughlin, M.J., Mosley, L.M., Fitzpatrick, R.W., 2020. Composition and dissolution kinetics of jarosite-rich segregations extracted from an acid sulfate soil with sulfuric material. Chemical Geology, 543: 119606. https://doi.org/10.1016/j.chemgeo.2020.119606.
Van Breemen, N., 1973. Soil forming processes in acid sulfate soils. In: Dost, H. (Editor), Proceedings of the International Symposium on Acid Sulfate Soils. Internal Institute for Land Reclamation and Improvement, Wageningen, The Netherlands, pp. 66-130
Vithana, C.L., Sullivan, L.A., Bush, R.T., Burton, E.D., 2013. Acidity fractions in acid sulfate soils and sediments: Contributions of schwertmannite and jarosite. Soil Research, 51(3): 203-214. https://doi.org/10.1071/SR12291.
Vithana, C.L., Sullivan, L.A., Bush, R.T., Burton, E.D., 2014. Jarosite quantification in soils: An enhanced sequential extraction procedure. Applied Geochemistry, 51: 130-138. https://doi.org/10.1016/j.apgeochem.2014.10.006.
Walenta, K., Theye, T., Hatert, F., 2007. Gengenbachit, $KFe_3(H_2PO_4)_2(HPO_4)_4.6H_2O$, ein zweites neues phosphatmineral von der grube silberbrünnle bei gengenbach, im mittleren schwarzwald, nunmehr eine anerkannte neue mineralart. Aufschluss (Der), 58: 125-128.
Welch, S.A., Christy, A.G., Kirste, D., Beavis, S.G., Beavis, F., 2007. Jarosite dissolution I — trace cation flux in acid sulfate soils. Chemical Geology, 245(3): 183-197. https://doi.org/10.1016/j.chemgeo.2007.07.028.
Yuan, C., Fitzpatrick, R., Mosley, L.M., Marschner, P., 2015. Sulfate reduction in sulfuric material after re-flooding: Effectiveness of organic carbon addition and pH increase depends on soil properties. Journal of Hazardous Materials, 298: 138-145. https://doi.org/10.1016/j.jhazmat.2015.05.013.

Exploring passivation-based treatments for jarosite from an acid sulfate soil

A.M. Trueman *[a,b], M.J. McLaughlin [a], L.M. Mosley [b], R.W. Fitzpatrick [b, c]

[a] School of Agriculture, Food and Wine, The University of Adelaide, Adelaide SA 5064, Australia
[b] Acid Sulfate Soils Centre (ASSC), School of Biological Sciences, The University of Adelaide, Adelaide SA 5064, Australia
[c] CSIRO Land and Water, Adelaide SA 5064, Australia

*Corresponding author. Email: austin.trueman@adelaide.edu.au, austin.trueman@outlook.com

Supplementary Material

1. Figures and tables related to the treatment of jarosite

All images in Fig. S.1-5 were captured using NIS Elements (V4.60.00) and a Nikon DS-Fi3 camera mounted on a Nikon SMZ 74ST stereomicroscope.

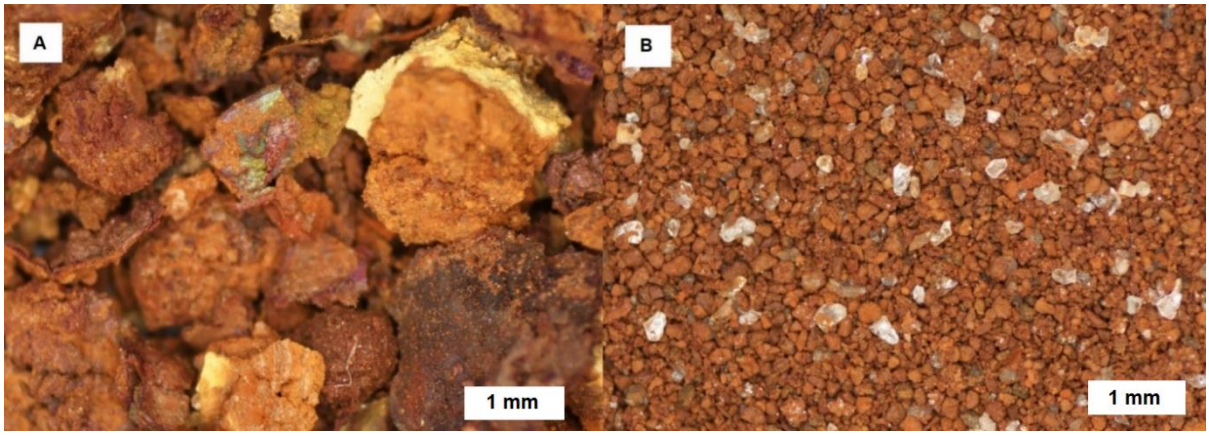

Figure S.1. Examples of jarosite-rich soil segregations treated with 1 M NaOH. Figure S.1A shows fragments of a jarositic phytotubule submerged in 1 M NaOH. Note that jarosite (yellow) was still present in some areas after the treatment, suggesting that the diffusion of NaOH through the pedotubule is variable. Also note that some fragments display a wider range of colours (e.g. green, purple), which is characteristic of iridescent or rainbow hematite. Figure S.1B shows the jarositic powder after being treated with NaOH.

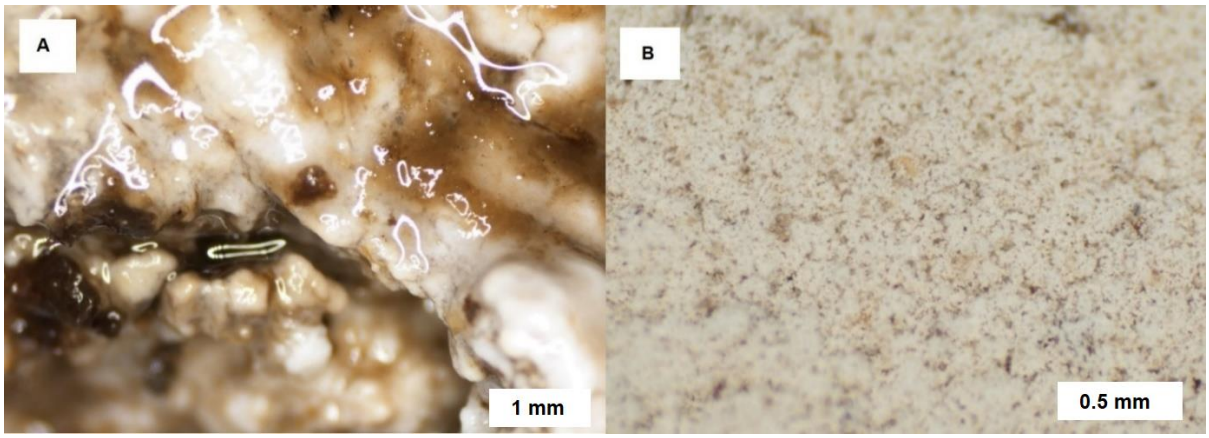

Figure S.2A shows the jarositic phytotubule submerged in 85% H_3PO_4 for 2 weeks. Figure 2.B shows phosphosiderite (monoclinic $FePO_4.2H_2O$), which formed through the reaction of the jarositic powder sample with 1 M H_3PO_4 at 80℃ for 48 hours. The white solid in Fig. S.2A is likely strengite (orthorhombic, poorly-crystalline $FePO_4.2H_2O$).

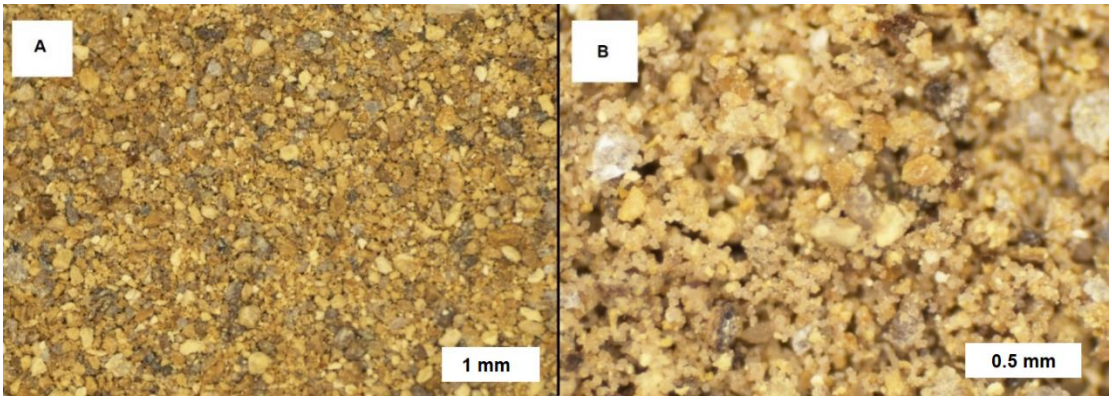

Figure S.3A shows the jarositic powder sample after it was heated in RO water at 80℃ as a control for the 80℃ treatments. Figure S.3B shows the jarositic powder after it was treated with MAP at 80℃. Note the small, spherical crystals in S.3.B, which are absent in the control sample. These are possibly $H_2(NH_4)Fe(PO_4)_2$.

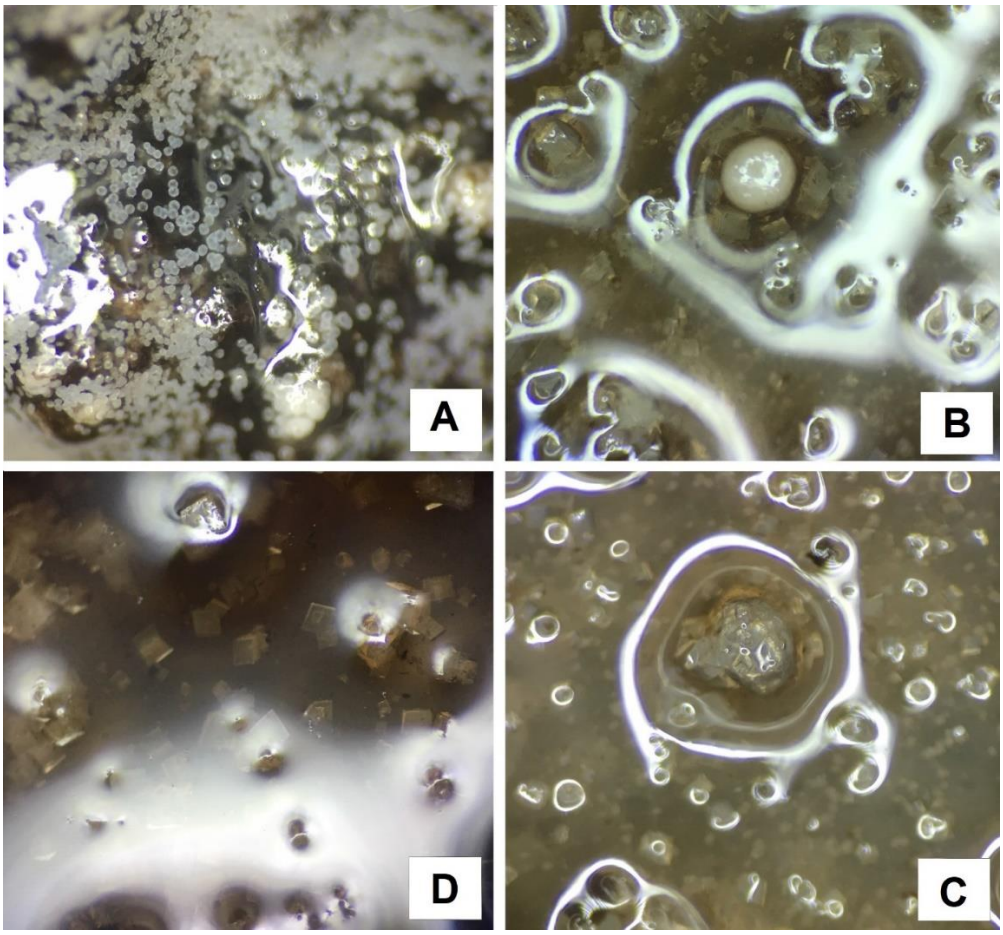

Figure S.4A shows waxy/dull, white to colourless, spherical aggregates of strengite that formed after treating a jarositic phytotubule with NaOH, then H_3PO_4. Heating the sample at 80℃ caused the aggregates to recrystallise, as shown in Fig. S.4B-D. The crystals display a vitreous lustre and possibly a monoclinic symmetry. Scale bars are not available, however the small aggregates in Figure S.4A were < 0.5 mm, the larger aggregate in Fig. S.4B and C was 2-3 mm in diameter, and the crystals in Fig. S.4D were typically 0.5-1 mm across the longest axis.

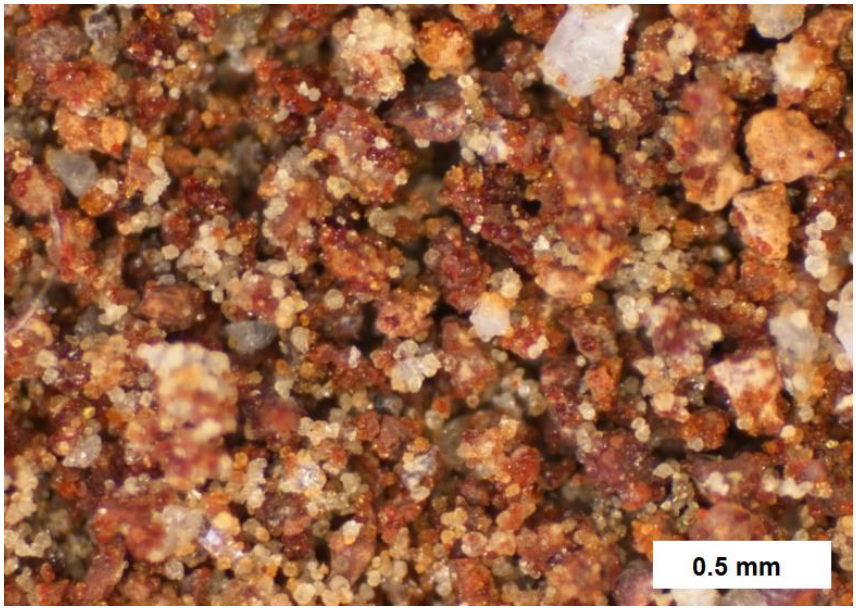

Figure S.5. The jarositic powder after being treated with NaOH then with MAP at 80℃. Note the small, spherical grains (red to colourless, vitreous lustre), which are likely spheniscidite: $(NH_4,K)(Fe, Al)_2(PO_4)_2(OH).2H_2O$.

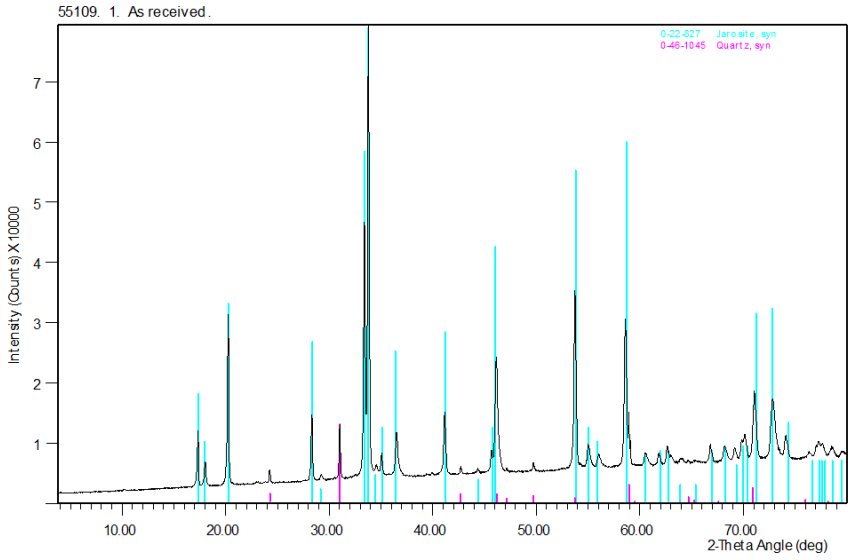

Figure S6. X-ray diffraction pattern of the jarositic powder after being treated with RO water at 80℃ for 48 hours. The XRD pattern shows that the resulting solids were principally composed of jarosite and quartz. Consequently, this treatment did not affect the mineralogy of the jarosite-rich sample.

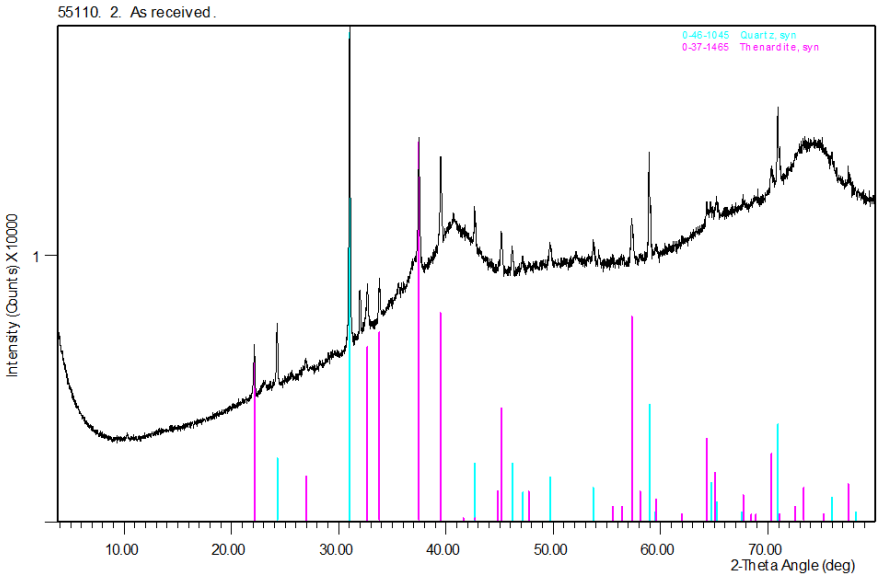

Figure S.7. X-ray diffraction pattern of the jarositic powder after being treated with 1 M NaOH at ambient temperatures for 48 hours. The broad XRD peaks indicates that the resulting solids were principally poorly-crystalline (likely 2-line ferrihydrite), and contained minor amounts of quartz and thénardite. The Game.

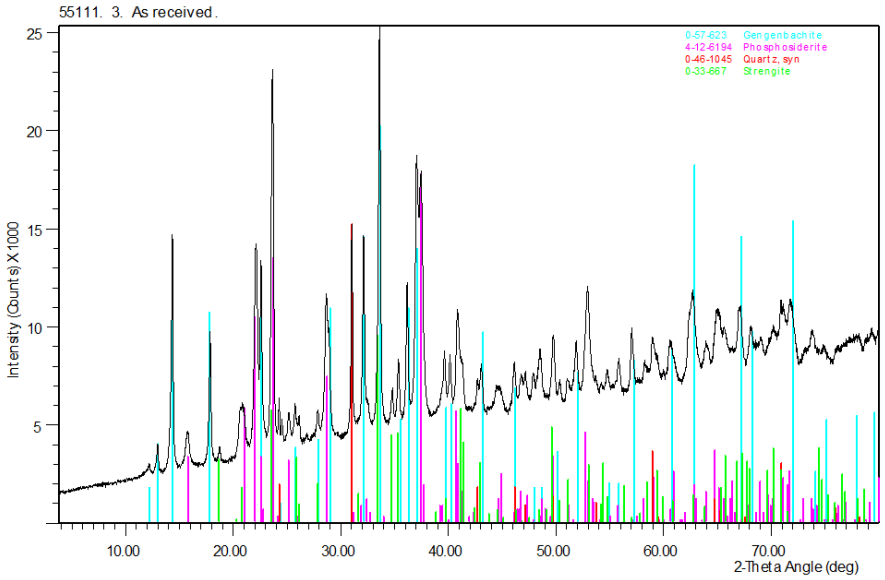

Figure S.8. X-ray diffraction pattern of the jarositic powder after being treated with 1 M H_3PO_4 at 80°C for 48 hours. The resulting solids were principally composed of phosphosiderite with minor amounts of gengenbachite, and trace amounts of strengite and quartz.

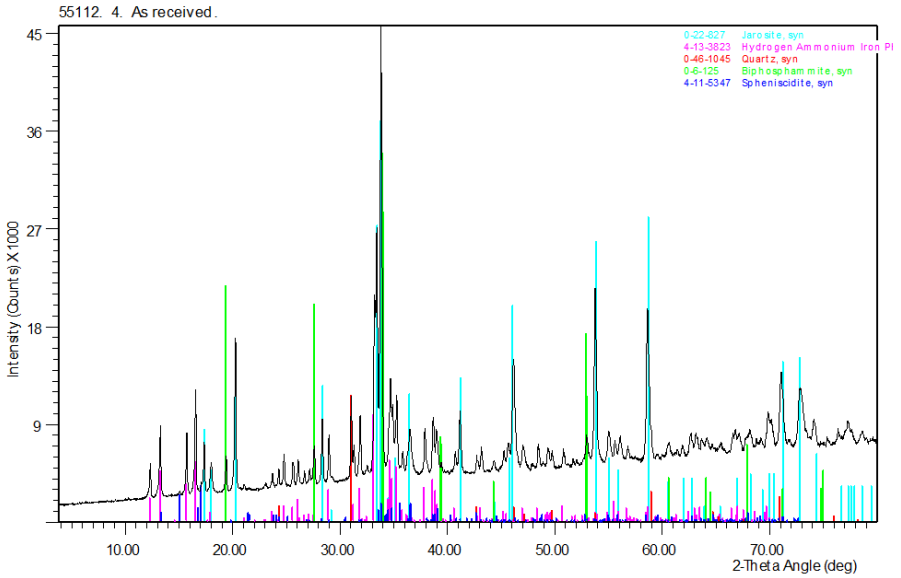

Figure S.9. X-ray diffraction pattern of the jarositic powder after being treated with 1 M $NH_4H_2PO_4$ at 80℃ for 48 hours. The resulting solids were principally composed of $H_2(NH_4)Fe(PO_4)_2$ and jarosite (in roughly equal proportions) with trace amounts of unreacted $NH_4H_2PO_4$, quartz and spheniscidite.

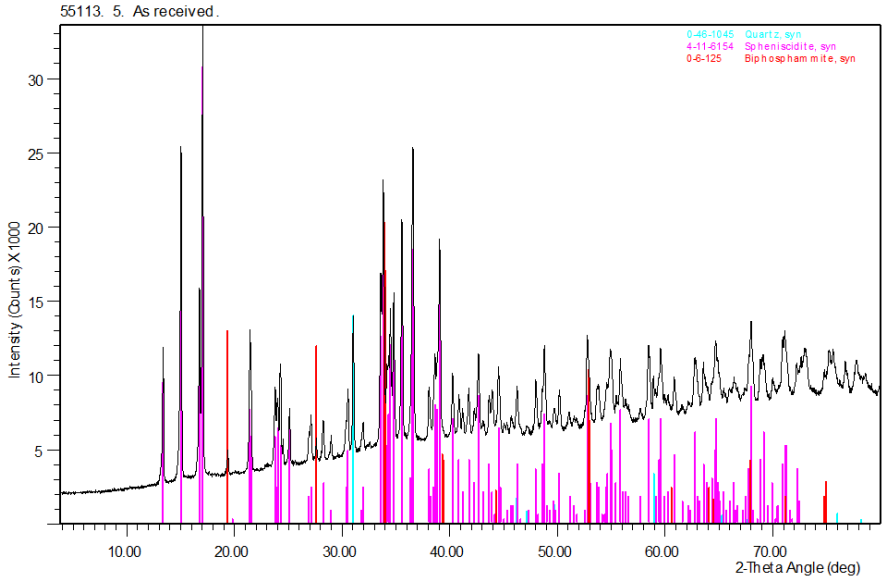

Figure S.10. X-ray diffraction pattern of the jarositic powder after being treated with 1 M NaOH for 48 hours at room temperature followed with 1 M $NH_4H_2PO_4$ for 48 hours at 80℃. The resulting solids were principally composed of spheniscidite with traces of quartz and unreacted $NH_4H_2PO_4$.

Table S.1. Elemental composition (μmol/g) and selected molar ratios of the untreated and treated jarosite. Values in bold are *not* statistically different with respect to the untreated jarosite. Corresponding RSD (%) values are included in brackets, while corresponding p-values are provided separately below mean values.

		25℃					80℃		
	untreated	NaOH	$CaOH_2$	MAP	H_3PO_4	NaOH H_3PO_4	H_2O	MAP	H_3PO_4
micromoles per gram									
Al	137 (11)	**119** (1.0)	**115** (4.5)	**129** (0.97)	**153** (7.9)	539 (9.5)	82.2 (7.5)	71.9 (12)	35.7 (4.1)
As	3.25 (7.8)	0.24 (66)	3.89 (0.98)	**3.07** (3.9)	2.21 (7.1)	0.18 (49)	5.85 (12)	0.10 (170)	0.30 (140)
Ca	23.2 (7.4)	30.7 (0.42)	2020 (3.1)	3.26 (4.3)	1.64 (16)	2.02 (15)	**20.8** (4.0)	16.9 (14)	1.45 (1.4)
Fe	5050 (4.2)	6770 (1.0)	4290 (2.7)	**5100** (6.3)	**5050** (6.0)	729 (13)	2440 (1.2)	2360 (13)	2390 (5.7)
K	1250 (8.3)	76.4 (4.1)	154 (3.2)	983 (5.7)	1000 (5.7)	70.7 (24)	518 (3.9)	25.7 (17)	20.9 (7.7)
Mg	74.7 (8.4)	**78.2** (1.5)	**70.9** (1.0)	11.8 (2.9)	12.9 (3.9)	50.3 (15)	**71.2** (4.3)	**68.1** (12)	3.32 (5.1)
Na	845 (8.9)	3380 (0.91)	54.3 (1.3)	270 (6.3)	255 (3.5)	45.2 (15)	541 (6.1)	87.8 (11)	18.8 (2.2)
P	9.33 (12)	2.99 (29)	12.6 (3.5)	725 (3.9)	589 (7.3)	1340 (9.5)	7.64 (7.3)	2630 (5.5)	1970 (13)
S	3530 (9.3)	173 (0.48)	1890 (4.9)	**2940** (1.6)	2810 (5.4)	35.5 (21)	1540 (7.1)	12.8 (17)	64.2 (5.0)
Zn	0.25 (14)	0.18 (2.1)	0.11 (0.19)	0.12 (17)	0.13 (7.1)	**0.27** (35)	0.15 (2.9)	0.19 (19)	**0.26** (19)
molar ratio									
Fe/Al	37.3 (8.5)	56.5 (0.01)	**37.4** (1.9)	**39.4** (5.4)	**33.1** (1.9)	1.35 (3.9)	29.8 (6.8)	32.7 (1.8)	67.0 (2.6)
Fe/K	4.05 (7.3)	88.7 (3.1)	27.8 (0.57)	5.19 (0.61)	5.05 (0.27)	10.5 (11)	4.72 (2.8)	92.0 (5.2)	114 (6.3)
Fe/P	549 (15)	2370 (30)	340 (0.80)	7.03 (2.5)	8.57 (1.4)	0.54 (3.9)	320 (6.9)	0.90 (16)	1.24 (17)
Fe/S	1.44 (7.4)	39.2 (1.5)	2.27 (2.3)	1.74 (4.7)	1.80 (0.60)	20.7 (8.0)	**1.60** (6.5)	184 (5.9)	37.4 (9.5)
S/K	2.82 (1.9)	2.26 (4.6)	12.2 (1.7)	2.99 (4.1)	**2.81** (0.34)	0.50 (3.0)	**2.97** (5.6)	0.50 (1.9)	3.07 (7.9)

p-vales (independent t-test)

	25℃					80℃		
	NaOH	$CaOH_2$	MAP	H_3PO_4	NaOH H_3PO_4	H_2O	MAP	H_3PO_4
micromoles per gram								
Al	**0.19**	**0.11**	**0.56**	**0.22**	<0.001	0.001	<0.001	<0.001
As	<0.001	0.02	**0.38**	0.002	<0.001	<0.001	<0.001	<0.001
Ca	0.001	<0.001	<0.001	<0.001	<0.001	**0.061**	0.002	<0.001
Fe	<0.001	0.003	**0.82**	**0.98**	<0.001	<0.001	<0.001	<0.001
K	<0.001	<0.001	0.02	0.02	<0.001	<0.001	<0.001	<0.001
Mg	**0.49**	**0.44**	<0.001	<0.001	0.004	**0.39**	**0.21**	<0.001
Na	<0.001	<0.001	<0.001	<0.001	<0.001	<0.001	<0.001	<0.001
P	<0.001	0.01	<0.001	<0.001	<0.001	0.041	<0.001	<0.001
S	<0.001	0.001	**0.05**	0.027	<0.001	<0.001	<0.001	<0.001
Zn	0.04	0.002	0.003	0.004	**0.78**	0.001	0.034	**0.86**
molar ratio								
Fe/Al	<0.001	**0.99**	**0.44**	**0.12**	<0.001	0.008	0.047	<0.001
Fe/K	<0.001	0.000	0.002	0.004	<0.001	0.008	<0.001	<0.001
Fe/P	<0.001	0.017	<0.001	<0.001	<0.001	0.003	<0.001	<0.001
Fe/S	<0.001	0.000	0.012	0.004	<0.001	**0.073**	<0.001	<0.001
S/K	<0.001	0.000	0.025	**0.78**	<0.001	**0.077**	<0.001	0.038

Table S.2. Analyte release rates ($log_{10}R$, R = mol/s) related to the column perfusion experiments described in Sections 2.3 and 3.2. The samples (either untreated, MAP-treated, or NaOH-treated jarosite) were eluted with dilute HCl (pH 4) for 72 hours, then with dilute NaOH (pH 10) for another 72 hours. The RSD (%) of the untransformed R values are included in brackets.

		$log_{10}R$									
	Trt. pH	**Al**	**As**	**Ca**	**Fe**	**K**	**Mg**	**Na**	**P**	**S**	**Zn**
Ctrl	4	-12.2 (26.2)	-13.2 (70.7)	-11.1 (0.6)	-10.6 (72.8)	-10.6 (19.2)	-10.9 (4.0)	-10.0 (8.3)	-12.2 (27.9)	-10.3 (26.2)	-12.8 (7.5)
MAP	4	-11.9 (0.9)	-12.3 (10.6)	-11.7 (2.6)	-11.5 (7.7)	-10.4 (16.9)	-11.6 (3.6)	-10.1 (2.8)	-8.8 (1.3)	-9.8 (11.2)	-13.1 (31.5)
NaOH	4	-10.2 (18.0)	-13.0 (7.2)	-12.4 (5.8)	-11.4 (16.5)	-9.6 (6.5)	-11.7 (16.4)	-7.9 (2.9)	-11.7 (7.0)	-9.3 (19.7)	-13.6 (3.9)
Ctrl	10	-13.2 (66.7)	-13.4 (43.0)	-12.0 (13.2)	-11.0 (50.6)	-11.0 (0.5)	-12.1 (16.7)	-11.6 (13.6)	-12.4 (10.7)	-10.4 (3.3)	-13.6 (31.5)
MAP	10	-12.9 (9.8)	-13.5 (11.9)	-12.6 (1.8)	-11.8 (15.0)	-11.9 (1.0)	-12.6 (38.9)	-11.0 (8.7)	-10.3 (8.2)	-11.4 (15.4)	-14.3 (33.6)
NaOH	10	-10.9 (34.1)	-13.7 (44.4)	-12.6 (12.7)	-11.1 (16.0)	-10.7 (18.4)	-11.8 (30.5)	-9.3 (21.6)	-12.6 (89.2)	-11.3 (44.7)	-14.2 (43.3)

2. Supplementary discussion related to the release of iron during the column perfusion experiments

The following relates to section 3.2 of the article, where the release of iron is discussed.

The rate of iron release (R_{Fe}, mol/s per gram solid) was calculated over two 72h intervals, namely, 0-72h and 72-144h. The former and latter intervals as referred to here as the "pH 4 interval" and "pH 10 interval", respectively, in reference to the eluant pH during that interval.

Consider the following average (arithmetic mean) iron release rates and associated error:

Control (pH 4 interval): R_{Fe} = 3.13E-11 (RSD = 73%)

MAP treatment (pH 4 interval): R_{Fe} = 3.49E-12 (RSD = 8%)

NaOH treatment (pH 4 interval): R_{Fe} = 34.32E-12 (RSD = 17%)

Control (pH 10 interval): R_{Fe} = 1.21E-11 (RSD = 50.6%)

MAP treatment (pH 10 interval): R_{Fe} = 1.51E-12 (RSD = 15%)

NaOH treatment (pH 10 interval): R_{Fe} = 7.62E-12 (RSD = 16%)

Note that the control appears to have released iron at a greater rate than both of the treatments; and that the control displays a much greater margin of error than the treatments.

Independent sample t tests were used to compare the rates. These tests suggest that there is one significant difference between the control and treatments:

Ctrl-MAP (pH 4): p = 0.120

Ctrl-NaOH (pH 4): p = 0.110

Ctrl-MAP (pH 10): p = **0.040**

Ctrl-NaOH (pH 10): p = 0.283

However, it could be argued that the control contains an outlier. To test this, control pseudoreplicates were obtained from similar experiments described by Trueman et al. (2020). In these experiments, the average iron release rate for jarosite eluted with dilute HCl (pH 4, unbuffered) was 6.36E-12 mol/s (RSD = 23%, n = 6). Conversely, for jarosite eluted with dilute NaOH (pH 10, unbuffered), the average Fe release rate was 4.28E-12 mol/s (RSD = 31%, n = 3). Analysing the control dataset along with the pseudoreplicates suggests that the upper extreme (fastest rate) in the control dataset is an outlier. For example:

Ctrl (pH 4) with outlier: skewness = 2.25, outlier standard score = 2.25

Ctrl (pH 4) without outlier: skewness = -0.09

Ctrl (pH 10) with outlier: skewness = 1.75, outlier standard score = 1.71

Ctrl (pH 10) without outlier: skewness = -0.14

If the tests are repeated using both the base dataset and additional pseudoreplicates – **including** the outlier – then there are no significant differences:

Ctrl-MAP (pH 4): p = 0.208

Ctrl-NaOH (pH 4): p = 0.234

Ctrl-MAP (pH 10): p = 0.103

Ctrl-NaOH (pH 10): p = 0.880

Moreover, if there tests are repeated using both the base dataset and additional pseudoreplicates – **excluding** the outlier – then there are no significant differences:

Ctrl-MAP (pH 4): p = 0.081

Ctrl-NaOH (pH 4): p = 0.181

Ctrl-MAP (pH 10): p = 0.064

Ctrl-NaOH (pH 10): p = 0.491

Therefore, in light of these results it is reasonable to conclude that the treatments did **not** significantly affect the release of iron relative to the control.

References

Trueman, A.M., Mclaughlin, M.J., Mosley, L.M., Fitzpatrick, R.W., 2020. Composition and dissolution kinetics of jarosite-rich segregations extracted from an acid sulfate soil with sulfuric material. Chemical Geology, 543: 119606. https://doi.org/10.1016/j.chemgeo.2020.119606.

Chapter 4 – Conclusions

1. Jarosite dissolution and implications for soil and water quality

Acid sulfate soil (ASS) is a general term for soils that contain or are capable of producing sulfuric acid in quantities that have a lasting effect on key soil characteristics. Effectively managing ASS heavily depends on accurately identifying and quantifying sulfidic and sulfuric materials and the hazards they pose to the environment and the communities that depend on them (Sullivan et al., 2018). Jarosite ($XFe_3(SO_4)_2(OH)_6$, where X is typically K or Na) is one of the most common secondary reaction products of iron sulfide oxidation, and is a ubiquitous component of sulfuric material (van Breemen, 1973; Vithana et al., 2013). Moreover, jarosite typically constitutes the primary form of retained acidity: an operationally defined pool of potential acidity, associated with slow release, and subsequent hydrolysis, of Al^{3+} and Fe^{3+} from sparingly soluble minerals (Vithana et al., 2013, 2014).

Under non-drought conditions, mobile pools of acidity and other contaminants are typically leached from the soil over time. As such, ASS management guidelines generally prioritise the collection and treatment of hazardous soil drainage (Sullivan et al., 2018). In contrast, jarosite and other forms of retained acidity represent a major management hurdle as they cannot be easily flushed from the soil. Consequently, soils with jarosite-rich sulfuric material may require more involved or detailed management strategies, which in turn requires more detailed information, including: an accurate measure of jarosite, and a robust understanding of how jarosite behaves in soil, how it effects long-term soil and water chemistry and quality, and how it responds to different treatments.

The body of knowledge related to jarosite mineralogy is well developed, but is often inconsistent and rarely considers natural jarosite dissolution under realistic environmental conditions and its effects on soil and water quality. In terms of its solubility product (K_{sp}), the reported solubility of jarosite varies from 10^{-9} and 10^{-14}. Similarly, reported jarosite dissolution rates (R, mol/m^{2}s) range from around 10^{-6} to 10^{-14}. This considerable magnitude of variation in K_{sp} appears primarily driven by differences in experimental design. For example, jarosite mineralogy and chemistry is frequently examined through a hydrometallurgical lens – with studies that focus on precipitating NH_4- or Na-jarosite at high temperatures (80-90℃) (c.f. Das et al. (1996) and Dutrizac and Jambor (2000)). Similarly the majority of investigations that focus on the dissolution kinetics of jarosite do so with a view to better understand the longevity of jarosite on the surface of Mars (Dixon et al., 2015; Madden et al., 2012; Pritchett et al., 2012; Zahrai et al., 2013). At the time this research project began, there were no studies that described the dissolution kinetics of natural jarosite using methods that mimic water-mineral interactions in soil (i.e. the perfusion or percolation of water through a porous, reactive medium). Rather, the majority of these studies employed synthetic jarosite (excluding Welch et al. (2008)) and batch dissolution techniques (excluding Dixon et al. (2015)). This knowledge gap motivated the first set of experiments, the results from which were subsequently published in Chemical Geology (Trueman et al., 2020).

In these first experiments, jarosite-rich soil segregations (pedotubules or phytotubules) were extracted from an ASS with sulfuric material in Gillman: ca. 770 ha of intertidal and supratidal land within the Southern Barker Inlet, South Australia. Large swathes of hazardous soils – with considerable amounts of retained acidity – have hindered development in the area since it was drained around 1935. XRD analysis showed that the jarosite-rich segregations were predominantly composed of jarosite with minor amounts of quartz and traces of halite, gypsum and muscovite. The jarosite and the soil from which it was extracted were analysed for major pools of actual and potential acidity and alkalinity using standard acid-base-accounting (ABA)

procedures recommended by the National Acid Sulfate Soil Guidance (Sullivan et al., 2018). Consequently, other results (i.e. jarosite composition and dissolution kinetics) can be reported in terms of retained acidity. This is unique in the literature and improves the utility of the results with respect to managing soils with jarosite-rich sulfuric material.

Mosley et al. (2017) suggested that the prolonged recovery of soil with sulfuric material was in part due to the dissolution of jarosite, which was likely buffering sub-surface layers of soil around pH 4. This pH buffering effect was clearly demonstrated during the column perfusion experiments. Where the eluant (input) pH was greater than 4, the eluate (output) pH was 2-4 units less than the eluant pH. The jarosite segregations contained a minor amount of actual acidity. Therefore, the drop in pH was primarily due to the release of retained acidity. Where the eluant pH was less than 4, there were no measurable difference between eluant and eluate pH. Therefore, jarosite dissolution plays a key role in driving the pH of sulfuric material towards 4. Conversely, further acidification is likely driven by the evaporative concentration of actual acidity rather than the release of potential acidity.

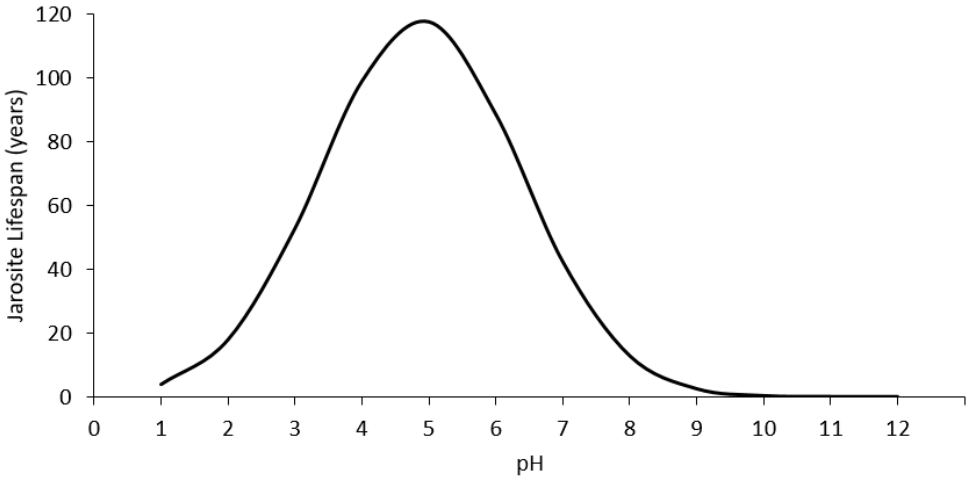

Figure 1. The lifespan of jarosite (years) under constant flow conditions as a function of pH. Dissolution rates – derived from Trueman et al. (2020) – are assumed to be zero order with an initial mass of 1 g.

The key output of the column perfusion experiments was the relationship between the dissolution rate of jarosite (R, mol m^2 s^{-1}) and pH: $\log_{10}R = 0.099pH^2 - 0.966pH - 9.914$, $R^2 = 0.94$. This shows that jarosite is relatively stable from pH 3 to 8, and could be very long-lived between pH 4 to 6 (Fig. 1). This is consistent with field evidence of limited recovery of pH in jarosite-containing acid sulfate soils in the Lower Murray region after nearly a decade of flood irrigation (Mosley et al. 2017). Note that this relationship was tested at a much broader range of pH values than previously described in the literature; and should hold relatively well between pH 1 and 12. Moreover, Dixon et al. (2015) suggests that the rate of jarosite dissolution is not significantly affected by flow rate. This is reasonable as the dissolution of sparingly soluble minerals tends to be controlled by the inherent mineral reactivity, rather than mass transport to and from the reaction site (Steefel, 2008). Therefore, although dissolution was tested under constant flow conditions, the rate estimations should be reasonably accurate under a moderate range of flow rates. However, rate estimates may not be accurate over long time frames, and are likely much greater than what would be expected in the field.

The dissolution rates were calculated assuming zero order reaction dynamics (i.e. where the rate is constant over time). This was a reasonable assumption under extremely acidic conditions (pH < 2), where the dissolution reaction was congruent and remained fairly constant over time. However, at higher pH values the reaction was incongruent and the dissolution rate decreased

over time. This rate change was extremely small, but will become increasingly significant over greater time scales. Moreover, conditions of the experiment were more controlled and conducive to dissolution than those expected in the environment. Therefore, the rates provided in this study are best suited for estimating jarosite dissolution and the release of acidity and other contaminants within relatively short time frames (e.g. days to weeks). *Ad hoc* treatment of the dissolution rates could be employed to improve their utility (e.g. time-dependent cofactors that mimic expected or plausible long-term changes in jarosite dissolution rate). However, more involved methods are required to accurately estimate the longevity of jarosite in soil (*c.f.* Section 2).

The dissolution experiments also considered the release of major cations (Ca, Mg and Na) and minor/trace cations (Al, As and Zn). Consequently, the data presented in Trueman et al. (2020) can be utilised to estimate multiple aspects of eluate quality under a broad range of pH conditions. Regardless of pH, the release of Ca, Mg, and Na was initially rapid and quickly decayed over the first 12-24 hours. Although Al, As and Zn displayed varying levels of pH-dependency, the release of these hazardous metal(loid)s was often greatest within the first day of perfusion. Consequently, jarosite represents not only a key source of acidity, but of salinity and hazardous metal(loid)s – which are likely to be rapidly released following the rewetting of jarosite-rich soil.

The dissolution experiments suggest that flushing jarosite from soil is not feasible (due to its low solubility over a broad pH range) and will invariably produce environmentally hazardous soil drainage. Neutralising retained acidity via liming may be prohibitively expensive and is often ineffective due to limestone armouring (Hammarstrom et al., 2003). Permanently saturating the soil should promote the reductive dissolution of jarosite (Baldwin and Fraser, 2009; Kölbl et al., 2017; Yuan et al., 2015). However, largescale flooding is logistically challenging and is typically unfeasible in drought-prone regions. Additionally, flooding may not be an option where the land is zoned for primary production, industry, housing etc. In such cases, a once-off treatment that permanently renders jarosite chemically inert is ideal. This concept motivated a second set of experiments, the aim of which was to alter jarosite to sparingly-soluble, relatively benign minerals such as goethite (α-FeOOH) and strengite ($FePO_4.2H_2O$), with a view to reduce to the risk of jarosite dissolution adversely affecting soil and water quality (Chapter 3).

Jarosite treated with alkaline solutions readily produced poorly-crystalline ferric (oxyhydr)oxide minerals under ambient conditions (Trueman et al., 2021). However, column perfusion experiments suggests that encouraging the alkaline decomposition of jarosite may exacerbate certain environmental risks associated with jarosite dissolution (e.g. Al toxicity). Conversely, the alteration of jarosite to ferric phosphate minerals such as strengite – although apparently spontaneous – is constrained under ambient conditions. Moreover, the column perfusion experiments showed that neither treatments offer any distinct advantages in terms of curtailing the release of potentially hazardous elements. Overall, this study provides key insights into jarosite alteration pathways, and sets a solid foundation upon which to further explore alternative methods of remediating jarosite-rich soils and mining wastes.

2. Further Research

There are a number of inherent difficulties involved in accurately characterising mineral solubility. Consequently, the reported solubility of jarosite (and many other minerals) varies considerably in the literature. Therefore, there is – and may always be – justifiable motivation for reassessing and building upon available geochemical data within a given investigative framework. For example, minerals such as sideronatrite ($Na_2Fe(SO_4)_2(OH).3H_2O$) and

tamarugite ($NaAl(SO_4)_2.6H_2O$) may play a key role in the regulation of acidity, metal(loids) and sulfate in ASS during wetting and drying cycles. However, due to a lack of relevant data, these minerals are not represented in standard geochemical libraries (e.g. MINTEQ, PHREEQC and WATEQ4F). Therefore, systematically describing the solubility and dissolution kinetics of these minerals would be helpful (e.g. for modelling aquatic speciation in acidic, metalliferous, sulfate-rich solutions), and may yield valuable insights into ASS hydrogeochemistry. However, this would be very time consuming. Therefore, narrowing the research focus in this way may yield diminishing returns in terms of resource inputs vs practical outputs and outcomes. Rather, it may be more resource effective to broaden the research focus from mineral solubility to the weathering of sulfuric material as its own distinct unit.

For example, repeating the column perfusion tests described in Trueman et al. (2020) using bulk samples of soil with sulfuric material could be employed to assess the chemistry of sulfuric soil drainage with respect to eluant pH and elution rate/porewater velocity. Additionally, assessing the ecotoxological risk associated with sulfuric material would improve ASS management guidance, and serve as a baseline for assessing the efficacy of remediation strategies. A relatively simple route would be to establish a relationship between acute biological toxicity (e.g. median lethal dose, LD50) and retained acidity. For example, this could be accomplished using a standard phytotoxicity test such as the OECD seedling emergence and growth test (OECD, 2006). This involves assessing the health and mortality of plants grown in soils with increasing amounts of a contaminant (in this case sulfuric material). Such tests can be expanded to include soil organisms – e.g. soil invertebrates, c.f. van Gestel (2012). Moreover, similar tests can be utilised to assess the toxicity of drainage from sulfuric soil – e.g. OECD static duckweed test (OECD, 2004). The results can be employed, for example, to estimate the dilution factor required to mitigate the toxicity of hazardous soil drainage relative to a receiving body of water. Additionally, although liming is an integral part of ASS management, it is difficult to determine the liming efficacy with respect to the removal of actual and potential acidity – especially jarosite. Liming efficacy could be investigated in a relatively simple fashion by liming soil containing jarosite-rich sulfuric material and periodically conducting ABA analysis. The efficacy of the liming agent and application method, and the effect of key factors (e.g. soil water content) should also be investigated. I believe the examples listed above are suitable for postgraduate research and would provide practical contributions to understanding and managing sulfidic and sulfuric soil systems.

References

Baldwin, D.S., Fraser, M., 2009. Rehabilitation options for inland waterways impacted by sulfidic sediments–a synthesis. Journal of Environmental Management, 91(2): 311-319.

Das, G.K., Acharya, S., Anand, S., Das, R.P., 1996. Jarosites: A review. Mineral Processing and Extractive Metallurgy Review, 16(3): 185-210.

Dixon, E.M., Elwood Madden, A.S., Hausrath, E.M., Elwood Madden, M.E., 2015. Assessing hydrodynamic effects on jarosite dissolution rates, reaction products, and preservation on Mars. Journal of Geophysical Research: Planets, 120(4): 625-642.

Dutrizac, J.E., Jambor, J.L., 2000. Jarosites and their application in hydrometallurgy. Reviews in Mineralogy and Geochemistry, 40(1): 405-452. https://doi.org/10.2138/rmg.2000.40.8.

Hammarstrom, J.M., Sibrell, P.L., Belkin, H.E., 2003. Characterization of limestone reacted with acid-mine drainage in a pulsed limestone bed treatment system at the Friendship Hill National Historical Site, Pennsylvania, USA. Applied Geochemistry, 18(11): 1705-1721. https://doi.org/10.1016/S0883-2927(03)00105-7.

Kölbl, A., Marschner, P., Fitzpatrick, R., Mosley, L., Kögel-Knabner, I., 2017. Linking organic matter composition in acid sulfate soils to pH recovery after re-submerging. Geoderma, 308: 350-362. https://doi.org/10.1016/j.geoderma.2017.07.031.

Madden, M.E., Madden, A.S., Rimstidt, J.D., Zahrai, S., Kendall, M.R., Miller, M.A., 2012. Jarosite dissolution rates and nanoscale mineralogy. Geochimica et Cosmochimica Acta, 91: 306-321. https://doi.org/10.1016/j.gca.2012.05.001.

Mosley, L.M., Biswas, T.K., Cook, F.J., Marschner, P., Palmer, D., Shand, P., Yuan, C., Fitzpatrick, R.W., 2017. Prolonged recovery of acid sulfate soils with sulfuric materials following severe drought: causes and implications. Geoderma, 308: 312-320. https://doi.org/10.1016/j.geoderma.2017.03.019.

OECD, 2004. Guidelines for the testing of chemicals. Test No. 221: *Lemna* sp. growth inhibition test. Guideline 221.

OECD, 2006. Guidelines for the testing of chemicals. Terrestrial plant test: seedling emergence and seedling growth test. Guideline 208.

Pritchett, B.N., Elwood Madden, M.E., Madden, A.S., 2012. Jarosite dissolution rates and maximum lifetimes in high salinity brines: Implications for Earth and Mars. Earth and Planetary Science Letters, 357-358: 327-336. https://doi.org/10.1016/j.epsl.2012.09.011.

Steefel, C.I., 2008. Geochemical kinetics and transport. In: Brantley, S.L., Kubicki, J.D., White, A.F. (Eds.), Kinetics of water-rock interaction. Springer New York, New York, NY, pp. 545-589.

Sullivan, L., Ward, N., Toppler, N., Lancaster, G., 2018. National acid sulfate soils guidance: National acid sulfate soils identification and laboratory methods manual, Department of Agriculture and Water Resources, Canberra, ACT. CC BY 4.0.

Trueman, A.M., Fitzpatrick, R.W., Mosley, L.M., Mclaughlin, M.J., 2021. Exploring passivation-based treatments for jarosite from an acid sulfate soil. Chemical Geology, 561: 120034. https://doi.org/10.1016/j.chemgeo.2020.120034.

Trueman, A.M., Mclaughlin, M.J., Mosley, L.M., Fitzpatrick, R.W., 2020. Composition and dissolution kinetics of jarosite-rich segregations extracted from an acid sulfate soil with sulfuric material. Chemical Geology, 543: 119606. https://doi.org/10.1016/j.chemgeo.2020.119606.

van Breemen, N., 1973. Soil forming processes in acid sulfate soils. In: Dost, H. (Editor), Proceedings of the international symposium on acid sulfate soils. Internal Institute for Land Reclamation and Improvement, Wageningen, The Netherlands, pp. 66-130.

van Gestel, C.A., 2012. Soil ecotoxicology: state of the art and future directions. ZooKeys(176): 275.

Vithana, C.L., Sullivan, L.A., Bush, R.T., Burton, E.D., 2013. Acidity fractions in acid sulfate soils and sediments: contributions of schwertmannite and jarosite. Soil Research, 51(3): 203-214. https://doi.org/10.1071/SR12291.

Vithana, C.L., Sullivan, L.A., Bush, R.T., Burton, E.D., 2014. Jarosite quantification in soils: an enhanced sequential extraction procedure. Applied Geochemistry, 51: 130-138. https://doi.org/10.1016/j.apgeochem.2014.10.006.

Welch, S.A., Kirste, D., Christy, A.G., Beavis, F.R., Beavis, S.G., 2008. Jarosite dissolution II - Reaction kinetics, stoichiometry and acid flux. Chemical Geology, 254(1): 73-86. https://doi.org/10.1016/j.chemgeo.2008.06.010.

Yuan, C., Fitzpatrick, R., Mosley, L.M., Marschner, P., 2015. Sulfate reduction in sulfuric material after re-flooding: Effectiveness of organic carbon addition and pH increase depends on soil properties. Journal of Hazardous Materials, 298: 138-145. https://doi.org/10.1016/j.jhazmat.2015.05.013.

Zahrai, S.K., Elwood Madden, M.E., Madden, A.S., Rimstidt, J.D., 2013. Na-jarosite dissolution rates: the effect of mineral composition on jarosite lifetimes. Icarus, 223(1): 438-443. https://doi.org/10.1016/j.icarus.2012.12.020.